Aus dem Bereich

Biophysik

Fachrichtung Theoretische und Klinische Medizin

Der Medizinischen Fakultät der Universität des Saarlandes

Transistor-Transferfunktionsmessungen mittels ionensensitiven Feldeffekt-Transistoren zur Ermittlung der Zellviabilität als neue Möglichkeit des pharmakologischen Hochdurchsatzscreenings

Transistor-transfer Function Measurements using Ionsensitive Field-Effect Transistors to Analyze Cell Viability as a Novel Tool for Pharmacological High Throughput Screening

Dissertation

Zur Erlangung des Grades eines Doktors der Naturwissenschaften

der Medizinischen Fakultät der

Universität des Saarlandes

Vorgelegt von

Dipl.-Biol. Dieter Koppenhöfer

aus

Zweibrücken

2016

Dekan: **Prof. Dr. med. Michael D. Menger**

Erstgutachter: **Prof. Dr. Markus Hoth**

Zweitgutachter: **Dr. Frank Kirchhoff**

INHALTSVERZEICHNIS

1.   INTRODUCTION

1.1   Motivation

With roughly 500 000 new cancer cases in 2008 (nearly 50 % having lethal outcomes), cancer is still one of the most common cause of death and counts as one of the most severe diagnoses patients can receive in modern medicine. In Germany the highest numbers can be found in descending order for colon cancer (65 390 diagnoses), prostate cancer (63 440 diagnoses), breast cancer (71 660 diagnoses) and lung cancer (see fig. 1, 49 530 diagnoses; Kaatsch *et al.*, 2012) with the probability to contract cancer rising with age.
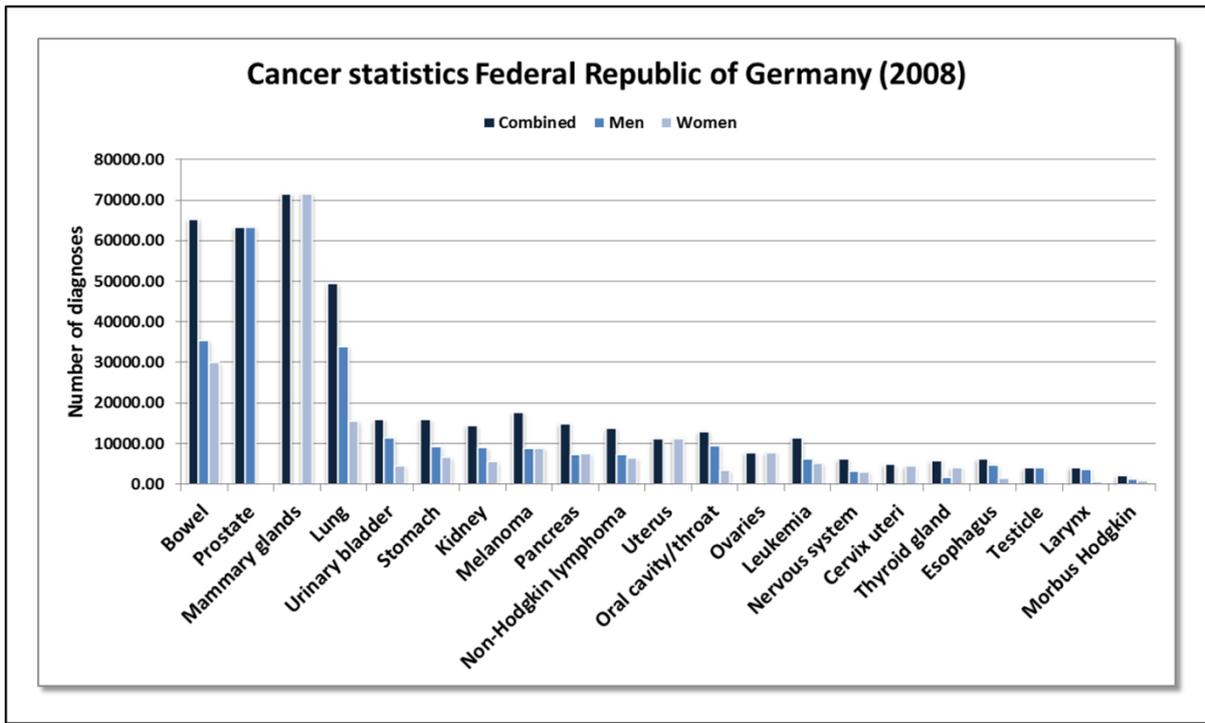
Fig. 1: Cancer statistics of the Federal Republic of Germany of 2008 (Kaatsch et al., 2012)

According to the German Cancer Research Center nearly 500 000 cancer cases were reported in Germany during the year 2008 with a mortality rate of nearly 50 %.

Similar numbers can be found in other nations like the United States of America with over a million estimated new cancer cases in 2008 (Jemal *et al.*, 2008). Cancer treatment normally involves a combination of chemotherapy, tumor resection and radiation therapy but is often

complicated by factors like accessibility of the tumor and the selectivity of the prescribed chemotherapeutic agents, and is often accompanied by severe side effects ranging from nausea and alopecia to neuropathy, immunodeficiency and myelosuppression (Love *et al*., 1989, Shapiro & Recht, 2001).

Table 1: Cancer statistics of the Federal Republic of Germany of 2008 (Kaatsch et al., 2012)

Localization	Men	Women	Combined
Bowel	35 350	30 040	65 390
Prostate	63 440	0	63 440
Mammary glands	0	71 660	71 660
Lung	33 960	15 570	49 530
Urinary bladder	11 460	4 510	15 970
Stomach	9 210	6 660	15 870
Kidney	8 960	5 540	14 500
Melanoma	8 910	8 890	17 800
Pancreas	7 390	7 570	14 960
Non-Hodgkin lymphoma	7 270	6 430	13 700
Uterus	0	11 280	11 280
Oral cavity / throat	9 520	3 490	13 010
Ovaries	0	7 790	7 790
Leukemia	6 340	5 080	11 420
Nervous system	3 180	2 990	6 170
Cervix uteri	0	4 480	4 880
Thyroid gland	1 710	4 160	5 870
Esophagus	4 800	1 380	6 180
Testicle	3 970	0	3 970
Larynx	3 610	510	4 120
Morbus Hodgkin	1 160	920	2 080
All malign tumors	246 700	223 100	469 800

1. INTRODUCTION

In recent years scientists try to shift cancer treatment from approaches generally attacking cells with high proliferation rates to selective and individualized cancer therapy using several new agents to selectively attack cancer cells. To enhance the effectiveness of cancer treatment, new approaches need to be analyzed and tested to minimize possible side effects and thereby lower the physical and psychological strain experienced by patients. Development of new pharmacological compounds and strategies always involves thorough testing and is therefore time consuming and expensive, furthering the need for fast and efficient screening platforms and testing methods.

A similar situation can be assumed for neurodegenerative diseases like Alzheimer's or Parkinson's disease, which are amongst the most common forms of dementia with 4.5 million people diagnosed in the United States alone (Hebert *et al*., 2003). A common contributing factor in both Alzheimer's and Parkinson's disease is oxidative stress caused by reactive oxygen species (ROS) like hydrogen peroxide or superoxide. Post mortem analysis of brain tissues obtained from patients affected by Alzheimer's or Parkinson's disease were reported to show increased signs of tissue damage induced by oxidative stress (Behl, 1999; Andersen, 2004). Even though these findings indicate a connection between elevated levels of oxidative stress and the observed neurodegeneration characteristic for these diseases, the connection remains unclear to a certain extent.

The objective of this thesis is the establishment of a new high throughput testing system to analyze the effectiveness of new pharmacological compounds like antineoplastic drugs based on the already established working mechanisms of silicon-based field-effect transistors in conjunction with impedance spectroscopy measurements. The presented system can be used to monitor the effects of cytotoxic compounds on single cells and in real-time. In addition, the proposed system is supposed to be used in toxicity studies to show its

general applicability in biological and pharmacological research providing researchers with a wide variety of possible applications ranging from studies on cellular adhesion to apoptosis induction and neurodegeneration.

1.2   Cancer biology

1.2.1   Homoeostasis

The human body normally consists of approximately 10^{15} cells and needs to constantly balance proliferation and differentiation against programmed cell death to maintain this condition. Proliferation and cellular turnover events are normally tightly regulated and induced by the secretion of growth factors (e.g. epidermal growth factor EGF, fibroblast growth factor FGF, platelet derived growth factor PDGF; Bertram 2001) by surrounding cells. Turnover events in which old non-functional or damaged cells are replaced by new cells can be found among others at the basal layer of the skin, the replacement of cells in the epithelial layer of the intestines or the hematopoietic system (Bertram, 2001). Even in organs with relatively low levels of cell division like the liver proliferation can be triggered by trauma or infection (Bertram, 2001). Factors influencing or altering tissue homeostasis can be mutations in genes involved in the reception of growth factors (like *erb*-b, which is involved in EGF reception), mutations in genes involved in signal transduction pathways (like *ras*, which represents a family of plasma membrane bound signal transduction molecules) or mutations in genes involved in nutrient uptake (Finkel *et al.*, 2007). Alterations to this delicate balance by biological, chemical or physical factors, if not corrected, do have the potential to alter the total number of cells in a tissue or a particular organ and thereby cause neoplasia or cancer.

Such neoplastic tumors can be categorized in two groups, benign tumors and malign tumors.

Benign tumors are characterized by their slow non-invasive growth, high level of differentiation and slow development of symptoms. On the contrary malign tumors show a fast, invasive and destructive growth, a comparatively low level of differentiation, high potential for the development of metastases, a variety of cellular atypia (e.g. nuclear hyperchromasia) and a faster development of symptoms (Leischner, *Oncology,* 3rd edition, 2014).
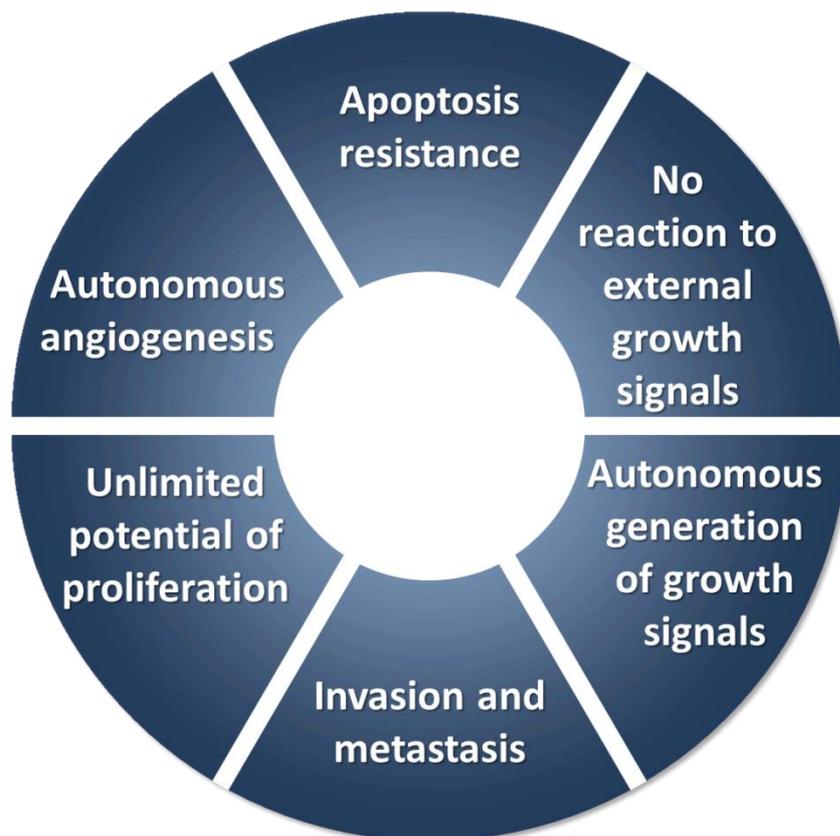
Fig. 2: Characteristics of cancer (Leischner, Oncology, 3rd edition, 2014)

Malign tumors require several characteristic traits allowing for aggressive and invasive growth. These include apoptosis resistance, independence from external growth factors, the ability to generate growth factors autonomously and the ability to induce angiogenesis.

1.2.2 Apoptosis

As mentioned it is necessary to sacrifice cells and replace them via controlled cell death. This is accomplished using the mechanism of apoptosis (see fig. 3). In a healthy human adult apoptosis is responsible for the death of roughly a billion cells per hour in the bone marrow and intestines alone (Carson *et al.*, 1993; Kerr *et al.*, 1994). Since apoptosis is also responsible for removing damaged and unhealthy cells, it is easy to see that disturbances of this process plays a significant role in developing malignancy.
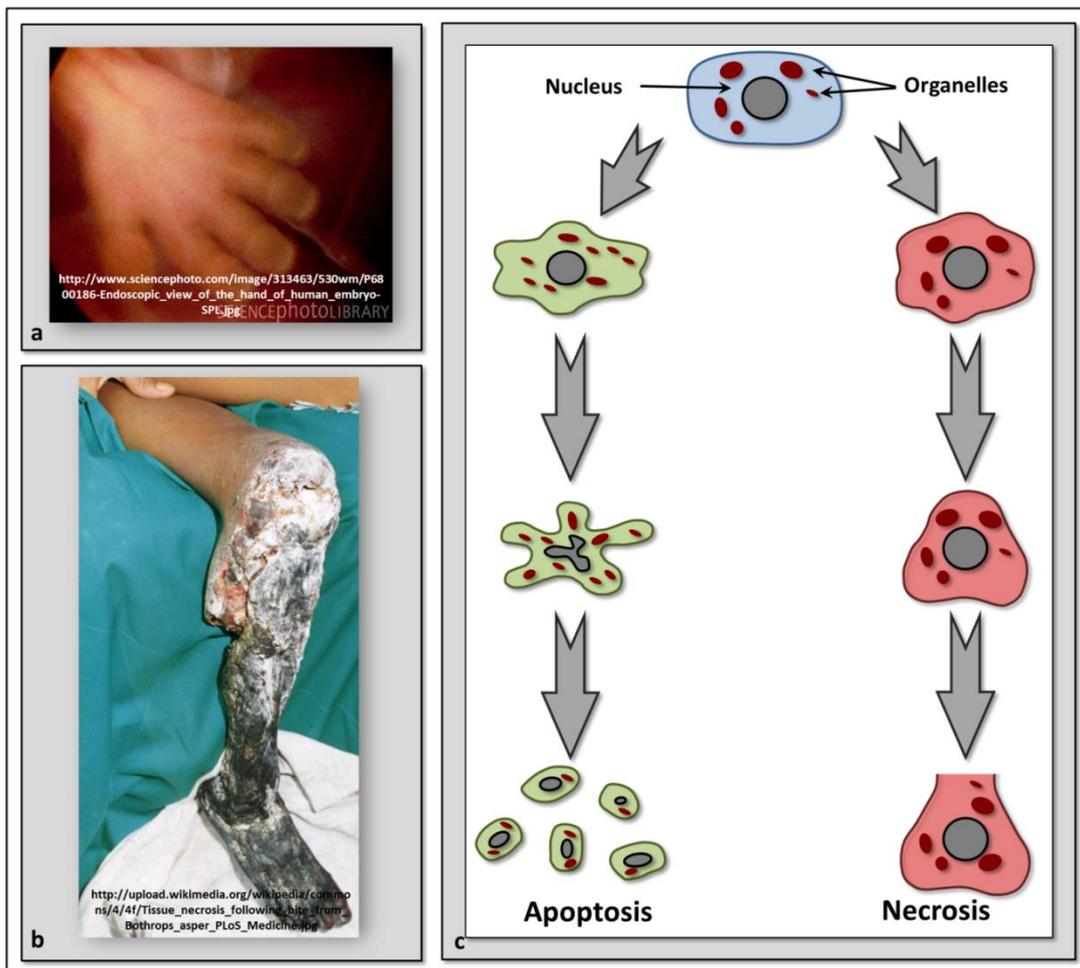
Fig. 3: Apoptotic and necrotic cell death

   a) **Apoptotic cell death is necessary for the development of extremities, in this case the development of a hand during ontogenesis**
   b) **Necrotic cell death caused by the venom of *Bothrops asper***
   c) **General mechanisms of apoptosis and necrosis: apoptosis = characterized by controlled degradation and fragmentation of the cell for removal from the organism via phagocytosis; necrosis = characterized by uncontrolled swelling of the afflicted to the point of rupture, thereby releasing the cell's contents into the surrounding tissue, damaging it.**

The process of programmed cell death can be divided into an initiation phase and an effector phase. As the tool for maintaining tissue homeostasis the initiation phase of apoptosis can be triggered by external and internal factors like DNA damage, UV light or gamma radiation. But either way the basic mechanism is the activation of a caspase cascade which leads to the activation of nucleases which will then in turn cause the fragmentation of the nucleus. Additionally the cytoskeleton and the nuclear membrane are degraded, which leads to the formation of DNA fragments containing vesicles. In total the affected cell starts to break down without releasing its contents and will be removed from the organism via phagocytosis in the end (Bold *et al.*, 1997). This happens in contrast to another major mechanism of cell death called necrosis (see fig. 3). This process can be seen as opposite to apoptosis in terms of control and affecting the surrounding tissue. Caused by extracellular damage, cells which undergo necrotic cell death will start to swell till they rupture and thereby release their contents into the surrounding area causing damage in the surrounding tissue.

1.2.3   Cellular adhesion and apoptosis

The connection between cell adhesion and cell cycle control is a topic of major interest in cancer research. It has become apparent that cell survival, cell death and general cell cycle control are heavily depending on cell adhesion between individual cells and the connection of cells to the extracellular matrix (Santini *et al.*, 2000). Therefore the fundamental principles of cell-cell and cell-matrix adhesion will be described in this chapter.

The ability of individual cells to connect to other cells and form complex structures and tissues is the basis for processes like the ontogenetic development of organs and tissue repair.

Tissues consist of many individual cells connected to each other and the extracellular matrix (ECM) via specialized contact points, which can be grouped into three functional categories (see fig. 4):

- Communicating connections (e.g. gap junctions)

- Sealing connections (e.g. tight junctions)

- Anchor connections (e.g. adherens junctions, desmosomes, hemidesmosomes, focal adhesions)
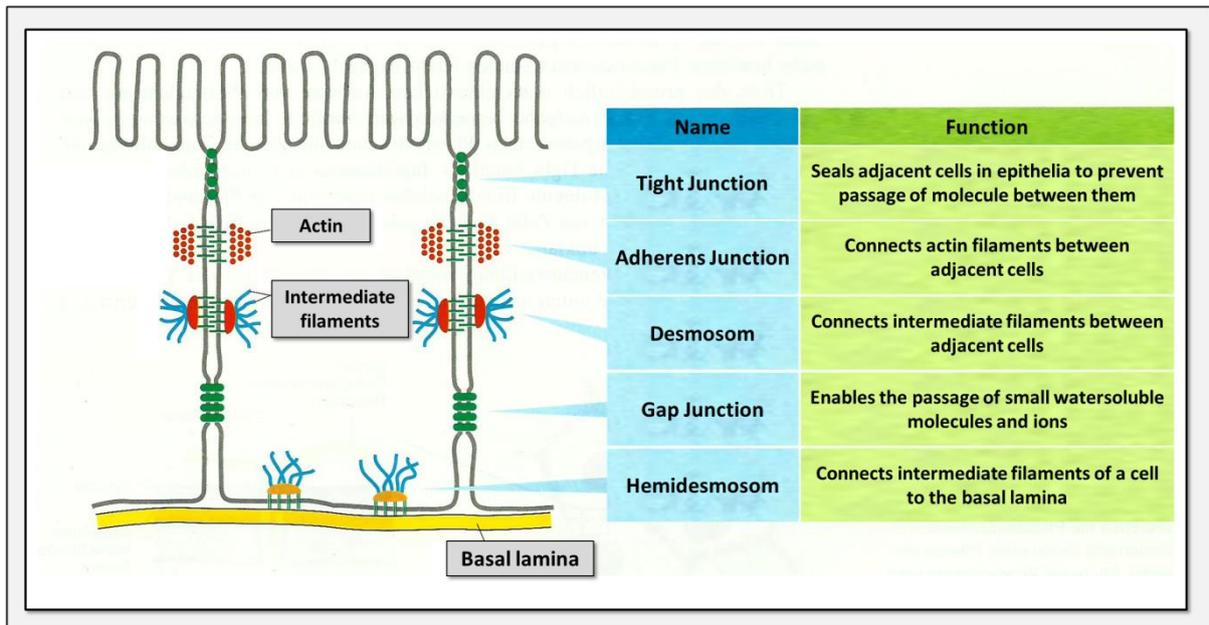
Fig. 4: Different cell connections in epithelia (Alberts et al., Molecular Biology of the Cell, 4th edition, 2004)

Gap junctions are communicating connections consisting of several connexons, which create bridges between the cytoplasm of adjacent cells. Individual connexons consist of a group of 6 connexin molecules forming a water filled connection between cells, enabling the transport of inorganic ions and small biomolecules. These connections are essential for the coordination the activity of electrically active cells (Alberts *et al., Molecular Biology of the Cell*, 4th edition, 2004).

1. INTRODUCTION

Tight junctions are impermeable connections between cells, which play an important role in the creation of the concentration gradient of small hydrophilic molecules in epithelia. They seal the plasma membranes of adjacent cells, thereby creating an impermeable diffusion barrier and hindering the diffusion of transport proteins between the apical and basolateral areas of the plasma membrane of epithelial cells (Alberts *et al., Molecular Biology of the Cell*, 4th edition, 2004).

Anchor connections are of great importance, especially in tissues which face heavy mechanical stress. This type of cell-cell connection transfers mechanical stress through the fragile cell membrane onto the tensile components of the cytoskeleton or the ECM.

These connections can be grouped in two categories characterized by the protein family mainly contributing to their respective structures. Adherens junctions and desmosomes are responsible for cell-cell connections and are normally consisting of adhesion proteins belonging to the cadherin family. Focal adhesions and hemidesmosomes connect cells to the extracellular matrix and consist of proteins belonging to the integrin family. Via such proteins cells are able to indirectly link their individual cytoskeletons or adhere to the extracellular matrix. This matrix makes up a considerable amount of the volume of tissues and consists of macromolecules (proteins and polysaccharides) secreted by the cells inhabiting this matrix.

Integrins are the most important matrix receptor connecting cells to matrix components like fibronectin, collagen or laminin. Integrins themselves are heterodimeric transmembrane glycoproteins (see fig. 5a), consisting of two not covalently bound subunits which can bind to a large group of extracellular matrix components (Alberts *et al., Molecular Biology of the Cell*, 4th edition, 2004).

Cadherins are responsible for Ca^{2+} dependent cell-cell adhesion and play important roles in cell sorting and embryonic development (Alberts *et al., Molecular Biology of the Cell*, 4th edition, 2004). Most cadherins are glycoproteins with a single transmembrane domain consisting of roughly 700 amino acids. They organize in oligomers with large repetitive extracellular domains facilitating cell-cell adhesion (see fig. 5b).

In tissue culturing fibronectin and polylysine are two of the most common substances to coat surfaces for cellular adhesion. In the case of polylysine the adhesion is based on the interaction between the polyanionic cell surfaces and the polycationic layer of the adsorbed polylysine (Mazia *et al.*, 1975). Adhesion of cells on fibronectin coated surfaces is facilitated via integrins.
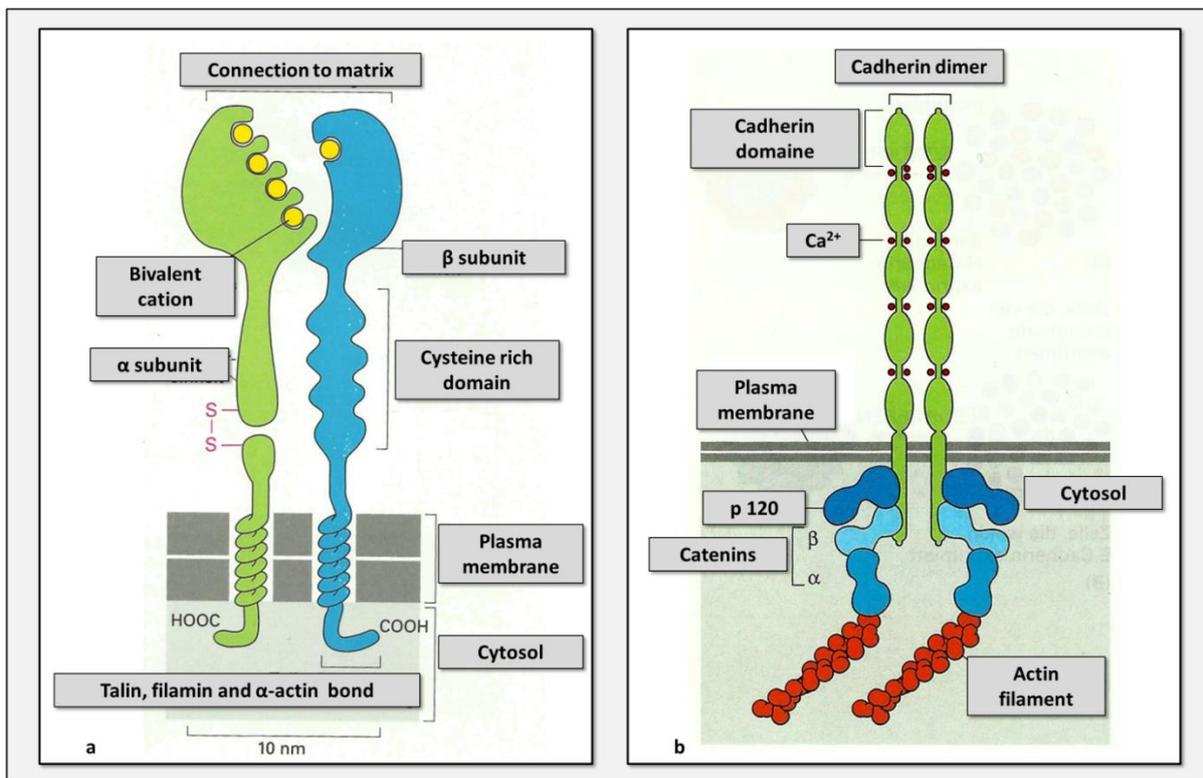
Fig. 5: Schematic drawing of the structure of integrins (a) and cadherins (b) (Alberts et al., Molecular Biology of the Cell, 4th edition, 2004)

1.2.4   Developing malignancy

During oncogenesis, benign cells start to change progressively into malign cells. This process is caused by the acquisition of mutations in cell cycle controlling or cell cycle associated genes. The majority of such changes is not inherited, but arises spontaneously caused by DNA damaging influences of a diverse group of potential risk factors. These factors can be of a physical, chemical and biological nature (see fig. 7).
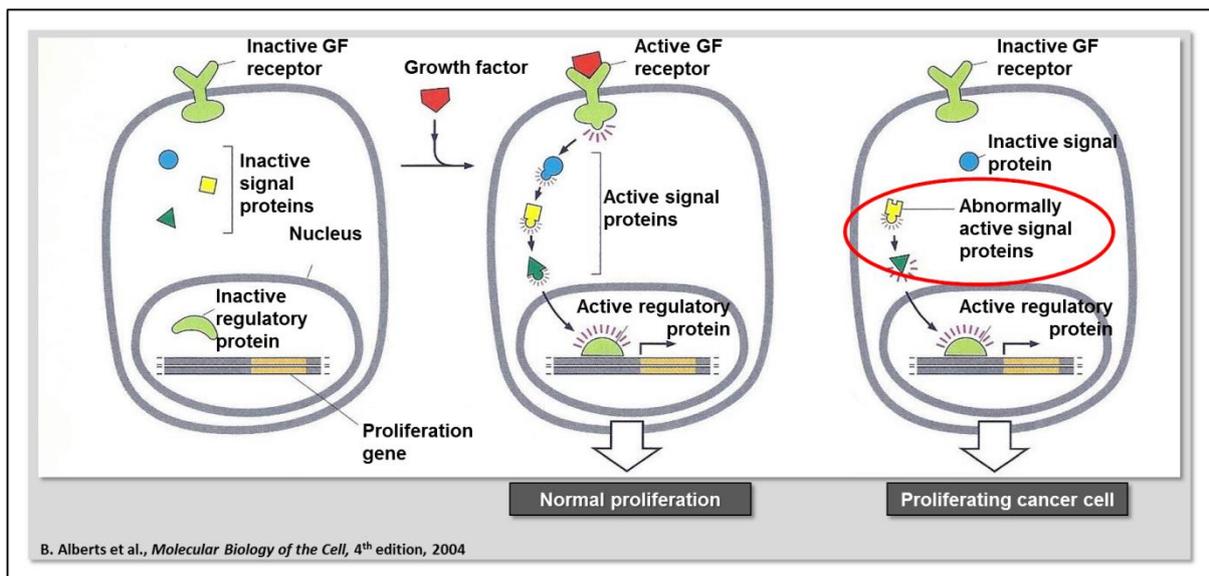
Fig. 6: Cell cycle control (Alberts et al., Molecular Biology of the Cell, 4th edition, 2004)

Developing malignancy is always caused by a loss of normal cell cycle control leading to the abnormal activation of signal pathways stimulating proliferation and invasion.

Physical risk factors like γ-radiation or UV-light cause damage to the chemical structure of the DNA due to their high energy content. Chemical factors (e.g. alkylating agents, carcinogens or procarcinogens) can cause mutations by intercalation into the DNA or via chemical modification.

This can even be caused by the organism itself, which is the case for procarcinogens. Such chemical compounds are metabolized by the organism and develop their carcinogenic potential after being metabolized. Biological carcinogens (e.g. oncoviruses) can cause mutations by inserting their DNA into cells thereby changing the genome and transcriptome to decouple cell cycle control. All of the mentioned possible ways for DNA damage to occur

cannot be thought of as mutagenic events of their own since DNA damage alone does not lead to DNA changes without replication and cell division (Bertram, 2001).
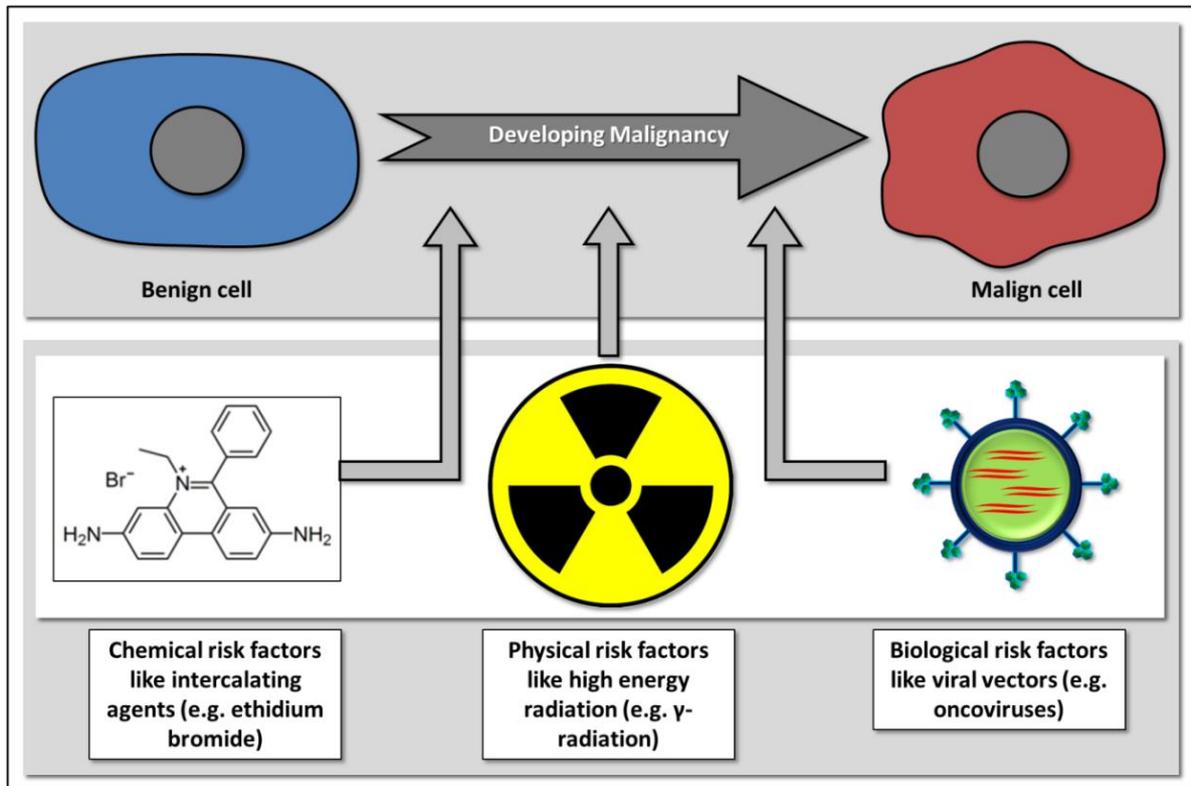
Fig. 7: Chemical, physical and biological risk factors beneficial for cancer development

Intercalating chemicals, high energy radiation and oncoviruses are amongst the most common causes of developing malignancy.

Many human cancer types seem to occur without obvious exposition to any chemical or physical carcinogen. Just as every other biomolecules, DNA constantly suffers chemical damage to its chemical bonds due to spontaneous thermal effects or attack by reactive molecules. The caused damage can lead to errors in reading and replicating DNA by DNA polymerases. During normal DNA replication there is a natural error rate of 1.3×10^{-10} mutations/base pair/cell division which leads to the introduction of one miscoding error in every 10 divisions.

As already mentioned DNA damage can also be caused by exposure to chemical and physical carcinogens. The most frequent chemical reactions damaging DNA are electrophilic attacks

on the DNA with the most significant target being guanine. The consequence of such attacks is a strong interference with base-pair recognition during DNA replication. Aromatic amines like nitrosamines or alkylating agents are examples of carcinogenic chemicals working in this manner. But not all chemical carcinogens are able to attack DNA directly; instead they have to be activated by cellular metabolism (Bertram, 2001).

Many chemotherapeutic agents act as carcinogens themselves since they target DNA replication in cancer cells (Boivin, 1990). One example of this phenomenon is topotecan, a derivative of camptothecin found in the roots and fruits of *Camptotheca acuminata*. The working mechanism of this particular compound is the inhibition of topoisomerase I, which is an enzyme localized in the nucleus and involved DNA replication and repair. Inhibition of topoisomerase I blocks the replication fork introducing an irreversible strand break and thereby inducing apoptosis (Devy *et al.*, 2004).

In addition to chemical carcinogens there are also physical factors like ionizing radiation (gamma radiation) or UV light that can be responsible for the development of malign tumors.

Ionizing radiation is able to cause direct damage to DNA by inducing single and double-strand breaks to the helix. Additionally to direct damage, ionizing radiation can also cause indirect damage via radiolysis of water which will lead to the release of free radicals. Ultraviolet radiation on the other hand is able to induce chemical reactions in the DNA; the most relevant is the formation of stable thymine dimers which will disrupt normal base pairing thereby inducing mutations (Bertram, 2001).

Besides spontaneous mutations or mutations caused by chemical or physical mutagens there is also the possibility to introduce mutations via DNA viruses. It is important to notice that

1. INTRODUCTION

the connection between a viral infection and cancer can be difficult to see since there can be years between infection and cancer diagnosis. One other factor is that viral infections are only one step in developing malignancy, therefore other mutagenic influences are normally needed. Viruses can introduce genes into the cell that interact directly with cell cycle control and thereby cause unchecked cell growth. Another way virus can act as a carcinogen is by acting as a tumor promotor. One example for the first working mechanism is the group of papillomaviruses which can lead to the formation of warts or can infect the cervix and lead to cervical cancer (Frazer, 2004).

Mutations responsible for carcinogenesis cover the complete range of possible mutations from point mutations and gene introduction over chromosome rearrangement due to chromosomal instability to chromosomal imbalance. Gene mutations in cancer cells normally have two basic functions. They either activate or increase the activity of oncogenes or they inactivate the gene function in tumor suppressor genes (Bertram, 2001).

Under normal circumstances mutations can be compensated and corrected to a certain degree by several cellular repair mechanisms. But if the introduced mutations lead to permanent changes in genes responsible for cell cycle control or genes responsible for genomic integrity, cells will start to accumulate further genomic mutations which will further lead to malignancy and uncontrolled proliferation. Bypassing the control mechanisms of proliferation, the aspiring tumor cells need to acquire the following traits:

- Independence from external growth signals, either by secreting growth signals by themselves or permanent activation of proliferation pathways.

- Development of a refractory state to growth inhibiting external signals.

•   Development of resistance to apoptosis induced by external signals.

•   Overcoming cellular senescence and development of infinite proliferative capacity.

•   Securing a continued supply with nutrients by development of angiogenic potential.

If developing tumor cells acquired these traits over multiple mutations and over several generations a malign tumor develops.

1.3   Classical approaches to cancer treatment

One key factor in cancer therapy is early diagnosis. If diagnosed in an early stage, cancer treatment is significantly more effective. Cancer treatment normally consists of a combination of the following approaches:

•   Tumor resection

•   Chemotherapy

•   Radiation therapy

Since there is a great diversity in tumor behaviors and responses to treatment, the treatment regiments need to be fitted individually to every patient. Therefore the individual treatment consists of a specialized combination of the already mentioned approaches (Bertram, 2001).

1.3.1   Tumor resection

Removing malign tissue surgically is the simplest approach to treat cancer and, in form of a biopsy, can also be used for diagnosis. The removed tissue can then be used to determine the developmental stage of the tumor and the severity of the disease. Final tumor resection does not only include removal of malign tissue but also the removal of surrounding benign

15

tissue and lymph nodes. This procedure is supposed to minimize the chance of survival of small colonies of (or even single) cancer cells. If done in an early stage the risk of metastases colonizing other parts of the body can be lowered considerably. If already metastasizing surgical removal can be used as a way of tumor control (Kreth *et al.*, 2000).

1.3.2   Chemotherapy

In the context of cancer, the term chemotherapy describes the treatment of malign tumors using a variety of chemical compounds to directly attack the tumor cells. In many cancer cases, chemotherapy is not used alone but is combined with radiation therapy and tumor resection. The used compounds, so called cytostatics, normally affect cell proliferation and therefore tend to damage cells with high proliferation rates. This holds true for cancer cells but also for several benign tissues in the human body like for example hematopoietic stem cells (Bold *et al.*, 1997).

Targets for cytostatic compounds can be cellular components like the spindle apparatus or enzymes associated with DNA replication or RNA synthesis. Since the spindle apparatus, which primarily consists of microtubuli, is essential for cellular division and, this forms an ideal target for antineoplastic drugs like vinca alkaloids or paclitaxel. Both drugs affect the reorganization of tubulin monomers to microtubuli and therefore affect cellular division. Other drugs directly affect the DNA replication and introduce strand breaks or DNA mismatches and thereby induce cell death.

1.3.3   Radiation therapy

This particular form of cancer treatment can be used to treat larger areas or regions that cannot be reached by surgery easily which can be the case for metastases.

Radiation therapy is utilizing ionizing radiation like gamma, X- or beta radiation to damage malign tissues. The working principle of radiation therapy is energy transfer into the irradiated tissue causing normally neutral molecules to change into positively or negatively charged ones and triggering the formation of free radicals. This can cause double strand breaks in the DNA and can cause apoptosis (Nutting *et al.*, 2000).

1.3.4   Side effects

Classical treatment approaches share a set of common side effects like nausea, hair loss, neuropathy, immunodeficiency, tiredness and pain in bones and joints (Love *et al.*, 1989) causing a high amount of distress for patients suffering from cancer. Consequently researchers are trying to optimize cancer treatment to make it more efficient and to lower the distress caused by severe side effects. Consequently new methods of personalized therapy need to be established to provide a fast and easy way to analyze the tumor at hand and to find an optimized treatment regime for the individual patient.

The system presented in this thesis work can be used for both aspects. By analyzing tissue samples obtained from biopsy the effectiveness of the planned treatment could be tested in vitro before being administered to the patient. In addition the system could be used to provide a histological analysis of the obtained tumor sample within a significantly reduced time and without the need for immunohistochemical staining[1].

1.4   New approaches (nanostructures & tumor targeting)

The effectiveness of classical cancer treatment approaches can be limited by several factors like low selectivity of chemotherapeutic drugs, the mutagenic properties of both chemotherapy and radiation therapy (possibly causing secondary cancer outbreaks) and the

---

[1] S. Ingebrandt, A.Susloparova, X. T. Vu, D. Koppenhöfer - *Device and method for measuring biological and/or electronic properties of a sample, and uses thereof,* Application number PCT/DE2015/100040

accessibility of the tumor for surgery, therefore it is obvious that more selective approaches are needed. New approaches include the use of nanocarrier systems and solid nanoparticles coupled with antibodies which can be used for active tumor targeting and the use of antibodies for immune modulation or vaccination are currently under investigation.

1.4.1   Immune modulation

Several approaches are currently under development to activate and modulate the human immune system and use it to attack cancers (Kottke *et al.*, 2011). Although cancer cells are not comparable to other pathogens in terms of immunogenicity, the immune system is still able to identify and attack tumor cells. However tumors frequently hinder an efficient immune response, the challenge is to develop strategies that augment antitumor responses. The possibility of using the human immune system is implied by both spontaneous tumor regressions in immune competent hosts and increased cancer incidence in immune compromised patients. Growing tumors can trigger cells of the innate immune system as a consequence of disturbances of their surrounding microenvironment. Under ideal conditions this will lead to inflammation and thereby trigger an adaptive immune response. But progressing tumors are often able to avoid detection using complex strategies like exclusion of immune cells from tumor sites or others (Blattman & Greenberg, 2004). The activation of the inherent immune response is one of many new approaches to cancer treatment with guiding and activating T cells being only one possible way to go necessitating approaches to effectively study T cell migration and adhesion (Law *et al.*, 2014).
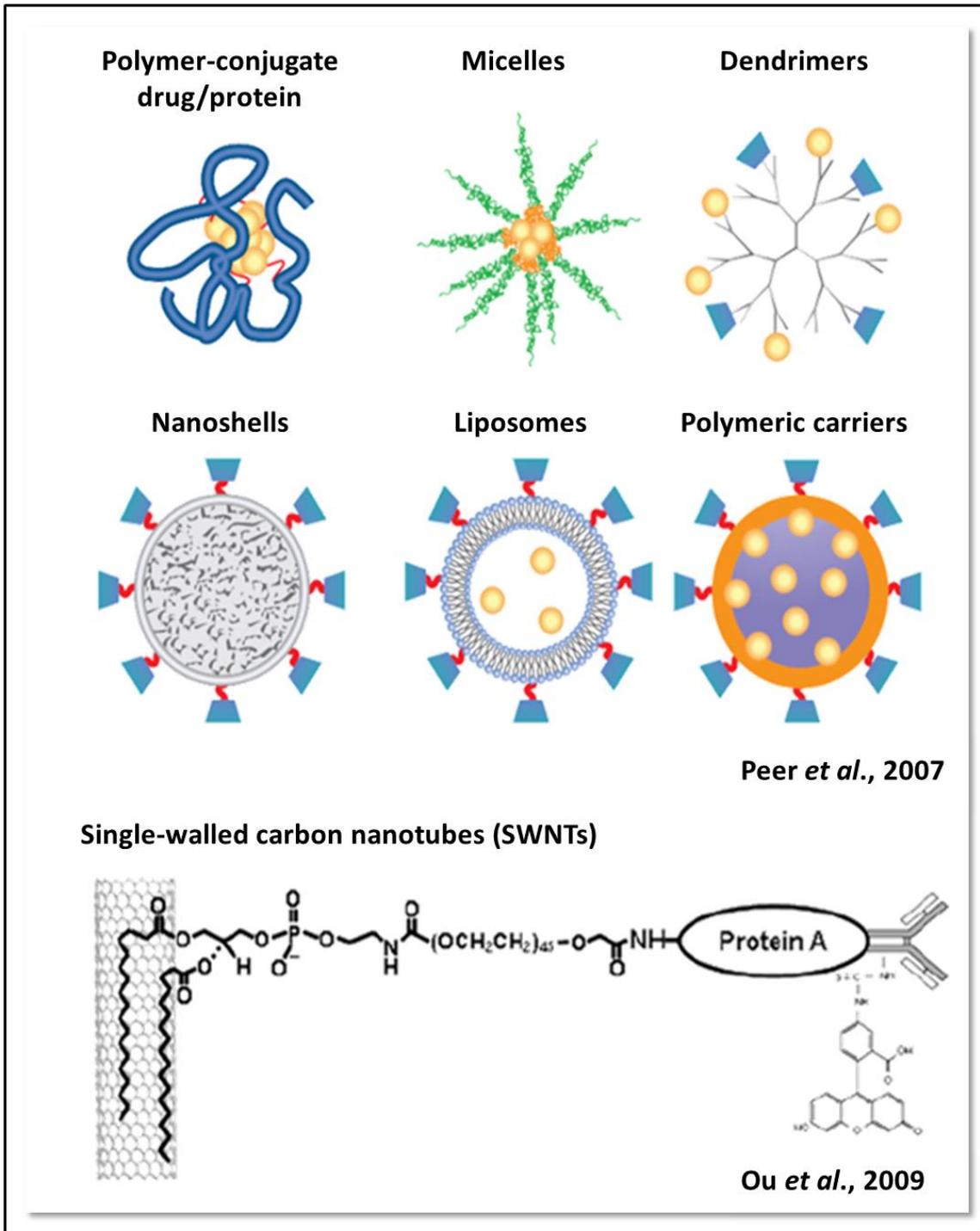
Fig. 8: Nano structures commonly used as carrier devices in cancer research and therapy (Ou et al., 2009)

Nano structures can be used for cancer diagnosis and therapy, becoming conjugated or loaded with therapeutic agents or targeting structures like antibodies for active tumor targeting

1.4.2   Nanostructures for cancer targeting

Another possibility for cancer treatment is the use of advanced nanomaterials (usually in the range of 1-100 nm diameter), either as antineoplastic compounds on their own or as drug

19

delivery systems (Brigger *et al*., 2002; Brannon-Peppas & Blanchette, 2004; Peer *et al*., 2007; Ou *et al*., 2009). The most common nanocarrier platforms include polymer conjugates and polymeric nanoparticles, lipid-based carriers (liposomes and micelles), dendrimers, carbon nanotubes and gold nanoparticles (including nanoshells and nanocages, see fig. 8).

These nanocarriers can be used to increase local drug concentration by releasing the loaded antineoplastic drugs in a controlled manner when bound to their targets. Such nanostructures can be used for tumor treatment and imaging via passive and active tumor targeting, with passive targeting off course being the easier way. This passive targeting can be done by using the enhanced permeability and retention (EPR, see fig. 9) effect which is characteristic for a large number of solid tumors.

 If fast growing tumors reach a certain size it is essential for them to induce angiogenesis to insure the accessibility of nutrients. This fast and artificial induced angiogenesis leads to higher permeability of the newly formed blood vessels and thereby makes it easier for nanoscale platforms to reach the tumor. In addition to a higher permeability of newly formed blood vessels it has been shown that tumors have a much lower lymphatic drainage then benign tissue. Combined with the aforementioned high permeability this leads to an easy accumulation mechanism in solid tumors since particles carrying compounds can enter the malign tissue passively but cannot be easily removed, thereby leading to longer exposition to the used particle and compound. Passive targeting approaches, while promising, are limited by factors like diffusion capability of the transported compound and problems controlling drug release. Such a lack of control might lead to multi drug resistance in tumor cells. If this occurs, a tumor cell starts to overexpress transport proteins to expel chemotherapeutic drugs causing chemotherapy to become ineffective.

Enhanced Permeability and Retention effect (EPR):
- General features of tumours (e.g. leaky blood vessels, poor lymphatic drainage) lead to extravasation of nanocarriers into the tumour tissues via leaky vessels.
- Increased permeability of blood vessels in tumours is characteristic of rapid and defective angiogenesis.
- Dysfunctional lymphatic drainage in tumours retains accumulated nanocarriers and allows the release of drugs into the vicinity of the tumour cells.

Fig. 9: Passive tumor targeting via the Enhanced Permeability and Retention effect (EPR, Peer et al., 2007):

Tumor induced angiogenesis normally leads to the formation of blood vessels with less dense cell layers, leading to higher permeability of the blood vessel. Coupled with relatively poor lymphatic drainage this allows for the passive accumulation of antineoplastic compounds delivered by nanocarriers inside of the tumor where the drug can then be released.

Active tumor targeting can be achieved by coupling the nanoparticle with tumor specific ligands to achieve specific localized effects. This is possible due to the high surface to volume ratio of most nanoscale structures which makes ligand binding highly effective (McDevitt *et al.*, 2007).

Targeting agents can be all types of molecules that can be specifically recognized by receptor proteins and are normally chosen from antibodies (which cannot just be used for targeting but also as chemotherapeutical compounds themselves), nucleic acid fragments, peptides, vitamins or carbohydrates. It is imperative that these ligands bind with high selectivity to highly expressed tumor specific surface markers. Monoclonal antibodies are the most

promising molecules for tumor specific targeting with several already approved for treatment like Rituxan or Herceptin. Both compounds consist of a monoclonal antibody which can be used for the treatment of non-Hodgkin's lymphoma or breast cancer respectively.

The most commonly used materials for the construction of nanoscale drug delivery systems are polymers like polylactic acid, chitosan or collagen. These polymers can be used to encapsulate chemotherapeutic drugs without further modification and later on release them in a controlled manner via surface erosion or diffusion.

1.5   Neurodegenerative diseases and oxidative stress

Dementia and neurodegenerative diseases in general are among the big medical challenges of our time with Alzheimer's, Huntington's and Parkinson's disease among the most common forms of dementia. 4.5 million people were diagnosed with Alzheimer's disease in the United States in the year 2000 alone. In both Alzheimer's and Parkinson's disease, signs of oxidative stress mediated damages can be found but the connection remains a topic of debate.

1.5.1   Alzheimer's and Parkinson's disease

Neurodegenerative diseases like Alzheimer's or Parkinson's disease are amongst the most common forms of dementia with 4.5 million people diagnosed with Alzheimer's disease in the United States alone (Hebert *et al.*, 2003).

Alzheimer's disease is a neurodegenerative disorder predominantly of the cerebral cortex which is clinically characterized by progressive mental deterioration, severe personality changes and memory loss. Memory loss in Alzheimer's disease can be divided in two categories, namely the early loss of episodic memory and the late loss of short-term and

working memory. Most reports can be characterized as late onset or sporadic forms of Alzheimer's disease; although early onset forms with a potential genetic background also exist (Behl, 1999).

Alzheimer's disease can be histologically characterized by the presence of neurofibrillary tangles (helical filaments consisting of tau protein) and amyloid β plaques in affected tissues leading to an ongoing sequence of degenerative changes (see fig. 10). The deposition of amyloid β is a major focus of research and is widely viewed as the central disease causing and promoting event in Alzheimer's disease. This view is strongly supported by the fact that the majority of mutations associated with Alzheimer's disease are connected to an increase of amyloid β production (Behl, 1999).

Parkinson's disease is an age related neurodegenerative disorder that affects roughly 1 million persons in the United States of America alone characterized by resting tremors, rigidity slowness or bradykinesia, gait disturbance and postural instability (Olanow and Tatton, 1999). The disorder is correlated to the degeneration of dopaminergic neurons in the substantia nigra pars compacta and the presence of intracytoplasmic inclusions known as lewy bodies (Olanow and Tatton, 1999, see fig. 11). These histological signs of Parkinson's disease can also be found in other parts of the nervous system, e.g. the locus ceruleus, nucleus basalis, hypothalamus and several peripheral components of the autonomic nervous system.
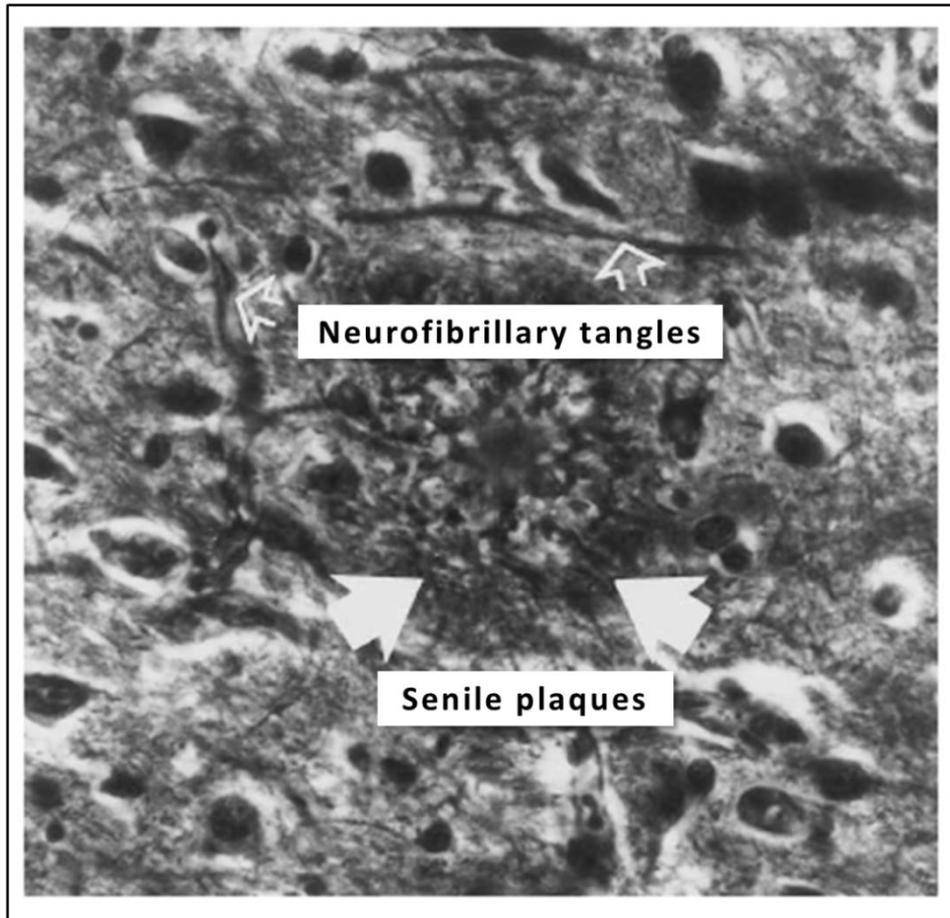
Fig. 10: Microscopic picture of neuronal tissue of an Alzheimer's disease afflicted patient (Behl, 1999)

Alzheimer's disease can be histologically characterized by the presence of neurofibrillary tangles (helical filaments consisting of tau protein) and amyloid β plaques leading to an ongoing sequence of degenerative changes.

Comparable to Alzheimer's disease, one can differentiate between early onset forms and late onset or sporadic forms of Parkinson's disease with the latter being influenced by several risk factors like exposure to herbicides or pesticides, cyanide or carbon monoxide, etc. Only 5 to 10 % of patients afflicted with Parkinson's disease are reported to have a familial form of Parkinsonism showing an autosomal-dominant heredity transmission (Olanow and Tatton, 1999).

One common important contributing factor in such neurodegenerative diseases is an observed elevated level of oxidative stress in afflicted tissues caused by reactive oxygen

species (ROS). Although the post mortem analysis of brain tissues of persons affected by Alzheimer's or Parkinson's disease were showing increased signs of oxidative stress induced damage (Behl, 1999; Andersen, 2004), the connection is not completely understood, making it unclear if oxidative stress damage is a possible cause or a symptom of such disorders.
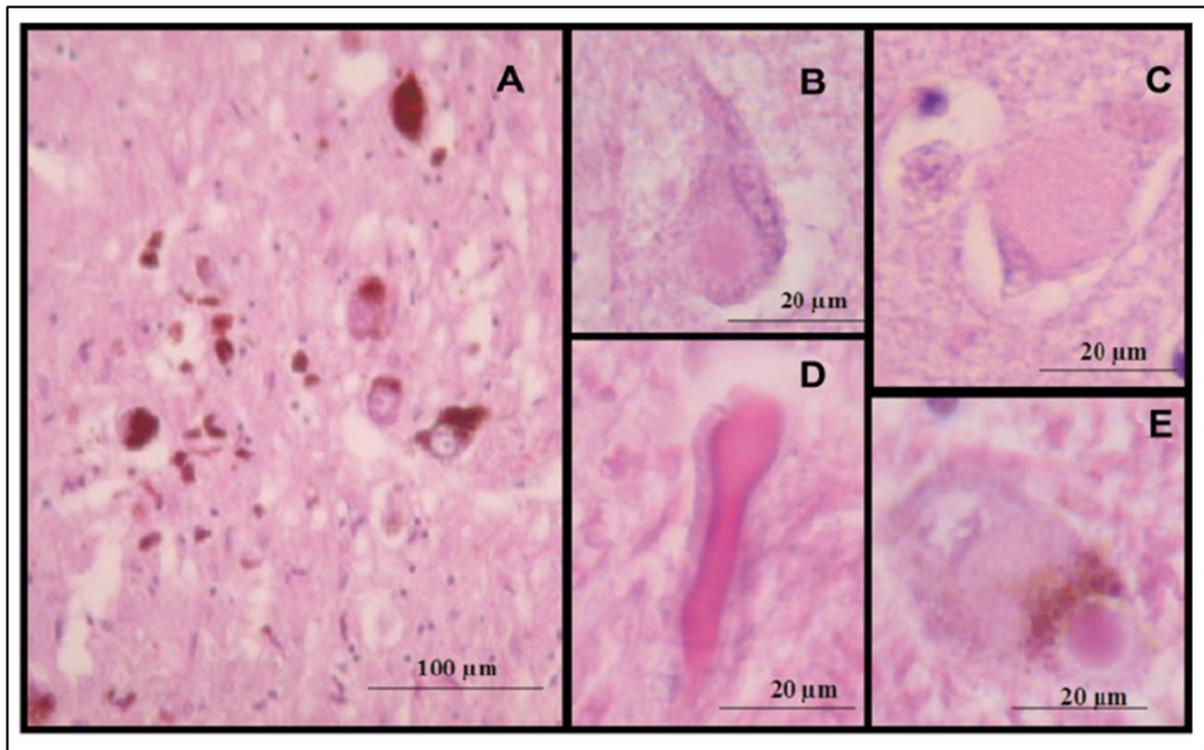
Fig. 11: Histological analysis of neuronal tissue of a Parkinson's disease afflicted patient (Zarranz et al., 2003):

a)   **Neuronal loss, secondary spongiosis, and pigment laden macrophages observed in the substantia nigra**
b)   **Concentric Lewy body in the cingular cortex**
c)   **Nonconcentric Lewy body in the cingular cortex**
d)   **Atypical elongated rod-like Lewy body in the pontine tegmentum**
e)   **Classic Lewy body in the locus caeruleus**

1.5.2   The Role of oxidative stress in neurodegeneration

Oxygen is essential for all eukaryotic cells to keep their metabolism up and thereby stay alive but it can also damage cells beyond repair if converted to reactive oxygen species (ROS). Such reactive oxygen species like hydrogen peroxide (H_2O_2), hydroxyl radicals or superoxide are generated during metabolism and are normally kept in check via various detoxification processes in the cell. Detoxification of ROS can be achieved via various enzymatic steps using

enzymes like catalases, superoxide dismutase or glutathione peroxidase and reductase to avoid lasting damage to essential components of the cell. Reactive oxygen species can cause significant oxidative stress for affected cells and thereby can cause a variety of detrimental effects.

Oxidative stress has been implicated as a contributing factor to several neurodegenerative disorders like Alzheimer's or Parkinson's disease due to signs of significant oxidative damage in brain tissues of patients afflicted with these disorders. Because of the relatively low antioxidant levels, low regenerative capacity and high oxygen consumption of neuronal tissue, a relatively high susceptibility is not surprising. The damaging effects of oxidative stress range from lipid peroxidation, enzyme impairment, protein modification to mutations (Barnham *et al.*, 2004) and apoptosis (Harrison *et al.*, 2005) induction. Lipid peroxidation can lead to the accumulation of HNE (4-hydroxyl-2,3-nonenal), inducing toxicity by crosslinking amino acids like cysteine, lysine and histidine. Chemical alteration of the DNA caused by ROS can lead to mutations unbalancing the metabolism, signaling and cell cycle control of afflicted tissues possibly leading to apoptosis induction. One example of misbalanced signaling can be found in both Alzheimer's and Parkinson's disease. Excessive production of ROS can ultimately lead to severe dysregulation of intracellular calcium signaling, possibly leading to an excitotoxic response caused by an ROS-induced calcium influx ultimately leading to apoptosis induction (Barnham *et al.*, 2004).

Damaging effects of oxidative stress also include protein modification (e.g. carbonylation and nitration) and misfolding leading to impaired degradation and thereby possibly contributing to the formation of tau protein and amyloid β plaques (Andersen, 2004) tightly associated with Alzheimer's disease. In addition to these effects, oxidative stress can also lead to mitochondrial damage leading to reduced ATP generation (Andersen, 2004).

1.6   Impedimetric biosensor applications

Impedimetric biosensors are promising tools for biomedical analysis. They allow for easy and fast computation of signals, making the ideal platforms for diagnosis and scientific analysis of diseases and functional disorders. Impedimetric biosensors can be counted among the group of affinity biosensors, with impedance spectroscopy being only one of a few physical approaches for the measurement of an analytical signal in real time (Ramanavièius *et al*., 2005).

Impedance spectroscopy is a versatile readout technique usable for a variety of sensor types, having already been successfully used for DNA analysis (Uslu *et al.*, 2004, Ingebrandt *et al.*, 2007), nicotine and histamine recognition via molecularly imprinted polymer (MIPs) sensors (Peeters *et al.*, 2013) or the detection of immunoreactions (Broeders *et al*., 2011). Gold electrodes are the most common sensor type used for impedance spectroscopy, having been used for bacteria detection (Varshneya *et al*., 2009), cellular adhesion measurements (Giaever and Keese, 1991) and for toxicity measurements (Curtis *et al*., 2008). Cell adhesion studies using metal electrodes are based on the principal that cells attach and spread on the electrode surface, thereby altering the effective area available for current flow causing an increase in the impedance of the system (Giaever and Keese, 1991). This technique has been used to study locomotion and can thereby generate new insights in processes like tissue formation our wound repair.

In recent years metal electrode based sensors have been used for several applications, among them being drug testing using 3-dimensional spheroid cultures (Kloß *et al.*, 2008), detection of bacterial cells using interdigitated array microelectrodes (IDAMs, Varshney *et al.*, 2009). In the first case interdigitated electrodes have been used as a means to study the

behavior of suspended tumor spheroids, which act as a model for tumor tissue *in vivo*. Varshney *et al.* (2009) or Alexander *et al.* (2010) indicate a general trend for metal based electrodes with an interdigitated design.

In the scope of this thesis another sensor type for impedance spectroscopy, the field-effect transistor is presented and applied to cellular adhesion measurement, cell toxicity analysis and oxidative stress response investigation. The presented device has possible applications in a variety of research fields such as rapid screening of antineoplastic drugs, analysis of oxidative stress response in neurodegenerative diseases and cancer diagnostics and histological tumor assessment.

1.7   Field-effect devices as possible platforms for pharmacological testing

1.7.1   Field-effect devices in research

Field-effect devices are a novel tool in biomedical research already in use for a variety of different research fields that are connected to cancer research. This includes nucleic acid detection (Uslu *et al.*, 2004), nucleotide polymorphism detection (Ingebrandt *et al.*, 2007), measurement of electrical cell-substrate impedance sensing (ECIS, Schäfer *et al.*, 2009; Lin *et al.*, 2010) or the detection of cancer associated proteins (Kim *et al.*, 2009).

In regards to cancer diagnosis the detection of tumor associated proteins via field-effect devices is another topic of major interest. In 2009 Kim *et al*. were able to show a discernible difference in prostate specific antigen (PSA) levels in human serum using carbon nanotube field-effect transistors (CNT-FETs). By using this specific type of sensor the authors were able to lower the detection limit of PSA to a protein concentration of 1.0 ng/ml.

One major research focus lies in the field of cell adhesion studies to monitor the effect of pharmacological compounds. Using the ability of cells to attach to various surfaces as an

indicator for their general viability, this method can be used as a fast cytotoxicity assay. The use of metal electrode systems is already established as a standard method in this particular field. Apart from the established ECIS method the use of FETs can improve the lateral resolution of impedimetric measurements to analyze cell adhesion on single cell level. Due to the intrinsic properties of these FETs binding events of cells or changes in the electrolyte composition can be monitored as variations of the drain-source current. In 2007, Ingebrandt *et al*. reported about the use of impedance spectroscopy with FET arrays to characterize the coupling of eukaryotic cells to transistors. In their work a 16-channel readout system was developed, which is able to provide a simultaneous, lock-in based readout by applying a test signal of known amplitude and phase via a reference electrode. The resulting frequency spectrum was then used for the investigation of the surface adhesion of individual HEK293 cells (Human Embryonic Kidney cells). A similar approach using organic electrochemical transistors (OECTs), a subtype of organic thin-film transistors (OTFTs) for cell-based biosensor applications was published by Lin *et al*. in 2010. The conductivity of the active layer of OECTs can be modulated by the gate voltage induced drift of cations between the electrolyte and the organic semiconductor film. The authors were the first to report a cell-based biosensor based on OECTs using PEDOT:PSS as the active layer. These particular OECTs were shown to have a stable performance under cell culture conditions with high biocompatibility to cancer cells (human esophageal squamous epithelial cancer cell line KYSE30) and fibroblasts. The OECTs proved sensitive to changes in surface charge and morphology of adherent cells and is therefore an interesting tool for further research.

1.7.2   Impedance sensing in cancer research

As mentioned before the therapy of cancer is a complicated and difficult process with only limited success depending on the type of cancer and its stage of development. Therefore the

1.   INTRODUCTION

need to develop new treatment approaches is big. Going hand in hand with the need to develop new agents and strategies is the need to test these agents and treatment approaches in a quick and efficient manner. Electric biosensors using impedance measurements to analyze cell reactions to drug treatment are promising tools to help further our understanding of chemotherapy and to optimize cancer treatment. Electrical impedance is the measure of the opposition that a circuit presents to the passage of a current when a voltage is applied. In quantitative terms, it is the complex ratio of the voltage to the current in an alternating current (AC) circuit.

Several systems working with impedance measurements are already commercially available (see fig. 12) with the ECIS (Electric cell-substrate impedance sensing) system being the most prominent. This system was the first commercial impedance system usable for the development of cell-based assays.

Using special culture dishes outfitted with metal electrodes in the range between 25 to 250 µm in diameter the system measures the AC impedance of cell-covered electrodes. The cells behave like dielectric particles due to the insulating properties of the cell membrane which leads to an increase in impedance when the coverage of the electrodes increases. If cell shape and electrode coverage change over time, for example due to treatment with antineoplastic or cytotoxic compounds, the impedance changes as well.

Fig. 12: Commercially available cell impedance measurements systems:

a) **ECIS system by Applied biophysics**
b) **96 well plate with incorporated metal electrodes**
c) **CellKey system by Molecular Devices**
d) **xCelligence system by Roche**

By recording time-resolved impedance measurements the influence of pharmacological compounds can be analyzed (Giaever & Keese, 1991 & 1993). Newer systems, like the xCelligence system from Roche or the Cellkey system from Molecular devices work in a similar manner by measuring electrode impedance across metal electrodes integrated into the culture plate and can be used to analyze the effects of different compounds on cellular adhesion (Urcan *et al.*, 2009; Scott & Peters, 2010; Fang, 2011).

In the specific context of cancer research electrode based biosensors have already been tested in the field. In 2010 Alexander *et al.* described a measurement system using interdigitated electrodes to impedimetrically monitor the environment of carcinoma cells.

Kloß *et al.* used a sensor platform consisting of microcavities with a width in the range of 200 to 400 µm (Kloß *et al.*, 2008). During this study the apoptosis inducing effect of

Camptothecin was studied using human melanoma spheroids. Tumor spheroids in general can be used as a model for tumor behavior *in vivo* due to their more complex structure mimicking the structure of 3-dimensional tissues much closer than *in vitro* cell cultures.

Impedimetric measurements can also be done using open gate FETs, which were initially developed to record spontaneous electrical activity from electrogenic cells (Offenhäusser *et al.*, 1997). This approach has one major advantage over metal electrode setups since the transistors can be constructed in much smaller scales and can reach sizes below 20 µm making single cell analysis easier.

1.7.3   Field-effect transistors

Transistors are semiconductor devices functioning as a variable resistor, which can be used to either switch or amplify a signal by controlling the transistor current via an electric voltage.

The FETs in this work were open-gate p-channel-type transistors with source and drain regions being p-doped (containing electron holes) on an n-type silicon substrate (Ingebrandt *et al.*, 2007; Poghossian *et al.*, 2009, see fig. 13). A conducting channel between these two normally separated regions can be established by a controlled electrical field at a third contact called the gate. The controlling gate contact is separated from the channel by a resistive silicon-dioxide barrier. Instead of the metallization at the gate area used in MOSFETs (Metal- Oxide-Semiconductor FET) the ISFET's (Ion Sensitive FET) gate area is in contact with an electrolyte solution (open-gate FET).

By applying a gate voltage via a reference electrode the concentration and mobility of the charge carriers in the channel region are changed forming the conducting channel. Once voltage between drain and source (V_{DS}) is applied, a conductive path for the drain-source

current (I_{DS}) is created. Field-effect transistors can be operated in depletion or enhancement mode. In depletion mode all mobile charge carriers have been forced away leaving a depleted carrier free region. In enhancement type FETs charge carriers are attracted to the gate region when a negative voltage is applied to form a conducting channel.
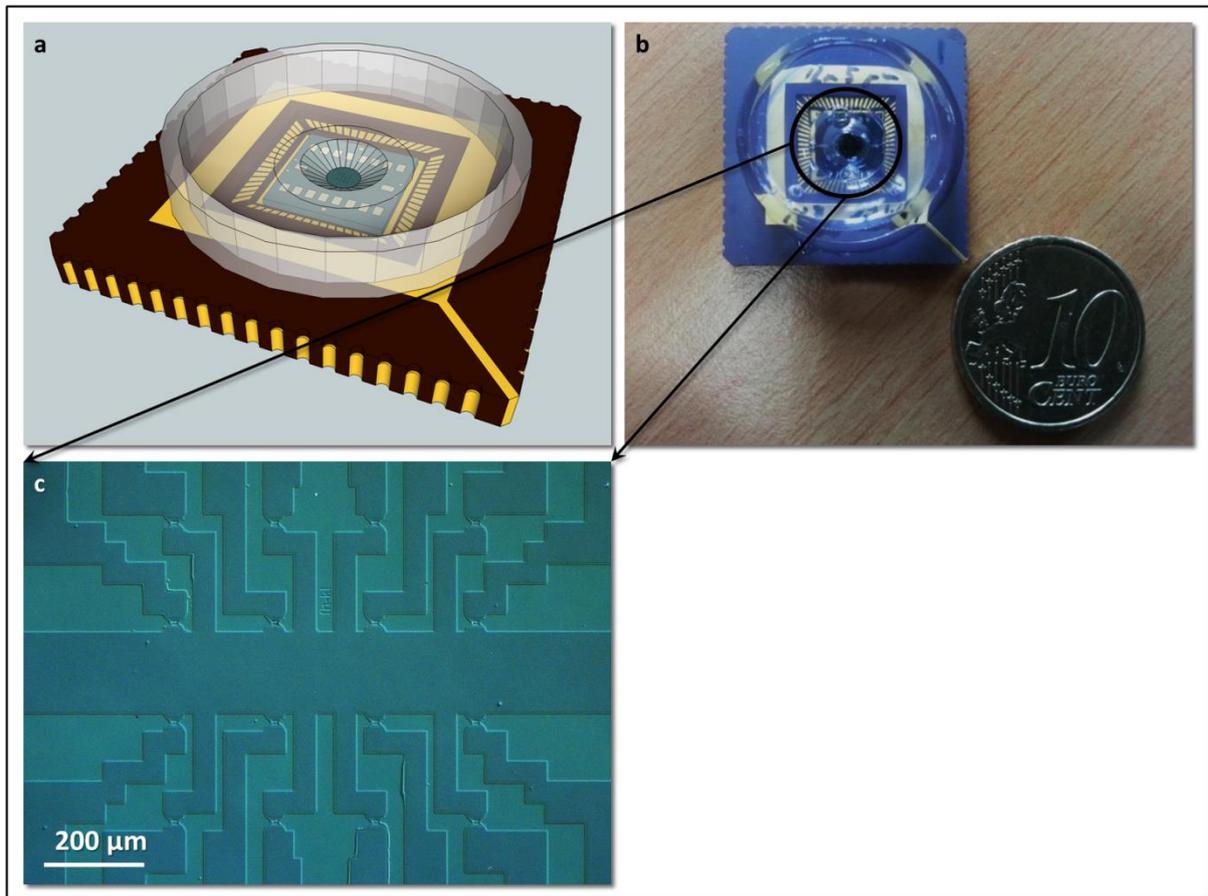
Fig. 13: Field-effect transistor platform used during this thesis:

    a)   **3D model of a fully encapsulated field-effect transistor chip**
    b)   **Encapsulated FET**
    c)   **Transistor array surface of the used chips**

Depending on the applied voltage, FETs can be operated in cut-off or sub-threshold region, linear region or saturation region. In the cut-off region, the gate-source voltage V_{GS} is smaller than the intrinsic threshold-voltage V_t, which is the minimum voltage required to open a channel, resulting in no gate-source current due to no conduction between the drain and source. In the linear region V_{GS} is larger than V_t while V_{DS} is smaller than the difference between V_{GS} and V_t. This allows a current to flow between drain and source. The saturation

region is characterized by V_{GS} being larger than V_t and V_{DS} being larger than $V_{GS} - V_t$ which

leads to an asymmetrical shape of the conducting channel.

FETs are characterized by the following parameters (see fig. 14):

- Output characteristics: I_{DS} (V_{DS}) measured with constant V_{GS}

- Transfer characteristics: I_{DS} (V_{DS}) measured with constant V_{DS}

- Transconductance: g_m (V_{GS}) measured with constant V_{DS}

The transconductance g_m describes the change of the drain-source-current I_{DS} in regard to

the applied gate-source-voltage V_{GS} at constant V_{DS}.
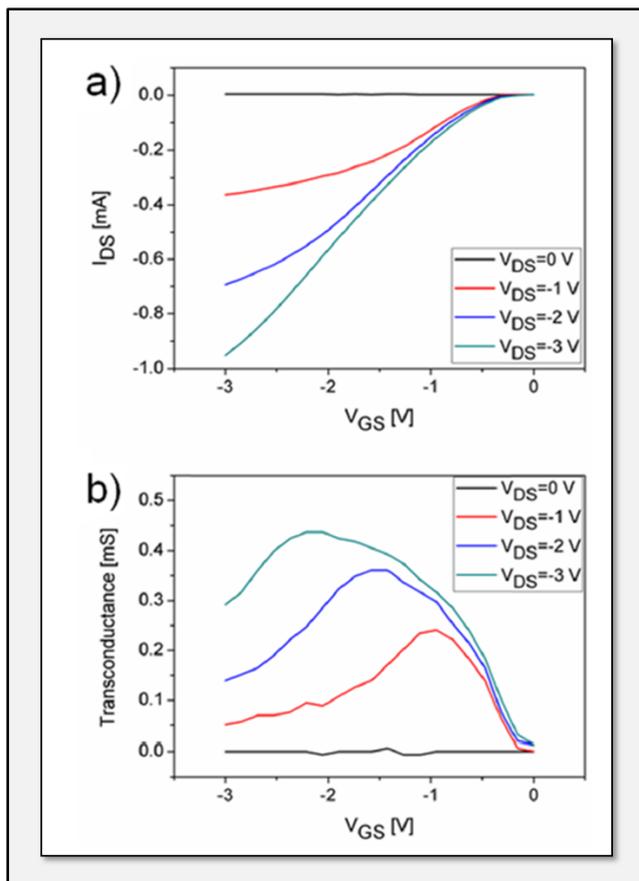
Fig. 14: Transfer characteristics (a) and transconductance (b) of quasi-planar open gate ISFET (graphs taken from Susloparova et al., 2015)

1.7.4   Impedance spectroscopy and transistor-transfer function measurement using field-effect transistors

The normalized transfer function H (see fig. 15b) is the mathematical representation of the relation between the output voltage and the input voltage of an electrical system comparable to a circuit of passive resistors and capacitors. Cell adhesion properties can be monitored by the capacitive changes or impedance changes an adherent cell causes on the gate area of an ISFET in the voltage applied to that gate.

The impedimetric measurement to analyze cell adhesion is based on the fact that attached cells act as insulating particles, which constrain the current flow between the reference electrode and the electrolyte solution. In this case the cell membrane can be approximated as a resistor and capacitor in parallel with the cell creating a cleft between the gate and its membrane. This gap is filled with the electrolyte solution surrounding the cell and acts as a resistor forcing the current to flow either through the cell or through the cleft.

Cell adhesion on top of the transistor surface is facilitated via focal contact points. Only at these points the cell membrane will be in contact with the underlying transistor surface, leaving the rest of the cell membrane free. At these focal points integrin molecules act as the mediators of cell adhesion to the surface below. Since the surface of a transistor gate is covered by a chemically stable SiO_2 layer the surface has to be made hydrophilic, thereby allowing the coating of the surface with additional proteins to facilitate cell adhesion. This can be done for example by treating the surface with hot sulphuric acid, thereby creating silanol groups on the transistor surface on which proteins like poly-D-lysine or fibronectin can be layered as contact points for the cell membrane (Yavin and Yavin, 1974; McKeehan and Ham, 1976).

The coupling of the cell and transistor can be modelled as an electrical circuit of passive resistors and capacitors. Modeling of an electrically equivalent circuit (EEC, see fig. 15a) and the cell was done by Susloparova *et al.* in 2014 [2] in order to find interpretations for the time constants, relating them to physical elements which can be described mathematically. C_{M1}/R_{M1} and C_{M2}/R_{M2} represent the capacitance and resistor of the free and cleft membrane, r_i represents the resistance inside the cell. For the current passing the cleft, the cleft resistance is shown as R_{seal}. C_{OX} stands for the oxide capacitance of the gate.

a   Schäfer et al., 2009

$$H(jw) = R_{feedback}g_m * \frac{1}{\sqrt{1+(\frac{f}{f_g})^2}} * \frac{1+jw(C_M R_{seal} - \frac{C_L}{g_m}) - w^2 \frac{C_L R_{seal}}{g_m}(C_M + C_{ox})}{1+jw(R_{seal}(C_{ox}+C_M)+R_{el}(C_L+C_{ox})) - w^2 R_{seal}R_{el}(C_L(C_{ox}+C_M)+C_{ox}C_M)}$$

b   Susloparova et al., 2014
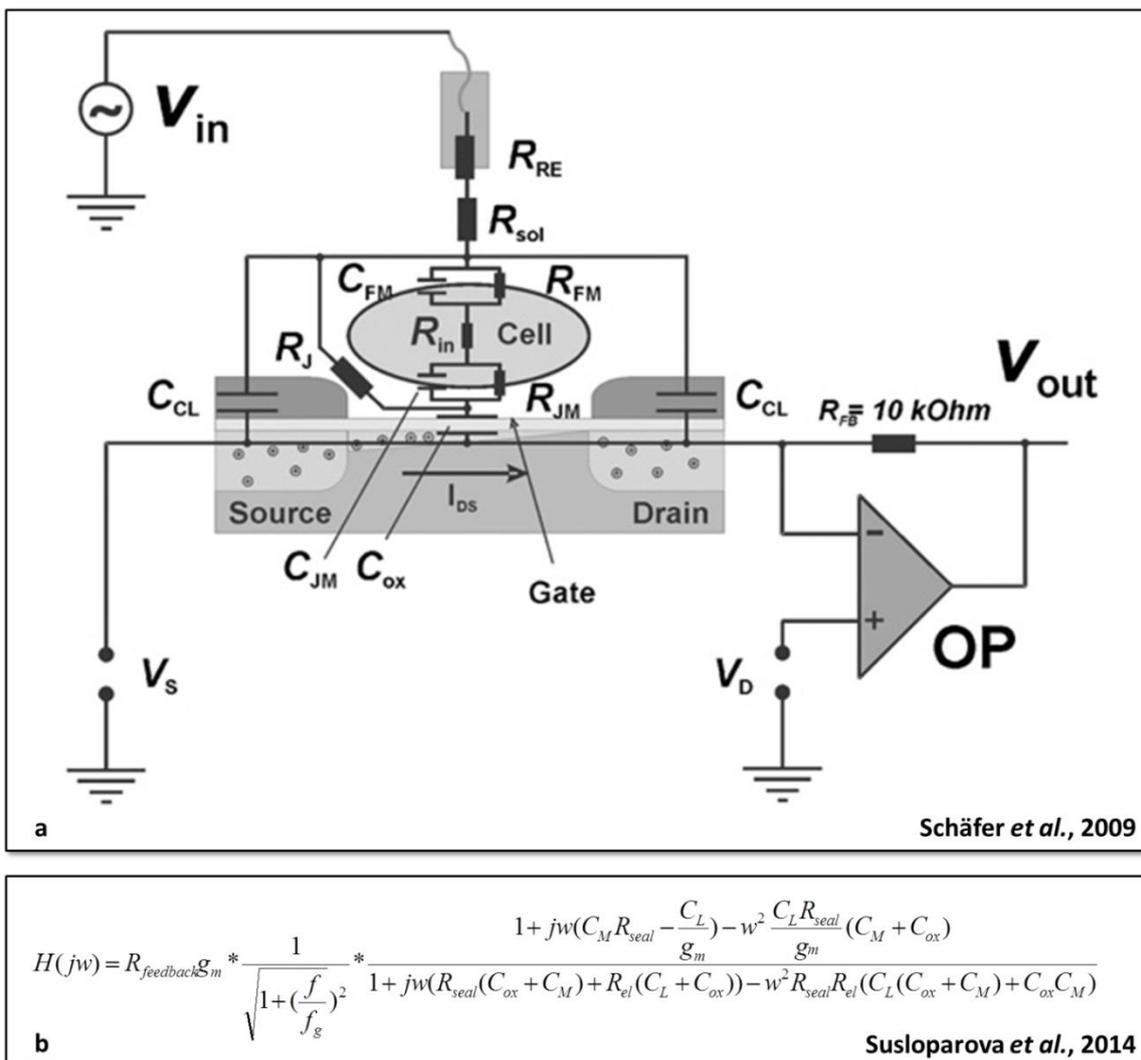
Fig. 15: Physical description of the cell-transistor contact

   a)   **electrically equivalent circuit (EEC, Schäfer *et al.*, 2009)**
   b)   **Transistor transfer function equation used for modelling the cell transistor contact (Susloparova *et al.*, 2014)**

The cell membrane acts as an efficient insulator, which means the membrane resistances R_{M1} and R_{M2} can be neglected in a first approximation. The inner cell resistance r_i is also very small and therefore can also be neglected. This reduces the gate input to the oxide capacitance and the seal resistance in parallel with the membrane capacitance. The various elements of the electrically equivalent circuit have different effects on the transfer function. The gate capacitance C_{OX} has a big influence on the transfer function. By increasing the size of the transistor gate or decreasing the thickness of the gate oxide the transfer function gets shifted towards lower frequencies, which leads to a steeper curve. The conducting line capacitance C_L affects the transfer function curve opposite to the gate capacitance. If the seal resistance is increased, it will lead to a shift of the low pass cut-off point towards lower frequencies and a decreased membrane capacitance C_M will result in a steeper curve shape in the transfer function (Susloparova *et al.*, 2015).

1.7.5   Possible applications in pharmacology, cancer research and diagnostics

Because of their promising characteristics, FETs can be considered as a promising tool for future pharmacological research. Being able to be downscaled to a size clearly below 20 µm, FETs can be used for high resolution studies of cellular adhesion to analyze the effects of chemical and physiological stimuli on single cell level while simultaneously analyzing potential pH changes in the surrounding medium.

In addition to the high lateral resolution provided by FETs, their flexibility and ability to be operated in real-time under cell culture conditions allow for possible applications as a versatile tool for high-throughput studies concerning the analysis of new pharmacological compounds.

1. INTRODUCTION

The possible applications for field-effect devices in cancer research are focused on rapid screening (Kim *et al.,* 2009; Huang *et al.*, 2013) and diagnostics (Mohanty *et al.*, 2014).

One topic of current research is the detection of Prostate Specific Antigen (PSA) as a method for early detection of developing malignancy of the prostate. Field-effect transistors are one promising tool for rapid detection by immobilized PSA antibodies. Huang *et al.* proposed an approach using polycrystalline silicon nanowire field-effect transistor (poly-Si NWFET) as a biosensor (Huang *et al.*, 2013). A similar approach was used by Mohanty *et al.* in 2014, where a breast cancer marker was detected by immobilized CA15.3 antibodies. Nanowire transistors have also been used for the analysis of electrical charge variations of cancer cell membranes, which act as a measure of their grade of invasion (Abdolahad *et al.*, 2014). In this particular study the nanowires were grown in a skein structure thereby creating a large and highly sensitive surface for measurements thus enabling the measurement of negative charges of the cell membrane of different metastatic grades of colon cancer.

Immune modulation has already been described as one approach for modern cancer treatment. Connected to this concept is the targeted migration and activation of T cells to stimulate the immune system to actively recognize and remove malign cells from the organism. The presented system has been used in research projects in our group to analyze the movement of cytotoxic T lymphocytes (CTS) on top of pre-coated surfaces (Law *et al.*, 2014). Via impedance spectroscopy the adhesion strength of individual CTS to different target proteins could be measured and compared providing a possibility for fast analysis of T cell interaction and migration on single cell level.

1.8   Scope of this work

In the scope of the present thesis possible applications of a novel FET-based measurement system in pharmacological research was analyzed. For this purpose on-chip cell culture protocols for various histologically and morphologically different cell lines and primary tissues were to be established for impedimetric studies using the proposed FET system for ECIS measurements (FETCIS). Since this thesis exploring possible applications for the proposed system in future research, it is also meant to reveal its possible short comings. To this end the following three subprojects were conducted.

1.8.1   Impedimetric detection of cell adhesion of confluent and low density cell cultures on ISFET surfaces

The first subproject of this thesis is aimed at analyzing the cellular adhesion of morphologically and histologically different cell lines to compare their respective impedance spectra and identify possible unique characteristics between the individual cell types. This experimental concept will demonstrate the general applicability of the proposed system to differentiate between individual cells of heterogeneous tumor samples.

Additionally low density cultures were used to further analyze the cell culture requirements for the detection of the adhesion of individual cells using field-effect transistors. This was done to determine if the proposed system is able to measure the adhesion of individual cells in an efficient manner and thereby can be used to monitor the adhesion of cell types not normally growing in confluent cell layers such as neuronal tissues or leukocytes.

1.8.2   Impedimetric analysis of the nanotoxicity of the industrial nanoparticle NexSil20

During the second subproject the toxicity of an industrial silica nanoparticle with a diameter of 20 nm was assessed using the proposed FET system to monitor toxic effects in real time under cell culture conditions. The toxicity of the used particle was already described by Prof. Dr. Roland Stauber of the department of Molecular and Cellular Oncology of the University Medical Center, Mainz (Germany), who also provided the particles used in this study.

By analyzing the toxicity of an already described particle type using real-time impedance monitoring, the applicability of the proposed system in pharmacological research was to be substantiated further in addition to the first subproject.

1.8.3   Impedimetric analysis of neurodegeneration caused by oxidative stress in primary neuronal tissues

The third and final subproject is supposed to show the applicability of the proposed measurement technique in conjunction with a specially designed parallel-culture setup to simultaneously monitor the reaction of primary neuronal tissue to external stimuli. In this case the primary cells obtained from the subventricular zone of postnatal BALB/c mice were exposed to hydrogen peroxide to induce oxidative stress and thereby apoptosis. Analyzing the effects of hydrogen peroxide toxicity in neuronal tissues is supposed to verify if the proposed system is capable of monitoring toxic effects in such delicate tissues as neurons and glia cells opening up research applications in Alzheimer's and Parkinson's disease.

2.   MATERIALS AND METHODS

2.1   Used Chemicals and Devices

A complete list of all used chemicals, cell culture media, supplements and devices used in this work can be found in the appendix.

2.2   Cell Culture Protocols

2.2.1   Cell Culturing

All used cell lines were grown in their respective standard culture mediums with supplements adjusted to their respective standard protocols. Incubation was done at 37°C and 5 % CO_2.

Primary subventricular zone (SVZ) cells used in this work were obtained via dissection from 1-4 days old BALB/c mice, which was done by Felix Kettenbaum (Enteric Nervous System Working Group, University of Applied Science, Kaiserslautern).

2.2.2   Passaging and Subculturing

Subculturing for all cell lines followed the same basic protocol with derivations explained in the respective paragraphs describing the used cell lines. All cells were grown till they reached between 90 and 95 % of confluence and were then split via trypsinisation in a ratio of 1:10. Before trypsinisation the cell culture medium was removed and the cells were rinsed with phosphate buffered saline (PBS, pH 7.4). After rinsing the PBS was discarded and the cells were removed from the cell culture flask surface via trypsinisation using 2 ml of 0.5 % Trypsin/EDTA and incubation at 37°C at 5 % CO_2. Cellular detachment was monitored microscopically and did not exceed 5 minutes. Trypsinisation was stopped by the application of 4 ml of fresh medium to inhibit the Trypsin and the cell suspension was transferred to a

15 ml falcon (Greiner Bio-One, Germany) for centrifugation (5 min. at 1000 rpm). Afterwards the supernatant was discarded, cells were resuspended in fresh medium, adjusted to the desired concentration and placed into a fresh cell culture flask.

2.2.3   Used Cell Lines

During this thesis work five different cell types were used (see fig. 16 & tab. 2).
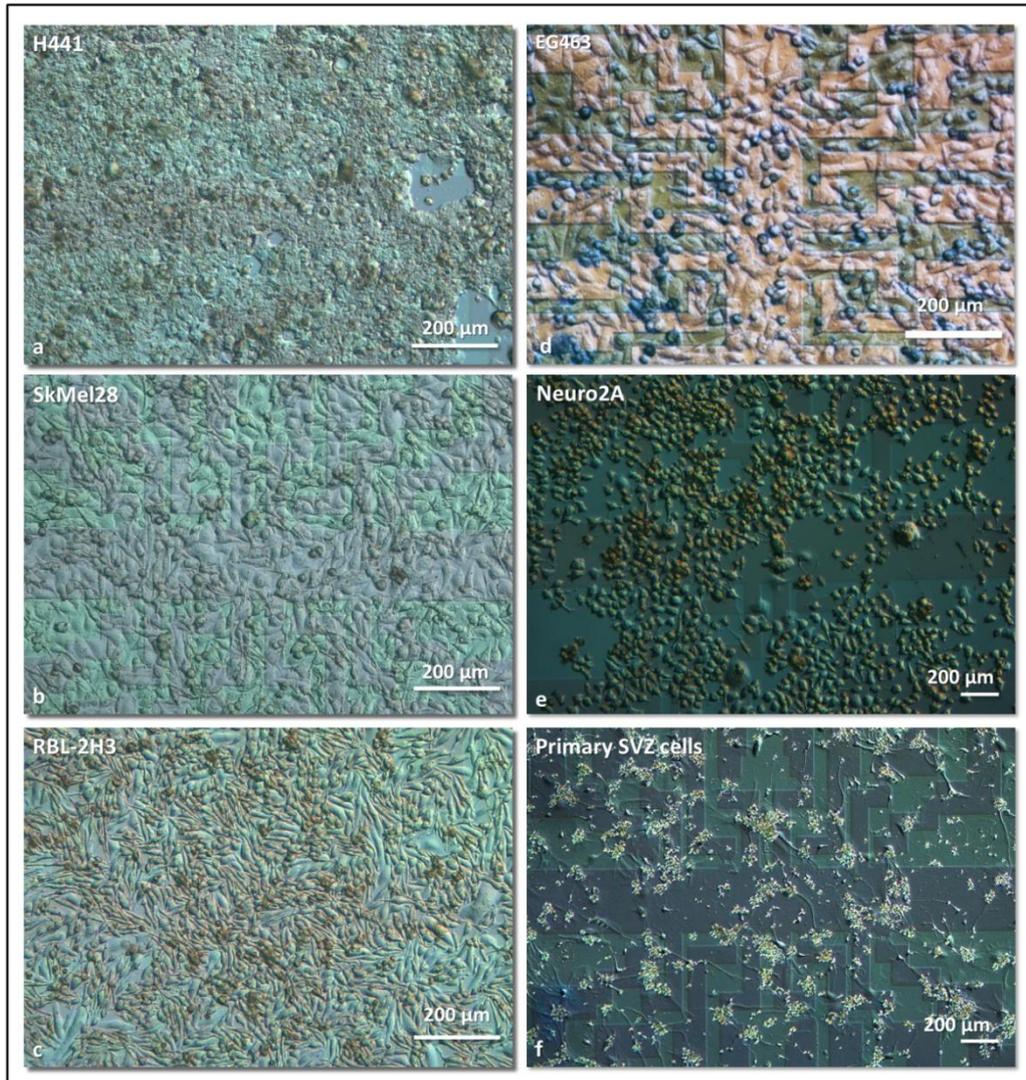
Fig. 16: Used cell types

- a) **H441**
- b) **SkMel28**
- c) **RBL-2H3**
- d) **EG463**
- e) **Neuro2A**
- f) **Primary cells from the subventricular zone of postnatal BALB/c Mice**

2.   MATERIALS AND METHODS

Table 2: Used cell lines and primary cell cultures

Cell Type	Description	Usage
H441	human papillary adenocarcinoma, epithelial morphology when grown in monolayers	• Impedimetric detection of cell adhesion of confluent cell cultures on ISFET surfaces • Impedimetric analysis of the nanotoxicity of the industrial nanoparticles NexSil20
SkMel28	human malign melanoma, polygonal morphology when grown in monolayers	• Impedimetric detection of cell adhesion of confluent cell cultures on ISFET surfaces • Impedimetric detection of cell adhesion of low density cell cultures on ISFET surfaces • Impedimetric analysis of the nanotoxicity of the industrial nanoparticles NexSil20
RBL-2H3	murine leukemia, fibroblast like morphology when grown in monolayers	• Impedimetric detection of cell adhesion of confluent cell cultures on ISFET surfaces
EG463	human malign melanoma, fibroblast like morphology when grown in monolayers	• Impedimetric analysis of the nanotoxicity of the industrial nanoparticles NexSil20
Neuro2A	established from a spontaneous tumor of a strain of an albino mouse, neuronal and amoeboid stem cell morphology	• Impedimetric detection of cell adhesion of primary neuronal tissues on ISFET surfaces • Impedimetric analysis of neurodegeneration caused by oxidative stress in primary neuronal tissues
Primary SVZ cells	primary cells obtained from the subventricular zone (SVZ) of 1 to 4 days old BALB/c mice	• Impedimetric detection of cell adhesion of primary neuronal tissues on ISFET surfaces • Impedimetric analysis of neurodegeneration caused by oxidative stress in primary neuronal tissues

H441 Cells

The cell line H441 is an epithelial cell line derived from human papillary adenocarcinoma (Kasper *et al.*, 2011). The method of culturing these cells followed the above description. The cells were provided by Prof. Dr. Roland Stauber from the Molecular and Cellular Oncology Department of the University Medical Center in Mainz, Germany. H441 cells are an already established model for the alveolar-capillary barrier *in vivo* and were used in this thesis work to demonstrate the applicability of the presented system in cytotoxicity studies since this cell line has already been used for comparable experiments by Kasper *et al.* in 2011.

Cells were cultivated in Roswell Park Memorial Institute medium (RPMI) containing 10% fetal calf serum (FCS), 1% L-Glutamine (200 mM) and 1% Penicillin/Streptomycin (10 000 u Penicillin, 10mg/ml Streptomycin) at 37°C and 5 % CO_2 with medium changes every 3 days. After reaching 95 % confluence cells were split for subculturing in a ratio of 1:10. Subculturing was done according to the protocol described above.

SkMel28 Cells

The cell line SkMel28 (Fogh *et al.*, 1977) is a cell line with polygonal morphology obtained from human malign melanoma and was provided by the project partner SymbioTec GmbH, Germany. Culturing was done following the protocol described in paragraph 2.2.

Cells were cultivated in Dulbecco's Modified Eagle's Medium (DMEM) containing 10% FCS, 1% L-Glutamine (200 mM), 1% Penicillin/Streptomycin (10 000 u Penicillin, 10mg/ml Streptomycin) and 1% of non-essential amino acids (NEAA). Medium changes and subculturing were done according to the described protocol.

EG463 cells

The cell line EG463 (Zeppezauer and Leinenbach, 1996) is a cell line obtained from human malign melanoma and was provided by SymbioTec GmbH, Germany. Culturing was done following the protocol described in paragraph 2.2.

Cells were cultivated in Dulbecco's Modified Eagle's Medium (DMEM) containing 10% FCS, 1% L-Glutamine (200 mM), 1% Penicillin/Streptomycin (10 000 u Penicillin, 10mg/ml Streptomycin) and 1% of non-essential amino acids (NEAA). Medium changes and subculturing were done according to the described protocol.

2. MATERIALS AND METHODS

Neuro2A Cells

The cell line Neuro2A (Windl *et al.*, 1999) is a neuroblastoma cell line derived from the brain of *Mus muscus*. The cell line was provided by the Enteric Nervous System Working Group of the University of Applied Science Kaiserslautern under the administration of Prof. Dr. Karl-Herbert Schäfer of the University of Applied Sciences Kaiserslautern, showing amoeboid stem cell like morphology. Culturing was done following the protocol described in paragraph 2.2.

Cells were cultivated in Dulbecco's Modified Eagle's Medium (DMEM) containing 10% FCS, 1% L-Glutamine (200 mM), 1% Penicillin/Streptomycin (10 000 u Penicillin, 10mg/ml Streptomycin) and 1% of non-essential amino acids (NEAA). Medium changes and subculturing were done according to the protocol described above.

RBL-2H3 Cells

RBL-2H3 (Eccleston *et al.,* 1973; Kulczycki *et al.*, 1974) is a basophilic leukemia cell line derived from *Rattus norwegicus* showing a fibroblast-like morphology.

Cells were cultivated in Alpha Medium containing 15 % FCS, 1% L-Glutamine (200 mM) and 1% Penicillin/Streptomycin (10 000 u Penicillin, 10mg/ml Streptomycin) at 37°C and 5 % CO_2 with medium changes every 2 days. After reaching 90 % confluence cells were split for subculturing in a ratio of 1:10. Subculturing was done according to the protocol described above.

Primary SVZ Cells obtained from postnatal BALB/c Mice

The primary cells used in this work were obtained from the subventricular zone (SVZ) of 1 to 4 days old BALB/c mice. The dissection of animals and the isolation of cells were done by Felix Kettenbaum. Required animals were sacrificed via decapitation with following removal of the whole brain from the skull. The obtained brains were transferred to a petri dish containing cold Minimum Essential Medium (MEM) to isolate the subventricular zone from both hemispheres. An overview over the dissection can be found in figure 17.
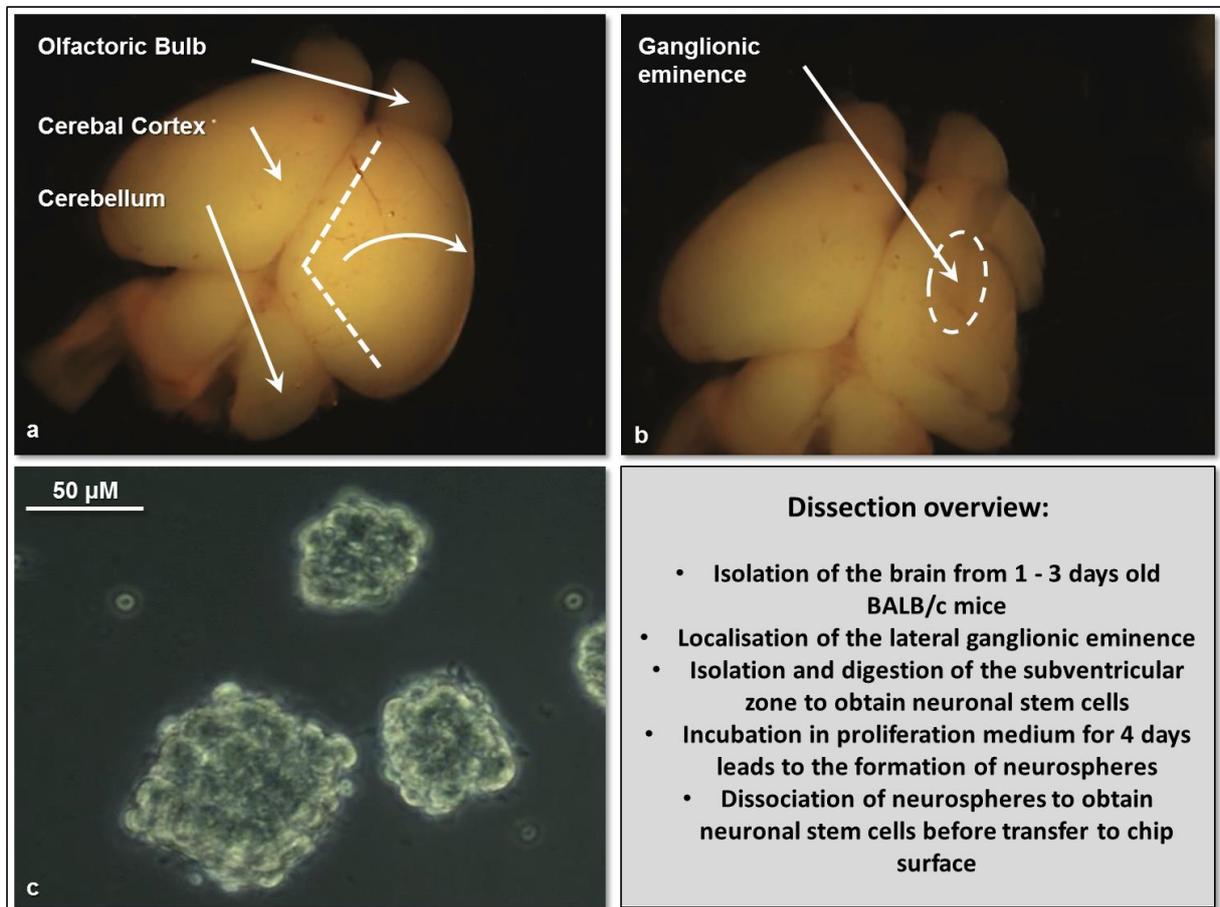
Fig. 174: Isolation and cultivation of primary cells from the subventricular zone of postnatal BALB/c mice

    a) **Brain of 3 days old BALB/c mouse after isolation from a sacrificed animal**
    b) **Right hemisphere cut open**
    c) **Neurospheres grown from isolated cells after 3 days in culture**

Isolated SVZs underwent 20 minutes of digestion with Accutase (PAA, Germany) at 37°C before dissociation using hollow needles (sizes 23 Gauge and 27 Gauge). Dissociated cells

were centrifugated at 500 rpm for 5 minutes before being resuspended and cultivated in proliferation medium consisting of DMEM F12 containing 1 % bovine serum albumin (BSA, 35 % in PBS), 1 % L-Glutamine (200 mM) , 0.1 % β-mercaptoethanol (50 mM), 1 % Penicillin/Streptomycin (10 000 u Penicillin, 10mg/ml Streptomycin), 2 % B27 (without retinoic acid), 0.2 % recombinant human fibroblast growth factor (rhßFGF, 10μg/ml), 0.1 % recombinant human epidermal growth Factor (rhEGF , 10μg/ml). The obtained stem cells were cultivated in proliferation medium for 5 days and formed neurospheres.

These neurospheres were digested using AccuMax (PAA) and subsequently dissociated using a pipette tip. Digestion was done for 10 minutes at 37°C with the process being repeated once.

The obtained cells were then adjusted to a concentration of 1.5 x 10^5 cells/ml with 50 μl of cell suspension being seeded on the prepared chip surface or 96-well plate (equaling 7500 cells per well or chip respectively). Cells were then cultivated in differential medium consisting of DMEM F12 containing 1 % bovine serum albumin (BSA, 35 % in PBS), 1 % L-Glutamine (200 mM), 0.1 % β-mercaptoethanol (50 mM), 1 % Penicillin/Streptomycin (10 000 u Penicillin, 10mg/ml Streptomycin), 2 % B27 (with retinoic acid) for 7 days to facilitate differentiation before measurements were conducted.

2.2.4   MTT Assay

The MTT assay is a caloric assay using the yellow insoluble tetrazolium dye 3-(4,5-dimethylthiazol-2-yl)-2,5-diphenyltetrazolium bromide (MTT) and its reduction to a soluble purple formazan by metabolically active cells (Mosmann, 1983). In this work the MTT assay was used in two separate projects to assess the viability of the tested cells as a standard control.

All MTT assays were conducted according to the following protocol. Cells were seeded in 96-well plates (Greiner Bio-One, Germany) in a density of 5000 to 10 000 cells per well and incubated at 37°C and 5% CO_2 overnight. After incubation the cells were treated with their respective testing compound for different durations. Afterwards 20 µl of MTT solution (5 mg/ml in PBS) were added to each well and incubated under cell culture conditions for 2 hours. The supernatant was then sucked of and replaced with 125 µl of undiluted dimethyl sulfoxide (DMSO) to dissolve the formed formazan dye. The well plates were incubated under a chemical hood on a shaker for 15 minutes and examined photometrically (Genios microplate reader, Tecan, USA). Each experiment was accompanied by empty control wells which were treated exactly like the cell containing wells to act as a blank measurement/control.

Cytotoxicity of NexSil 20 Nano Particles

H441 cells were seeded in 96-well plates in a density of between 5000 and 10 000 cells per well and incubated according to the protocol mentioned in paragraph 2.2.2. After cultivation for 24 hours the cells were treated with 60 µg/ml (4.4 x 10^{12} particles/ml) and 600 µg/ml (4.4 x 10^{13} particles/ml) of silica NexSil 20 particles. The used particles, provided by Prof. Dr. Roland Stauber from the Molecular and Cellular Oncology Department of the University Medical Center in Mainz, Germany, had an average diameter of 20 nm and were administered in serum free Roswell Park Memorial Institute medium (RPMI). The same was done for SkMel28 cells and EG463 cells.

For long term studies cells were incubated with particles for 36 hours with consequent MTT testing every 4 hours as described above. Short term effects of particle treatment were

analyzed by the same method using particle exposure for an overall duration of 6 hours with consequent testing every hour after particle administration.

Cytotoxicity of Hydrogen Peroxide in SVZ and Neuro2A Cells in Medium

5000 to 10 000 cells of both cell types were seeded in 96- well plates and cultured for 7 days (primary SVZ cells) and 24 hours (Neuro2A), respectively. Well plates containing primary SVZ cells had to be coated with PDL (100 µg/ml) and laminin (20 µg/ml). Cells were treated with medium containing various concentrations of hydrogen peroxide (50 mM, 10 mM, 1 mM, 100 µM, 10 µM), incubated under cell culture conditions overnight and subsequently tested following the protocol described above.

Cytotoxicity of Hydrogen Peroxide in SVZ and Neuro2A Cells in Hank's Balanced Salt Solution (HBSS)

5000 to 10 000 cells per well of both cell types were seeded in 96- well plates and cultured as already mentioned in the paragraph before and were afterwards treated with Hank's Balanced Salt Solution (HBSS) containing various concentrations of hydrogen peroxide (50 mM, 10 mM, 1 mM, 100 µM, 10 µM). Cells were then incubated under cell culture conditions for 6 hours and tested following the protocol described in 2.2.2.

2.3   Chip Fabrication and Assembly

During this work two types of ion sensitive p-type open-gate field-effect transistors (ISFETs) were used:

a.   16 channel quasi-planar ISFETs

b.   8 channel dip-chip ISFETS

The 16 channel quasi-planar ISFET chips used in this study were produced in our research group by Dr. Xuan Thang Vu in our research group at the facilities of the University of Applied Sciences Kaiserslautern in Zweibrücken. The process flow of chip fabrication can be found in figure 18.

The 8 channel dip-chip ISFETs were produced at the Institut für Mikrotechnik, Mainz during a former project at the Max-Planck Institute for Polymer Research Mainz, Germany (Offenhäusser *et al.*, 1997). These ISFET devices were fabricated on n-doped silicon wafers with boron doped contact lines for in order to obtain robust, reusable devices, usable in cell culture experiments.

2.3.1   Fabrication of Quasi-Planar ISFETs

The devices were fabricated on 4 inch n-type silicon wafers with a resistivity of 2 to 10 Ohm cm (Simat, Germany). As a first step a silicon oxide layer (thickness 1 μm) was thermally grown on top of the wafer via wet oxidation (1000°C, 5 hours) to act as masking layer for following ion implantation.

Photolithography and following wet etching with buffered hydrofluoric acid (BHF) were used to define the contact lines. The resistance of the contact lines was lowered via boron ion implantation by an external supplier (IPS, France) using a high dose and energy of $1 \cdot 10^{16}$ ions/cm^2 and 150 keV. Afterwards the wafers had to be cleaned in piranha solution (1% hydrofluoric acid) and annealed (1050°C, 2 hours). In the next step the quasi planar topography was established by complete removal of all silicon oxide layers using wet etching in BHF with subsequent cleaning following a standard RCA protocol. This second wet etching step was followed by 10 minutes of annealing in N$_2$ at 900°C to activate the dopants.

Afterwards a wet oxidation process (30 minutes) was done to achieve a uniform SiO_2 passivation layer with a thickness of 220 nm.
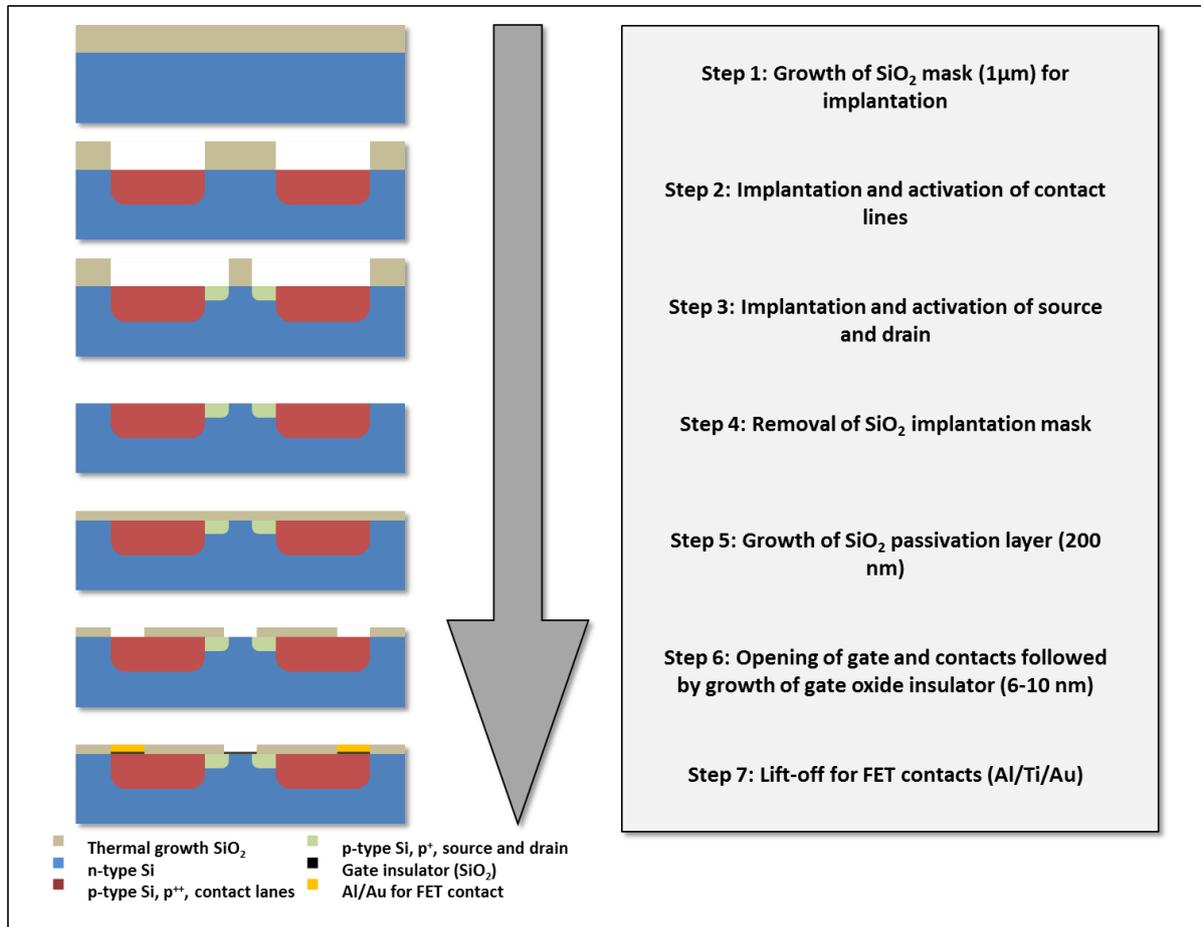
Fig. 18: Process flow of quasi-planar ISFET fabrication

The devices used during this work were produced in our research group at the University of Applied Sciences (campus Zweibrücken) and were fabricated by Dr. Xuan Thang Vu. The individual steps are described in paragraph 2.3.

The actual gate area and outer source and drain contacts were defined in an additional lithography step. There the passivation layer was opened via wet etching in BHF (3 minutes) and subsequently in HF (hydrofluoric acid, 1%) until the silicon oxide was opened completely. After the removal of the resist using acetone, the gate oxide layer was thermally grown to a thickness of 6 nm to act as dielectrics for the devices using dry oxidation (4 minutes at 820°C). As a final step during the production of our FET chips the outer source and drain contact lines were metallized. This was done by etching of the silicon oxide

covering the source and drain contact by 1% HF and by deposition of 200 nm of aluminium, 20 nm of titanium and 100 nm of gold via electron beam evaporation. The newly created metal contacts were then annealed for 10 min at 400°C in a N_2 atmosphere in order to form good ohmic contacts.

The used design for this work had individual transistor gates with a gate size of 12 x 5 µm (effective gate length of about 1.3 µm due to under-diffusion in the above described process) arranged in a 4 x 4 grid located at the center of a 7 x 7 mm² chip. The individual gates were arranged with a distance of 200 nm between them (fig. 19).

2.3.2   Encapsulation of Quasi-Planar ISFETs

Selected chips were put in a beaker and cleaned of photoresist via ultrasonication in acetone for 5 minutes. Afterwards the used acetone was replaced with fresh acetone and the process was repeated. The acetone was then replaced with 70 % isopropanol and sonicated for another 5 minutes.

Chips were clued to 68-pin Leaded chip carriers (LCC) using a two components epoxy adhesive (Epoxy Technology, USA) which components were mixed in a ratio of 1:1 and applied to the surface of the chip carrier. The chip was then placed in the center of the carrier and slightly pressed onto the carrier surface. Afterwards the carrier and chip were baked for 1 hour at 150°C.

After baking the chips were connected to the contact pads on the carrier via wire bonding using an Al (1% Si) wire following the bond plan shown in fig. 20.

The bonded chips were encapsulated in biocompatible Polydimethylsiloxane (PDMS, Sylgard 96-083, Dow Corning, Germany) to insulate the metal contacts and bonds and to form a

miniature cell culture receptacle. The mentioned cell culture receptacle was created by gluing a silicon hopper (formed out of Sylgard 184 silicone) and outer glass ring onto the chip surface and the chip carrier surface respectively using PDMS (Sylgard 96-083).
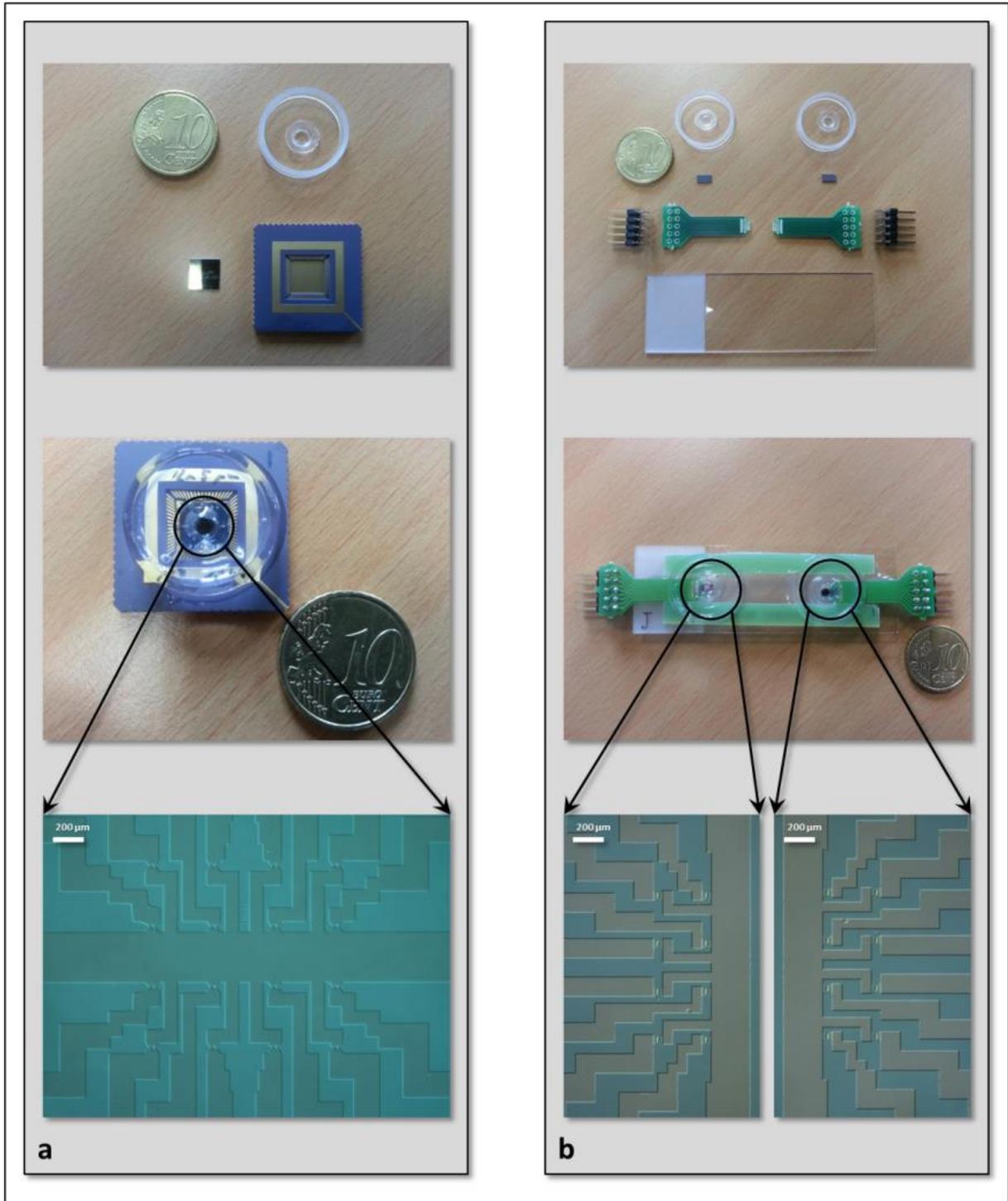
Fig. 19: *Components used in chip encapsulation for both quasi-planar ISFETs and parallel-culture ISFETs*

    a)   **Quasi-planar ISFETs**
    b)   **Parallel-culture ISFETs**
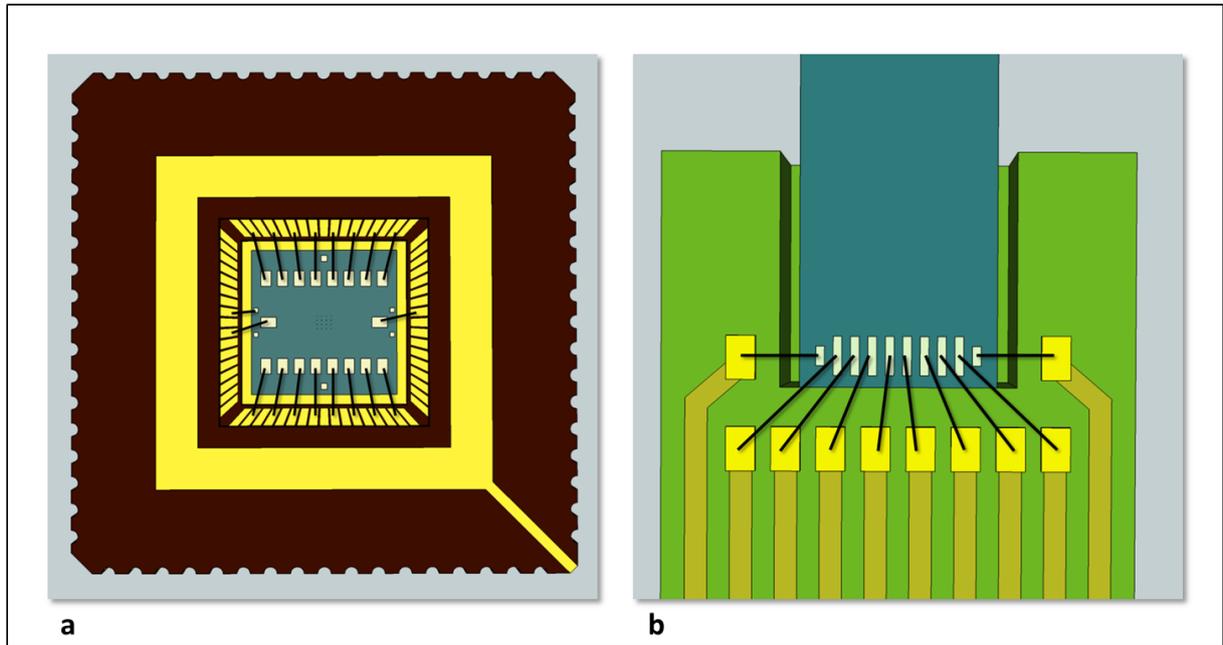
Fig. 20: Bondplan for quasi-planar ISFETs (a) and parallel-culture ISFET (b)

Wire bonds are visualized as black lines with each black line representing two bonds.

Following the attachment of the glass ring and the silicon hopper the chips were baked at 150°C for 1 hour. Afterwards the gap between the silicon hopper and the outer glass ring was filled with PDMS, degassed in a desiccator and again baked for 1 hour at 150°C.

2.3.3 Encapsulation of Dip-Chip ISFETs for Parallel Cell Culture

The encapsulation of the used dip chips to create a chip system allowing for parallel cell culture followed the same protocol like the encapsulation of quasi-planar ISFETs. Before encapsulation the chips were clued to a PCB (printed circuitry board, LeitOn GmbH, Germany) carrier. Two such chip-carrier complexes were then glued to a microscope slide accompanied by two pieces of PCB to act as a base for the glass rings used to create the cell culture receptacle. After gluing the chips were baked for 1 hour at 150°C.

The chips were connected to the contact pads of the carrier via wire bonding. The bond plan for this particular setup can be seen in figure 20. Wire bonding was followed by the application of the silicon hoppers and outer glass rings using PDMS as it was described for

quasi-planar ISFETs. Encapsulation with PDMS and baking were also done according to the aforementioned protocol. A schematic drawing of the encapsulation process can be found in figure 21.
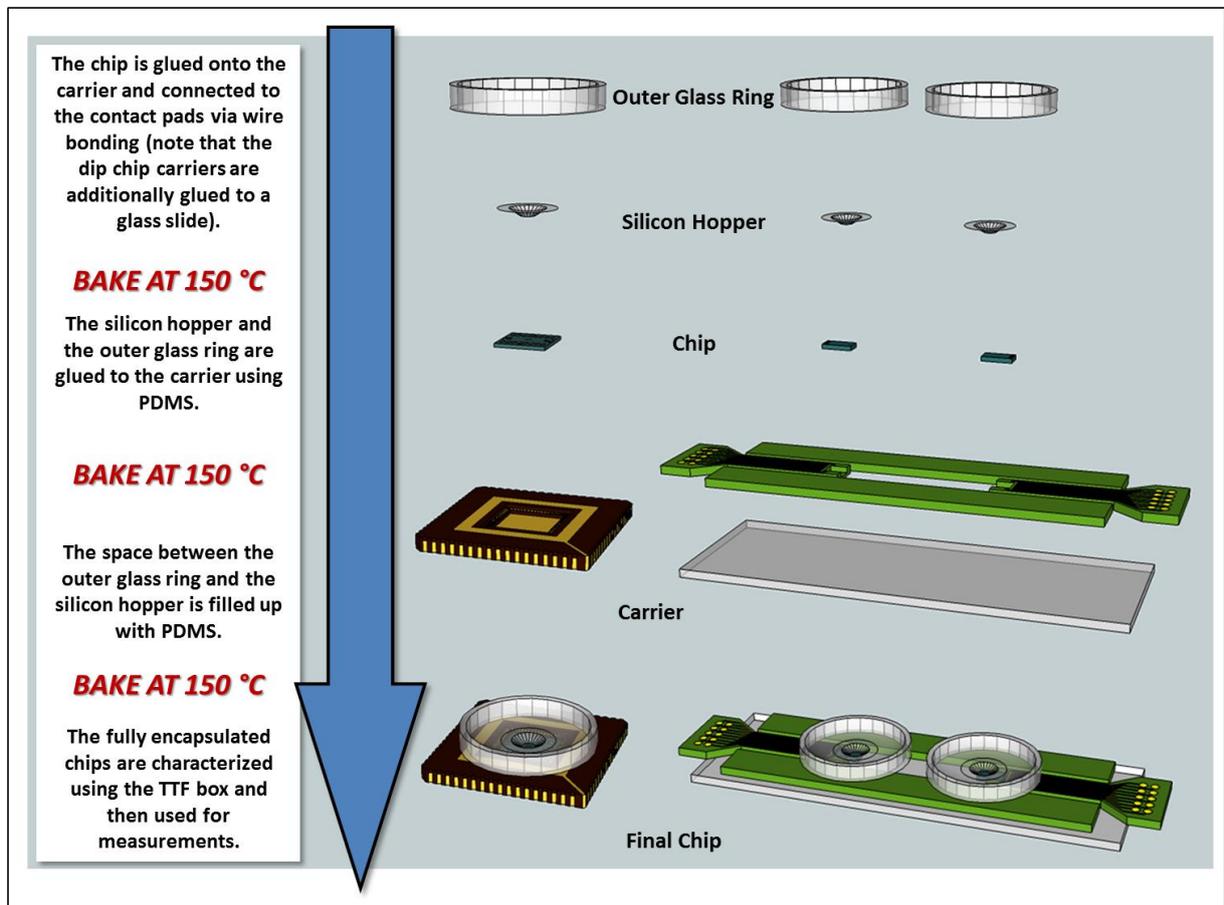
Fig. 21: Encapsulation procedure for quasi-planar ISFETs and parallel-culture ISFETs

Encapsulation of both chips followed the same basic protocol with the individual steps being described on the left side of the schematic drawing.

2.4   Measurement Setup

The measurement setup (fig. 22) used in this work is called a transistor-transfer-function-box (TTF-box for short, fig. 22b) and is used as a portable 16 channel amplifier system (Ingebrandt *et al.*, 2005, Schäfer *et al.* 2009). Chips can be connected to the amplifier system either via a square contact port on the top side of the device (quasi-planar ISFETs) or via

cable connection to two contact ports on the left and right side of the device (parallel culture chips).
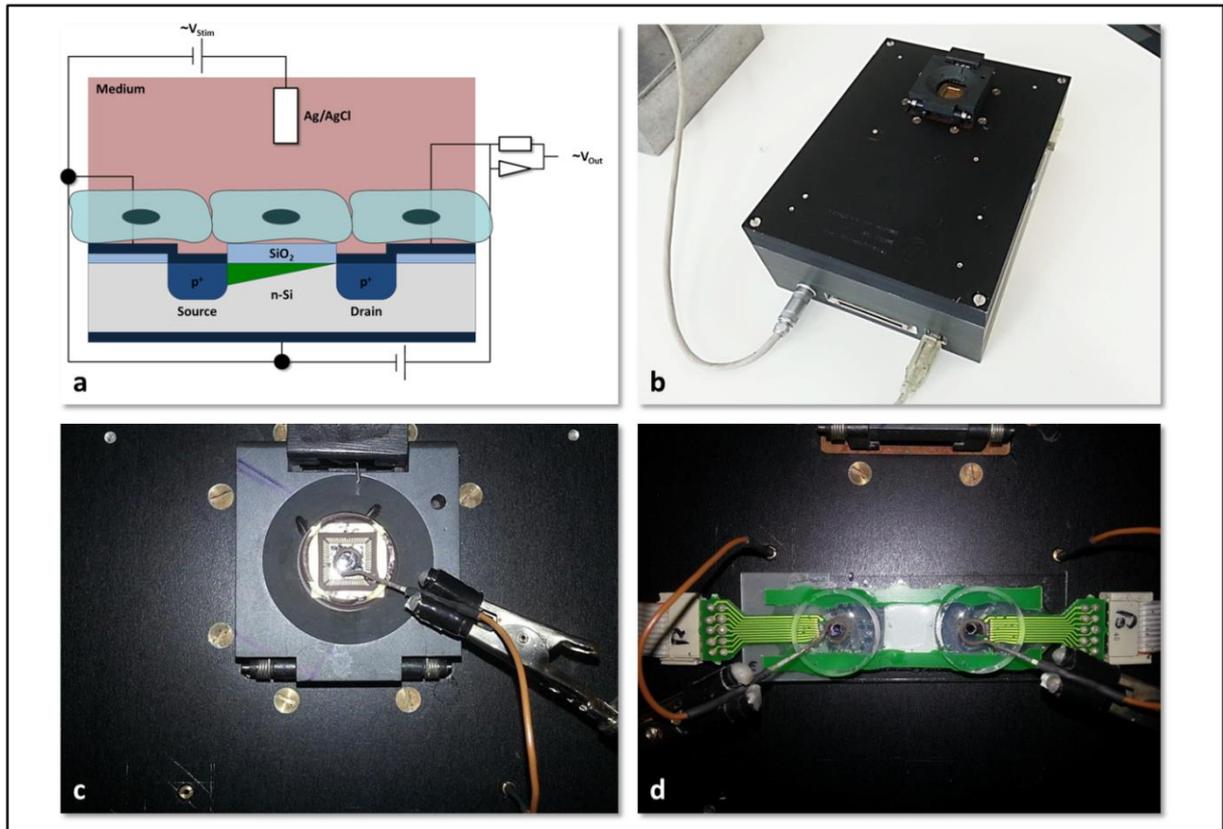
Fig. 22: Measurement setup

    a)   **Schematic drawing of the measurement setup on the level of an individual transistor gate**
    b)   **Transistor-transfer function box (TTF box)**
    c)   **Top view of the chip adapter to connect quasi planar ISFETs to the TTF box**
    d)   **Top view of parallel-culture ISFET connected to the TTF box**

The system is operated via custom made software called Biomol, which was developed at the Research Center Jülich (FZ Jülich, Germany).

2.4.1   Chip Characterization

During this work an assessment of the transfer characteristics of each chip was done before measurements were conducted (fig. 23). After assessing the transfer characteristics for each individual transistor the transistors were set to a common working point of maximum transconductance. This was achieved by adjusting V_{GS} and V_{DS} to the highest point in the

plotted transconductance curves (showing the drain-source current I_{DS} correlated to constant V_{DS} values) corresponding to the transfer characteristics for four defined steps of V_{DS} (0 V, -1 V, -2 V, -3 V). Since the sensor chip was fabricated in a common-source layout, all channels need to be set to the same working point, which resulted in small variations in I_{DS} from channel to channel.
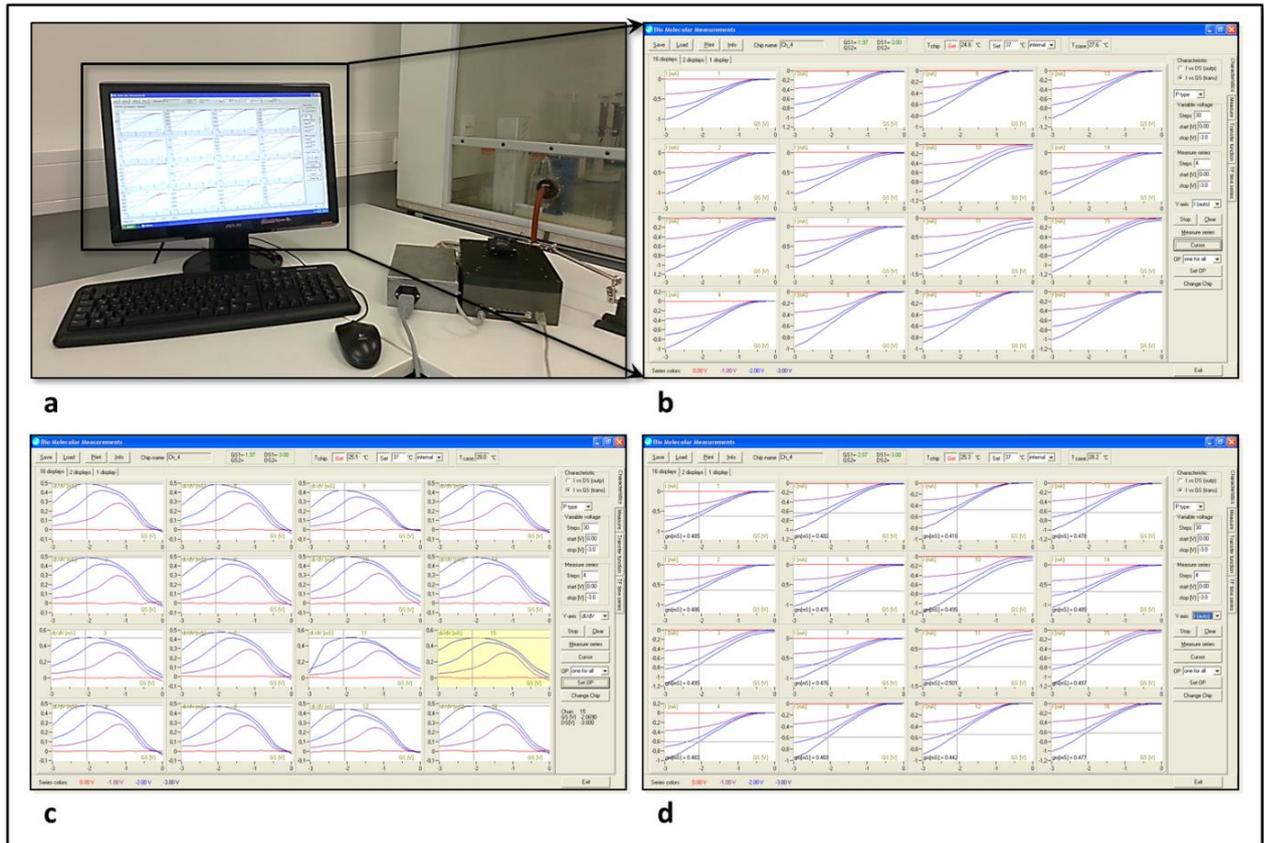
Fig. 23: Chip characterization and working point adjustment

    a) **Measurement setup showing the BioMol software graphied user interface**
    b) **Characterization lines before working point adjustment**
    c) **Adjustment of the working point**
    d) **Characterization lines with included working point**
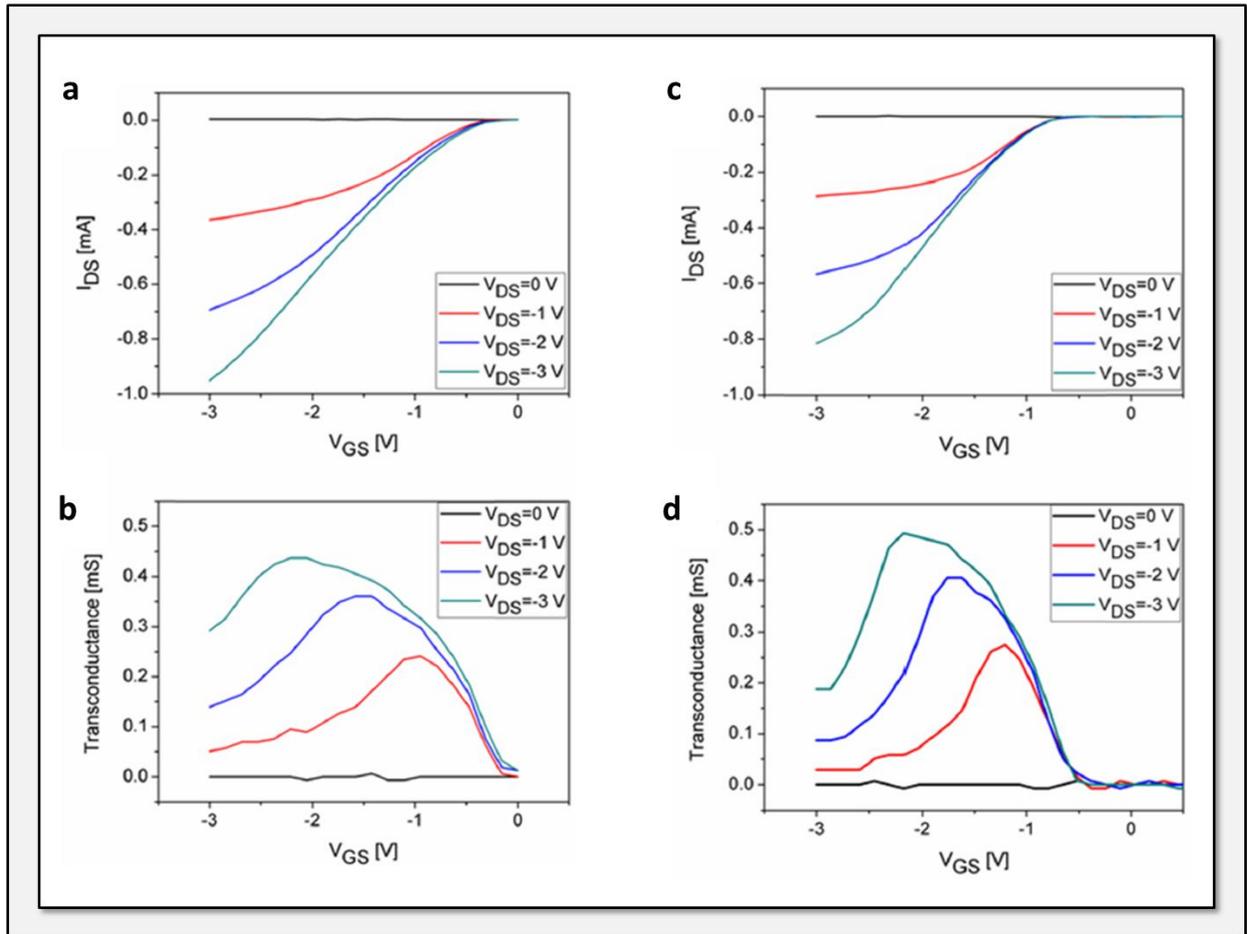
Fig. 24: Typical transfer characteristics of 8 channel dip-chip ISFETs devices and 16 channel quasi-planar ISFET devices (pictures taken from Susloparova et al., 2015)

- a)   **Transfer characteristics of 8 channel dip-chip ISFETs devices**
- b)   **Transconductance of 8 channel dip-chip ISFETs devices**
- c)   **Transfer characteristics of 16 channel quasi-planar ISFET devices**
- d)   **Transconductance of 16 channel quasi-planar ISFET devices**

The transfer characteristics of both used devices were measured in a voltage range (0 to -3 V for V_{GS} and V_{DS}, see fig. 24 a & c). Fig 24 b & d show the transconductance of both the 8 channel dip-chip ISFET devices and the 16 channel semi-planar ISFET devices. A maximum transconductance of 0.45 mS and 0.5 mS was achieved for the 8 channel dip-chip ISFET devices and the 16 channel semi-planar ISFET devices, respectively (Susloparova *et al.*, 2015).

2.4.2   Analysis of Chip Deterioration

In general FET sensors could be repeatedly used. However, extended usage times lead to deterioration of the sensor performance. To assess the deterioration of the used quasi-planar FET chips g_m-values obtained via repeated characterization (13 times) of nine chips were analyzed. For this the following definitions were set up:

- Channels with g_m-values above 0.3 mS are best suited for impedance spectroscopy.

- Channels with g_m-values below 0.2 mS are considered as failing.

- Channels with g_m-values below 0.1 mS are considered as insensitive and therefore broken.

Channels which were considered as broken from the beginning were excluded from the analysis.

2.4.3   Impedance Spectroscopy

Characterization was followed by the measurement of the transistor-transfer function (TTF). This was done by applying a signal of 10 mV with varying frequency in the range from 1 Hz to 1 MHz to an Ag/AgCl wire used as a pseudo-reference electrode. The typical behavior of the used devices is shown in fig. 25.

The method of our analysis is based on the recording of the transistor-transfer function (Schasfoort *et al.,* 1989; Antonisse *et al*., 2000; Kharitonov *et al*., 2001), representing the combination of the bandwidth-affecting effects of the used reference electrode, measurement solutions (in this work the cell culture media), attached biological samples (in our case cells), the actual transistor and the first amplifier stage inherent in our

measurement setup. The resulting response of an attached sample to an applied AC voltage forms the basis for deducing the properties and the behavior of attached cell samples.
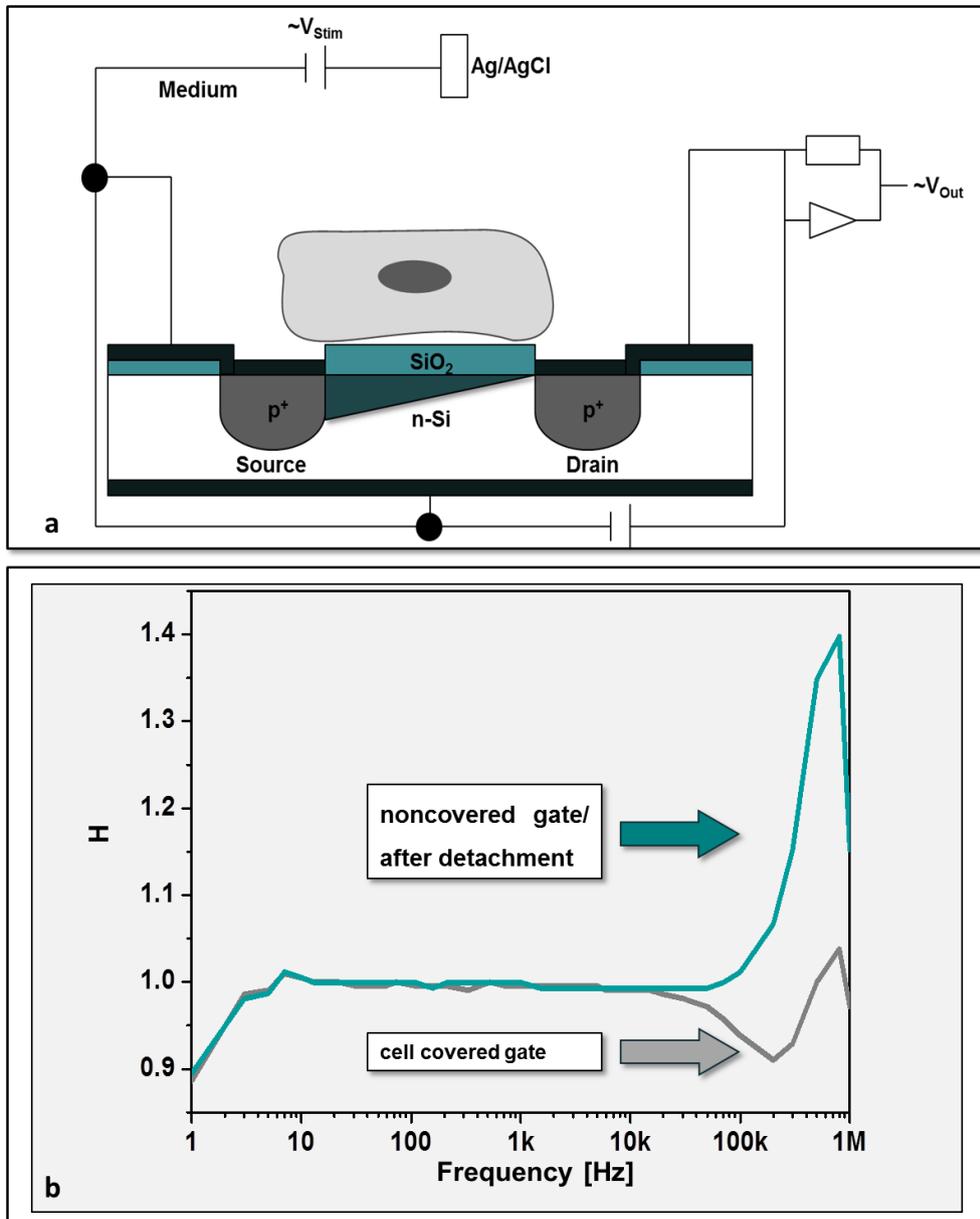
Fig. 25: Cellular adhesion on FET surface:

    a)   **Schematic drawing of an adherent cell on top of a FET surface**
    b)   **Typical behavior of an open gate ISFET with and without attached cells**

Alternatively to scans of a whole spectrum in the frequency range of 1 Hz to 1 MHz, the measurement setup can be used to conduct measurements to analyze time dependent responses of attached cell samples in real time. To do so, the amplifier was set to a defined frequency and variations in the transistor-transfer function were monitored over time.

2.4.4   Real-Time Observation of Transfer Function Changes

For the observation of transfer function changes in real time, the measurement setup was set to a defined frequency of 200 kHz and measurements were typically taken for 2 hours. With our TTF system these measurements can be done inside or outside of the cell culture incubator. The frequency of 200 kHz was chosen after conducting the chip characterization and a first impedance scan as described above using chips with a confluent layer of cells attached to the transistor surface, which was also checked microscopically. With our TTF system we were able to perform these measurements under cell culture conditions inside or outside of the incubator.

2.5   On Chip Cell Culture Protocols

2.5.1   Chip Cleaning

Before use all chips were thoroughly cleaned according to the following standard procedure (Wrobel *et al.*, 2005). The chip surface was cleaned using a cotton bud soaked with 70 % ethanol and subsequently ultrasonicated for 5 minutes in distilled water. The water was removed afterwards and replaced with a 2 % Hellmanex III solution (Hellma Analytics, Germany) followed by another round of ultrasonication for 5 minutes. Afterwards the Hellmanex solution was discarded and replaced with distilled water for a third ultrasonication step. The chips were subsequently dried and prepared for coating.

2.5.2   Chip Coating

Chips used during this work were coated with either fibronectin (100 µg/ml; for H441, RBL-2H3, SkMel28, EG463 and Neuro2A, adapted from Lindl*, Cell- and Tissue culture*, 5th edition, 2002) or PDL (100 µg/ml) and laminin (20 µg/ml; for primary SVZ cells), respectively (following a protocol for primary neurons described by Medert *et al.*, 2013). Before the

coating was administered, the chip surface was activated via incubation at 80°C for 30 minutes with 20 % sulfuric acid applied to the center of the chip surface. After surface activation the chips were again ultrasonicated in distilled water for 5 minutes and dried afterwards. The activated dry chip surface was then sterilized using 70 % ethanol (5 min) and rinsed with distilled water before the coating was applied.

Fibronectin (100 µg/ml) was administered to the chip surface in 50 µl droplets and incubated at 37°C and 5 % CO_2 for 3 hours before removal of the fibronectin and subsequent washing with distilled water took place. This was done for the cell lines H441, RBL-2H3, SkMel28 and Neuro2A.

For cultivating primary SVZ cells the chips were coated with PDL (100 µg/ml) for 24 hours (37°C, 5 % CO_2) before the PDL was replaced with laminin (20 µg/ml) and incubated for 1 hour (37°C, 5 % CO_2). Afterwards the chips were again washed with distilled water.

2.5.3   On-Chip Cell Culture

Cells were cultivated on the surface of FET chips according to their respective protocols mentioned above. Cell culture receptacles on chip have a capacity of between 500 and 600 µl of cell culture medium.

Confluent cell cultures were used to observe the cytotoxic effects of NexSil 20 nanoparticles in H441 cells, SkMel28 cells and EG463 cells and the cytotoxic effect of hydrogen peroxide in Neuro2A cells. Cellular adhesion was also analyzed using confluent on chip cultures of SkMel28 cells, H441 cells and RBL-2H3 cells. To establish confluent cell cultures on top of the chip surface, cell suspensions obtained through subculturing were adjusted to a concentration of 2×10^5 cells/ml and were seeded on top of the chip surface in 50 µl droplets (equaling 10 000 cells per chip). The chips were then incubated for 30 minutes at

37°C and 5 % CO_2 so the cells could sink down to the chip surface and adhere to it. Afterwards the cell culture receptacle was filled up with 500 µl of the respective cell culture medium.

Low density cell cultures of SkMel28 cells were used to further analyze cell adhesion and possible differences between adhesions of individual cells compared to larger cell populations. Therefore 1.5×10^4 cells/ml to 2×10^4 cells/ml were seeded on top of the chip surface in 50 µl droplets (equaling 750 to 1000 cells per chip). Further proceedings were identical to confluent cell cultures.

2.5.4   Primary Cell Cultures

On chip cultivation of primary cells from the subventricular zone was done according to the protocol described in paragraph 2.2.1. It is important to note that the dissociation and digestion needed to obtain individual stem cells which will differentiate on top of the chip surface is inducing a varying degree of physical stress for the cells. Therefore the amount of viable cells cannot be adjusted to a specific concentration with the same amount of accuracy given for established cell lines.

2.6   Impedimetric Analysis of Cell Attachment

2.6.1   Impedimetric Analysis of Cell Adhesion in Confluent Cultures

Cells were grown on top of fibronectin-coated chip surfaces according to their respective protocols described in 2.2 and were cultivated for 24 hours under standard conditions (37°C, 5 % CO_2) before measurements were started. To verify the confluent cell layer on top of the chip microscopic photographs were taken using Axiotech vario 100 HD (Carl Zeiss AG, Germany) utilizing a Zeiss epiplanar 10x objective and a Zeiss AxioCam color (type 412-312). Photographs were taken before and after measurements.

Chips were characterized as described above and set to a working point of maximum transconductance for impedance spectroscopy. After impedance spectroscopy the cells were removed from the transistor surface via Trypsin treatment (30 minutes, 37°C). Afterwards the Trypsin was removed and fresh cell culture medium was applied to the chips for further measurement. The chips were set to the exact same working point as before Trypsin treatment and the measurement was repeated.

2.6.2   Impedimetric Analysis of Cell Adhesion in Low Density Cultures

Measurements done with low density cultures of SkMel28 cells were done in exactly the same manner like with confluent cell cultures. Transistor gates with attached cells were categorized into groups with 25 – 50 %, 50 – 75 % and 75 – 100 % gate coverage according to their respective area of coverage. This was done using microscopic pictures of individual cell-covered gates taken with the Axiotech vario 100 HD microscope.

2.6.3   Data Fitting

The fitting procedure followed a protocol established in our group (Susloparova *et al.*, 2015). By using an equivalent-electrical circuit model (EEC, fig. 26 a) the behavior of a functional FET with an adherent cell can be simulated using the equation shown in figure 26 b. Using this approach makes it possible to extract the cell-related parameters C_M and R_{seal} from the measurements. The following parameters presented in table 3 are relevant for the fitting procedure with the first three being chip-related.

Table 3: Chip- and cell-related parameters relevant for data fitting

Chip related parameters	
C_L [pF]	Contact line capacitance; parallel combination of C_{drain} & C_{source}
C_{Ox} [pF]	Gate oxide capacitance
g_m [mS]	Transistor transconductance; measured during chip characterization
Transimpedance circuit parameters	
R_{el} [kΩ]	Series resistance of electrolyte and reference electrode
$R_{feedback}$ [kΩ]	Feedback resistance
f_g [kΩ]	Cutoff frequency of the operational amplifier
Cell-related parameters	
C_M [pF]	Combined membrane capacitance
R_{seal} [MΩ]	Seal resistance
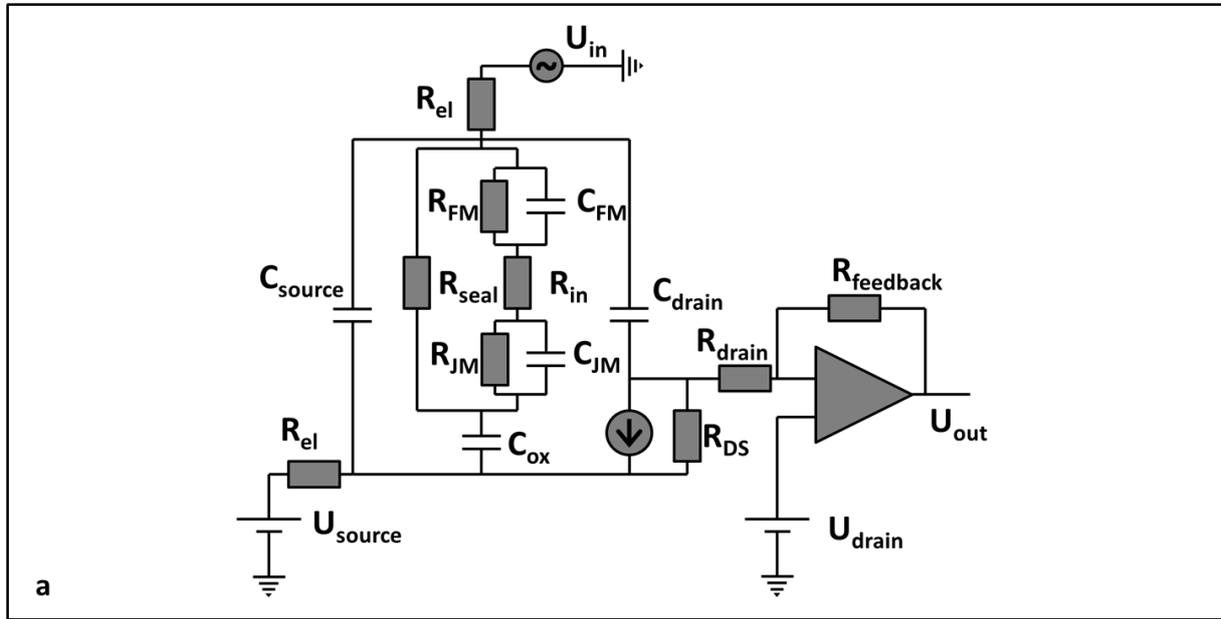
$$H(jw) = R_{feedback} g_m * \frac{1}{\sqrt{1+(\frac{f}{f_g})^2}} * \frac{1+jw(C_M R_{seal} - \frac{C_L}{g_m}) - w^2 \frac{C_L R_{seal}}{g_m}(C_M + C_{ox})}{1+jw(R_{seal}(C_{ox}+C_M)+R_{el}(C_L+C_{ox})) - w^2 R_{seal} R_{el}(C_L(C_{ox}+C_M)+C_{ox}C_M)}$$

b

Fig. 26: Equivalent-electrical circuit model

   a)   **EEC model of a cell-covered field-effect transistor**
   b)   **Fitting equation**

The combined membrane capacitance C_M should not be confused with the total membrane

capacitance typically measured by patch-clamp pipettes. Due to the serial combination of

both free membrane parts and parts in the cellular junction this projected membrane

capacitance C_M is generally smaller than the typical whole-cell membrane capacitances of cells, which is measured from the cells interior to the surrounding bath.

The equation was fitted to the measured data and the obtained values for C_M and R_{seal} were extracted from the fittings of averaged impedance signals. Fitting was done using the software Origin (OriginPro 9.0, OriginLab Corporation, Germany).

2.7   Real Time Analysis of Cytoxicity of NexSil 20 Particles

H441 cells were grown as a confluent cell layer on top of the transistor surface according to the protocol described in paragraph 2.2. After cultivation for 24 hours the chips were characterized and an impedance spectroscopy was done as described in 2.4. Afterwards the cells were treated with 60 µg/ml (4.4 x 10^{12} particles/ml) and 600 µg/ml (4.4 x 10^{13} particles/ml) of NexSil 20 particles (in serum free RPMI medium) and their effect was analyzed by monitoring the transistor-transfer function time-dependently for 2 hours at a frequency of 200 kHz under cell culture conditions.

2.8   Apoptosis Induction via Hydrogen Peroxide

Primary cells from the subventricular zone and Neuro2A cells were grown on top of coated chip surfaces according to their respective protocols detailed in paragraph 2.2.

Cells were treated with medium and HBSS containing hydrogen peroxide (SVZ: differential medium with 50 mM H_2O_2, HBSS with 1 mM H_2O_2; Neuro2A: DMEM with 10 mM H_2O_2, HBSS with 1 mM H_2O_2) and incubated for a specific amount of time (24 hours in medium and 6 hours in HBSS). Impedance spectroscopy in the respective standard media containing no hydrogen peroxide was done for before and after incubation with hydrogen peroxide.

2.9   Scanning Electron Microscopy (SEM) Documentation

Samples of cells attached to a transistor gates were prepared from low density cell cultures of all used cell lines. Cells were cultivated on the chip surface according to their respective protocols described earlier for 24 hours to achieve proper cell adhesion. Afterwards the samples were rinsed with 1xPBS twice and then fixated (see fig. 27).

Fixation

Cells samples were fixated on top of the chip surface using a Glutaraldehyde solution (3 % in HEPES buffer, pH 7.3). The used samples were incubated in the Glutaraldehyde solution under a chemical hood for 24 hours. After Fixation the samples were rinsed with distilled water twice and prepared for drying.

Drying

The samples were incubated in several concentrations of Isopropanol in ascending order starting with 30 % Isopropanol and ending at 100 % Isopropanol. The details are shown in figure 27. After finishing the incubation in 100 % Isopropanol the samples were examined microscopically and air dried in the clean bench.

Documentation

Cell samples were analyzed using a Supra40 scanning electron microscope (Carl Zeiss AG, Germany). The dry samples were glued to a SEM sample holder and sputtered with a 10 to 20 nm thick layer of gold. Afterwards the sample was inserted into the SEM and scanned with an acceleration voltage of 3 kV and an aperture size of 20 μm.
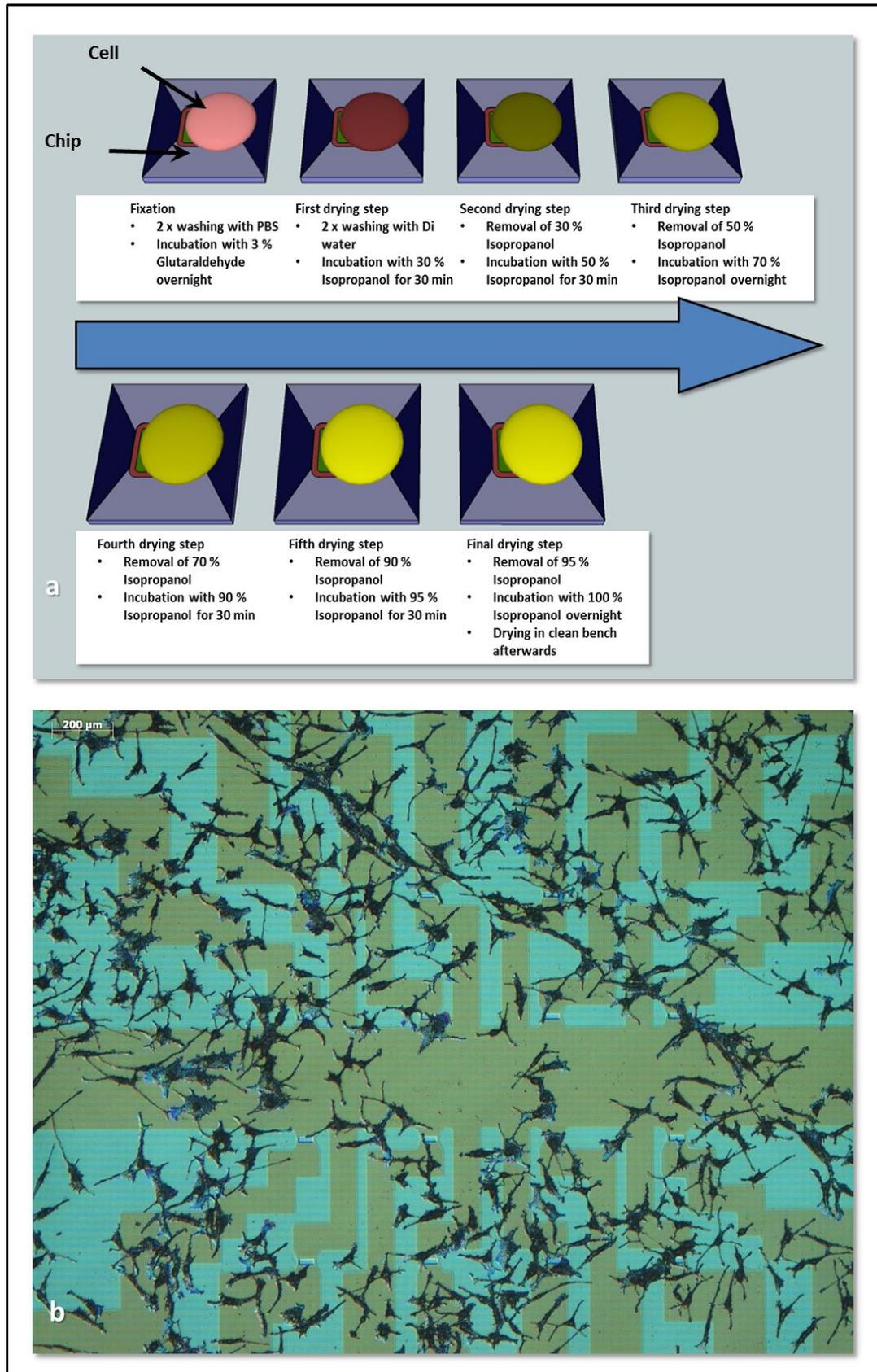
Fig. 27: Fixation and drying steps

a) Schematic drawing of fixation and drying steps used during this work
b) Microscopic picture of a dry sample of fixated SkMel28 cells on chip surface

3.   RESULTS

The following chapter is meant to show the results of the conducted experiments including a short summary of said experiments. A detailed discussion of the data can be found in chapter 4.

3.1   Deterioration of individual transistor gates used in cell culture

Over the course of this thesis the used chips showed a sharp decline in their performance resulting in low sensitivity to cellular attachment. The g_m-values of individual transistor gates were analyzed as described in chapter 2.4.4 with a total amount of 144 channels being considered for analysis.

Out of these 144 channels 88 channels showed g_m-values above 0.1 mS for all 13 measurements and were therefore considered working while 38 channels broke down over time (g_m-value dropped below 0.1 mS) and 18 channels not working from the beginning (fig. 28 a). Working channels which did not break down over time (n = 88) were used to analyze the decline of the g_m-value to provide a simple measure of chip quality over time (fig. 28 b). At their first use an average g_m-value of 0.47 mS was observed. At the fourth use of the tested chips the average g_m-value dropped to 0.36 mS, at the seventh use it dropped to 0.3 mS, at the tenth to 0.25 mS and after thirteen uses to 0.21 mS. Over thirteen individual uses of the tested channels the average g_m-value showed a decline of 55 % compared to the first use. To test the functionality of the used chips the g_m-values were monitored during the performed experiments.
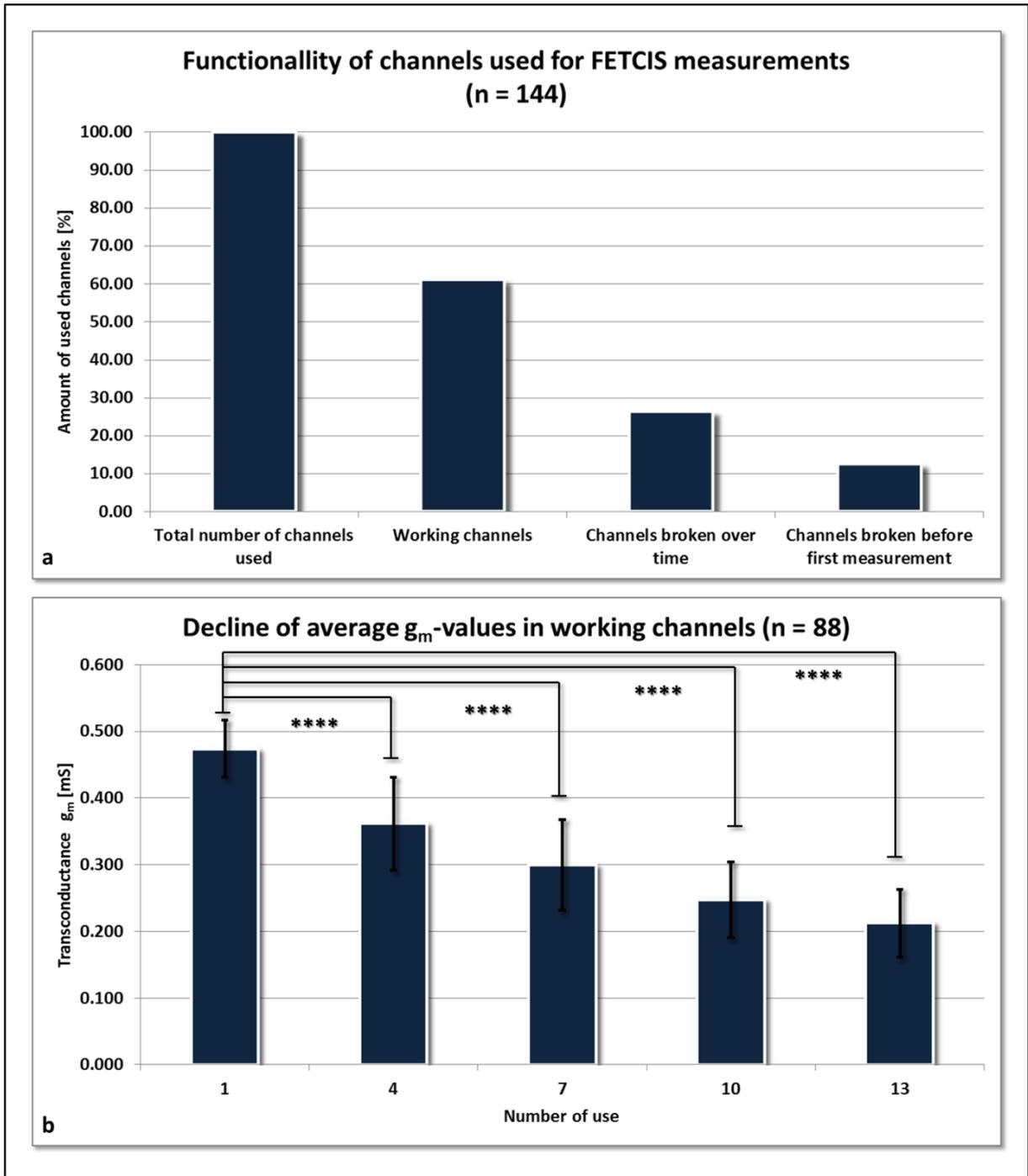
Fig. 28: Deterioration of FET channels used for impedance spectroscopy

a) **Functionality of channels used for FETCIS measurements:** From a total amount of 144 channels 88 channels showed g_m-values above 0.1 mS for all 13 measurements while 38 channels broke down over time (g_m-value dropped below 0.1 mS) and 18 channels were not working from the beginning.

b) **Transconductance deterioration in working channels (n = 88):** over 13 measurement cycles the g_m-value of the used channels dropped 55 % to a g_m-value of 0.21 mS.

$* = P < 0.05; ** = P < 0.01; *** = P < 0.001; **** = P < 0.0001$

3.2   Impedimetric detection of cell adhesion of confluent cell cultures on ISFET surfaces[3]

One of the major topics in this thesis was the analysis of cell adhesion of several morphologically different cell lines in confluent cell layers with the in-house developed FET sensor setup.
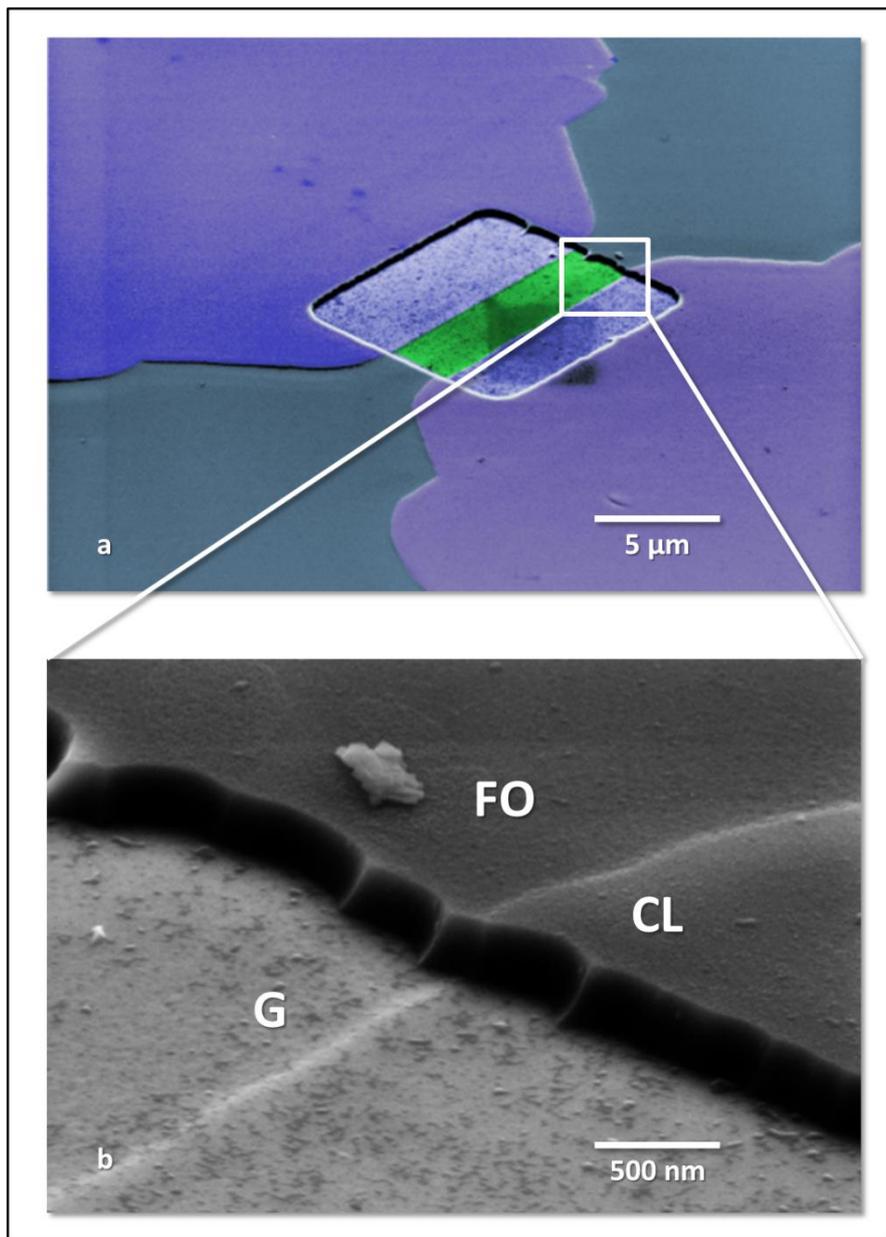
Fig. 29: Close-up images of the planar field-effect transistor surfaces

   a)   **Zoom in to an individual gate contact opening (scanning electron microscopy (SEM), colored).**
   b)   **Only the 220 nm thick opening in the passivation layer at each of the 16 gate contacts is visible in SEM. FO is the field oxide area, CL the contact line area and G the gate area.**

---

[3] Results partially published in Sensors and Actuators, B: Chemical (2015) - Electronic monitoring of single cell-substrate adhesion events with quasi-planar field-effect transistors - Koppenhöfer, D; Susloparova, A; Law, J K Y; Vu, X T; Ingebrandt, S
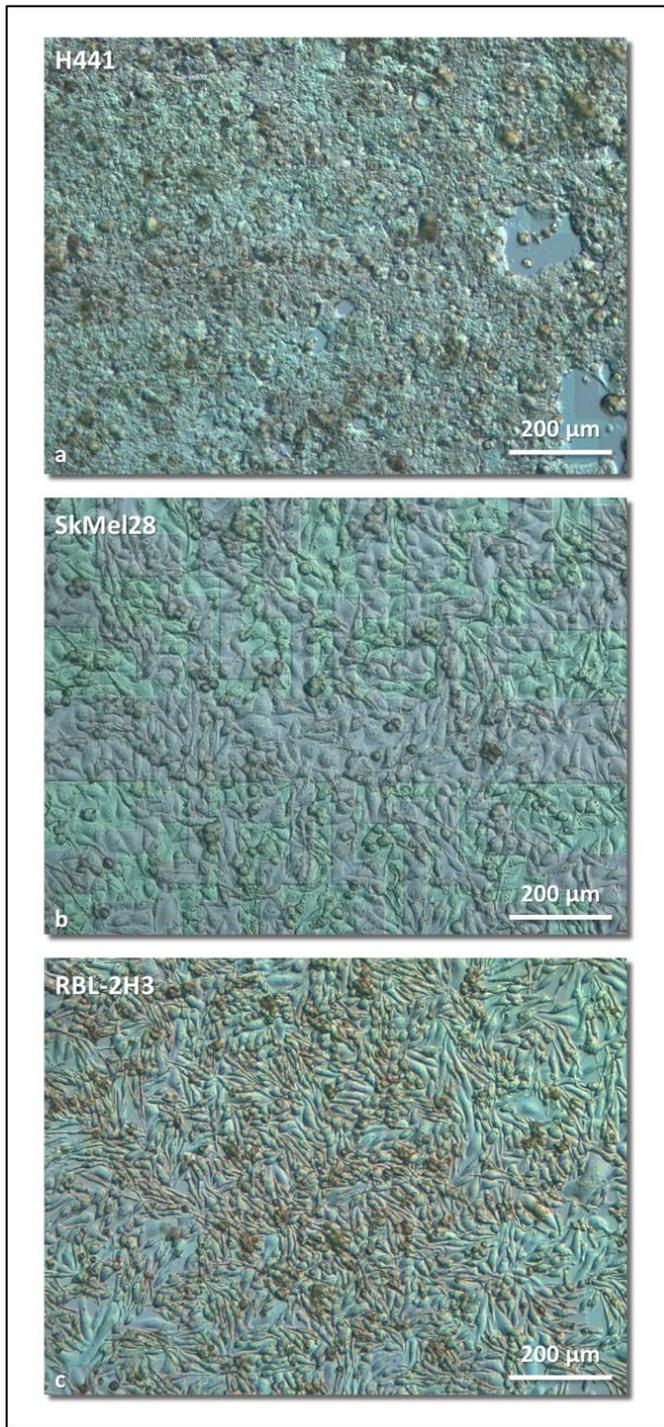
Fig. 30: Confluent cell cultures on fibronectin-coated FET surfaces

All three tested cell lines are covering the 4×4 transistor array in a confluent layer. The different morphologies can be identified from the pictures below:

a) **H441 – epithelial morphology,**
b) **SkMel28 – polygonal morphology,**
c) **RBL-2H3 – small fibroblast like, elongated cells.**

Therefore the cell lines H441 (human papillary adenocarcinoma), SkMel28 (human malign melanoma) and RBL2H3 (murine leukemia) were cultivated in high density cultures on pre-coated ISFET surfaces (protocols provided in chapter 2). All tested cell lines were seeded in a density of 7 500 to 10 000 cells in 50 µl droplets per chip and incubated for 24 hours (37°C, 5 % CO_2) to achieve full coverage of the transistor surface. Microscopic examination of all three used cell lines shows their distinctly different cell morphologies on the ISFET sensor chips, which were all as described in literature. H441 cells were showing an epithelial morphology with relatively small cell bodies while SkMel28 and RBL-2H3 cells showed polygonal and fibroblast like morphology, respectively.

The SkMel28 cells seem to possess the largest cell body of all tested cell lines while the RBL-2H3 cells where developing small and elongated cell bodies.

After incubation the cell-covered chips were characterized according to the protocol described above and set to a working point of maximum transconductance as described in paragraph 2.4.1. All used chips showed a g_m-value of above 0.3 mS (fig. 31).
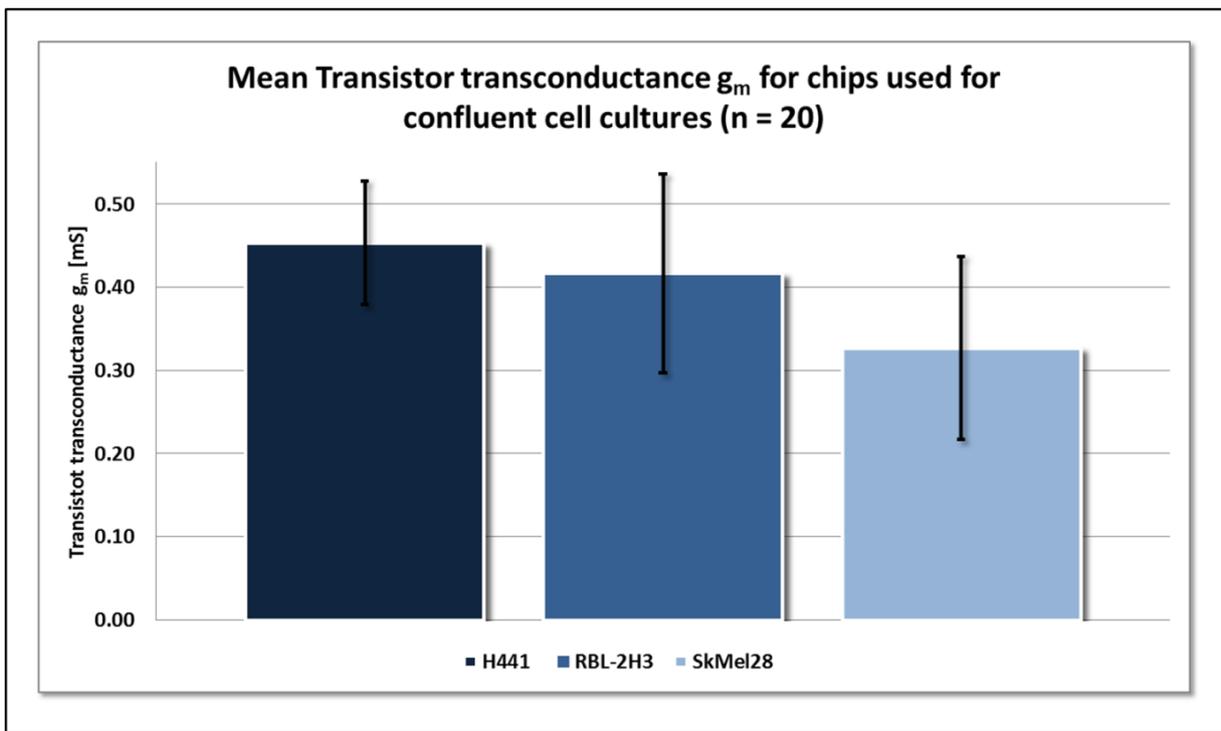
Fig. 31: Average g_m-values (obtained from chip characterization) for cell-covered transistor gates in confluent cell cultures (n = 20)

Statistical analysis of the mean g_m-values of transistor gates covered by different confluent cell cultures did not show any significant difference between the gates used for the individual cell lines. Statistical analysis was done using paired t-test with error bars representing the standard deviation.

Chip characterization was followed by impedance spectroscopy in the frequency range of 1 Hz to 1 MHz as described in the materials and methods section. After trypsinisation impedance spectra were again measured as described in paragraph 2.6.

3.2.1 Impedance spectra of confluent cell layers

All cell lines showed a similar behavior for cell-covered transistor gates, showing a suppression of the transistor-transfer function in a frequency range of 100 kHz to 1 MHz with individual frequency ranges with significant difference in transfer function amplitude for cell-covered and cell-free transistor gates.
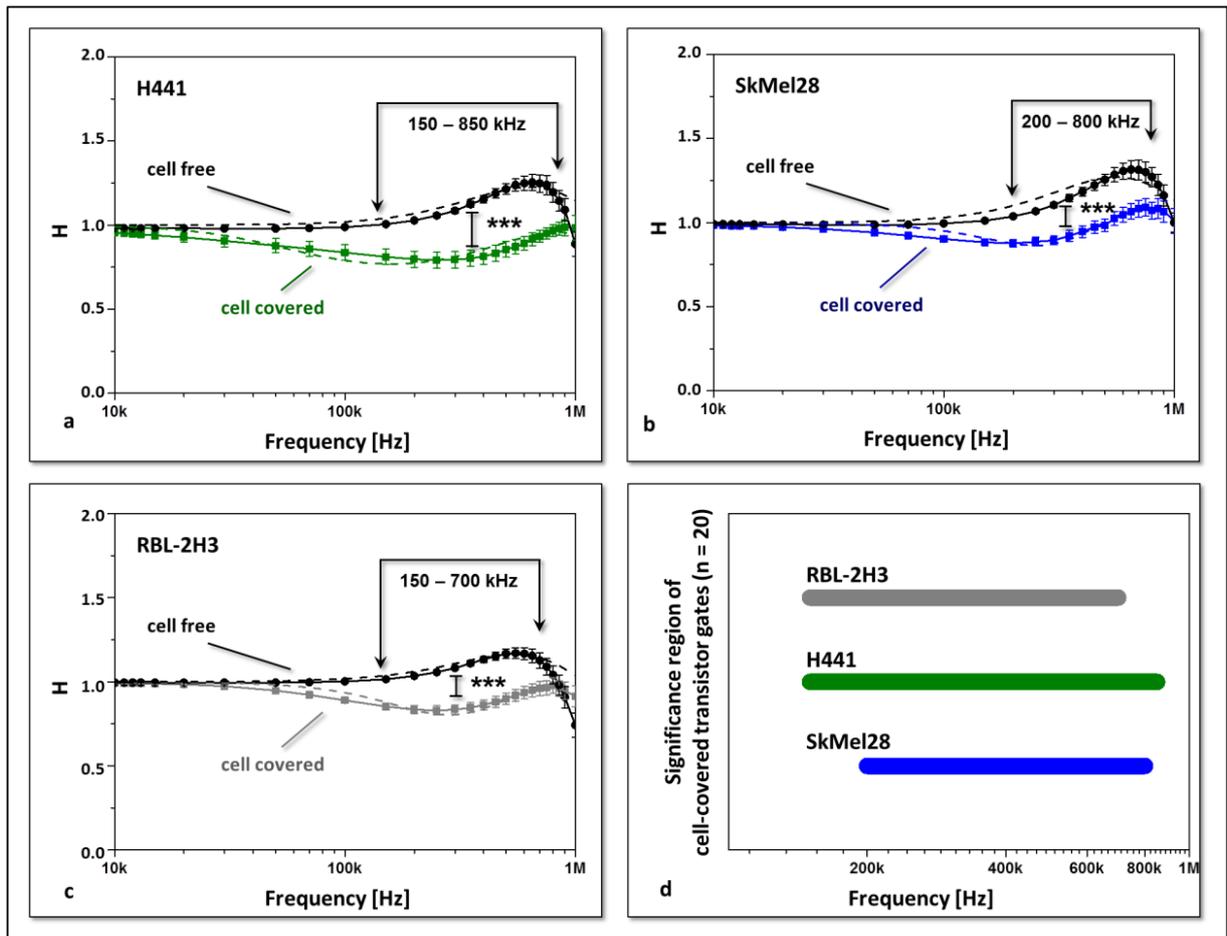
Fig. 32: Average impedance spectra for cell-covered and cell-free transistor gates: Cell-covered chips were used to perform impedance measurements (n =20 individual channels)

a) **H441**
b) **SkMel28**
c) **RBL-2H3**

All cells showed a significant difference between cell-covered and cell-free transistor gates in a frequency range of 150 to 850 kHz (H441), 200 to 800 kHz (SkMel28), and 150 to 700 kHz (RBL-2H3; d). Dotted lines represent fitted data. Statistical analysis was done using two-way ANOVA with error bars representing the standard error. * = P < 0.05; ** = P < 0.01; *** = P < 0.001

Transistor gates without cells show an ascent of the transfer function amplitude starting at around 100 to 150 kHz and becoming steeper till reaching the maximum height at around 800 kHz (fig. 32). Cell-covered transistor gates showed a distinct suppression of the transfer function. This suppression starts between 10 and 20 kHz for confluent cultures of H441 cells and becomes steeper till the amplitude reaches its lowest point between 200 and 300 kHz (fig. 32 a). Transistor gates covered by SkMel28 and cells RBL-2H3 cells showed a comparable behavior with the suppression of the transfer function starting at 20 kHz and reaching its lowest point between 200 and 300 kHz, respectively (fig. 32 b & c). Each tested cell line showed a significant difference between cell-covered and cell free transistor gates ($P <$ 0.001) in an individual frequency range. H441 cells showed a significant difference between cell-covered and cell-free transistor gates in the frequency range of 150 to 850 kHz while SkMel28 cells and RBL-2H3 cells showed a significant difference in the frequency range of 200 to 800 kHz and 150 to 700 kHz, respectively (fig. 32 d).

3.2.2   Analysis of membrane capacity and seal resistance in confluent cell layers

Using the fitting procedure described in chapter 2.6.3 the membrane capacitance C_M and the seal resistance R_{seal} were obtained from the averaged impedance spectra. H441 cells showed the highest value for both R_{seal} and C_M with values of 0.78 pF for C_M and 2.8 MΩ for R_{seal}. SkMel28 and RBL-2H3 cells showed lower values of 0.25 pF and 0.33 pF for C_M and 0.93 MΩ and 0.97 MΩ for R_{seal}, respectively (fig. 33).

3.3   Impedimetric detection of cell adhesion of low density cell cultures on ISFET surfaces[4]

Analysis of individual cellular binding events was conducted using the same technique of measuring the impedance spectra of individual cells to a transistor gate. Therefore SkMel28 cells were cultivated in low density culture on pre-coated ISFET surfaces. Cells were seeded in a density of 750 to 1 000 cells per chip and incubated for 24 hours at 37°C and 5 % CO_2.
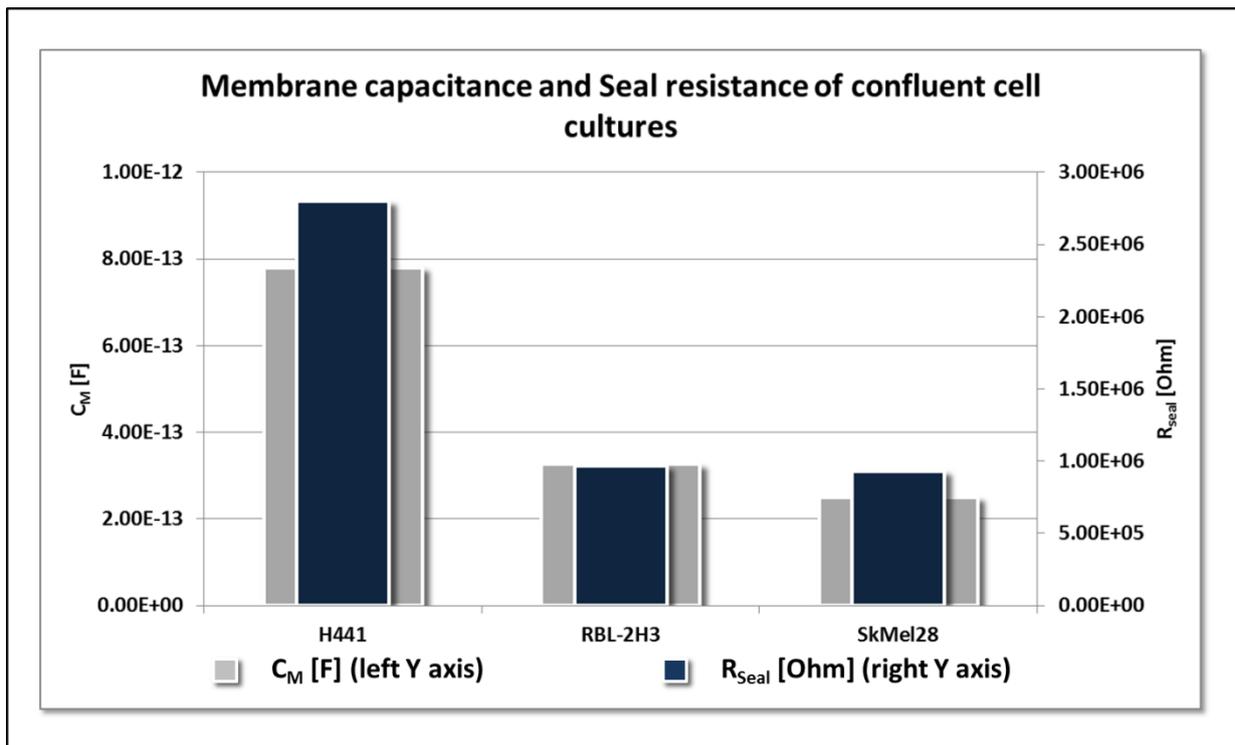
Fig. 33: C_M- and R_{seal}-values for transistor gates covered by confluent cell cultures

C_M- and R_{seal}-values of transistor gates covered by confluent H441, RBL-2H3 and SkMel28 cell cultures were extracted from averaged impedance spectra using the fitting procedure described under 2.9. The lowest membrane capacitance and seal resistance was observable in SkMel28 cells.
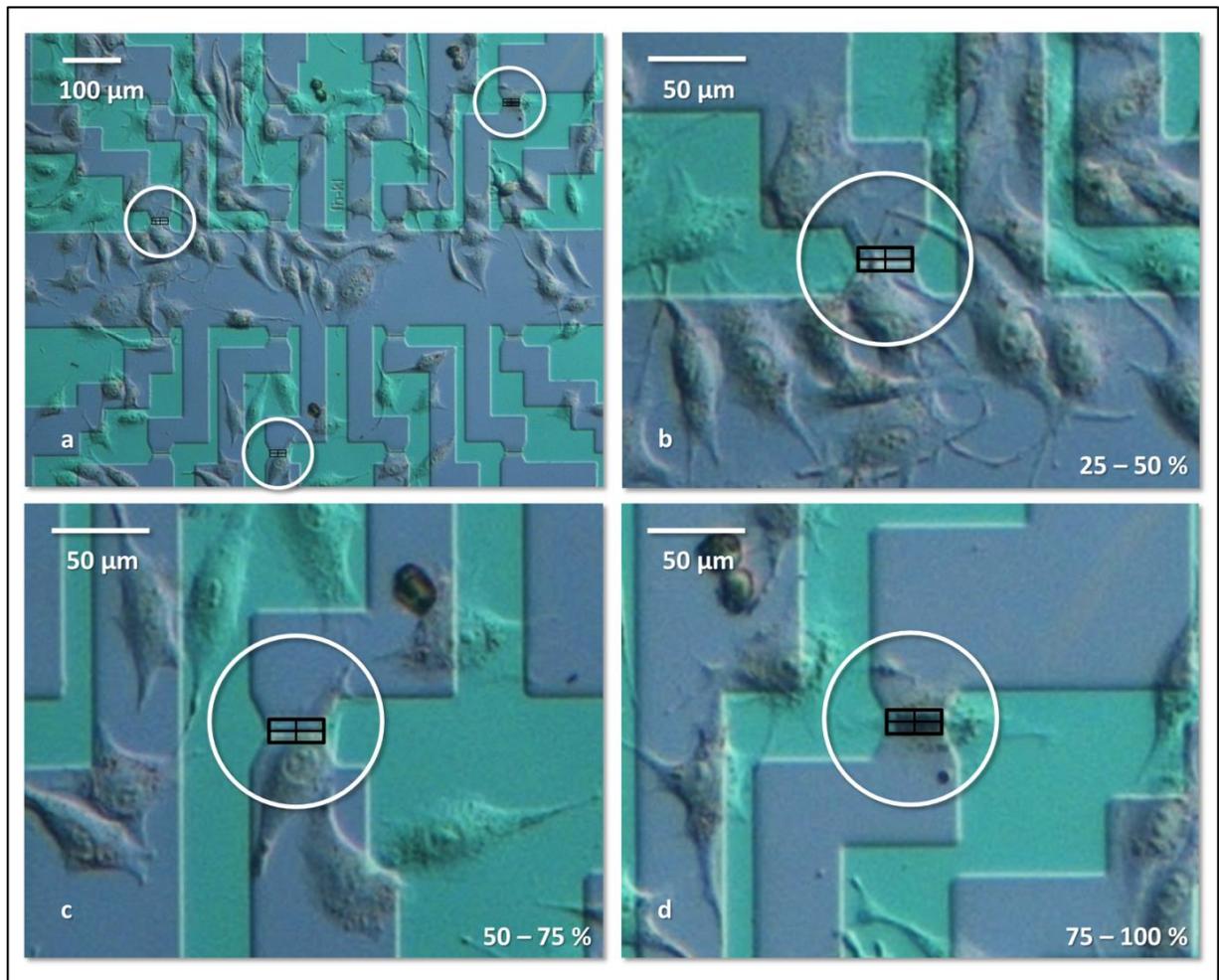
Fig. 34: Low density culture of SkMel28 covering transistor gates:

a) Lowering the density of seeded cells to 1 000 cells per chip leads to individual cells binding on transistor gates;
b) - d) show exemplary pictures of cell-covered transistor gates with different amounts of covered gate area:
> **b) 25 – 50 % gate coverage**
> **c) 50 – 75 % gate coverage**
> **d) 75 – 100 % gate coverage**

After 24 hours cells attached to transistor gates were categorized in three groups according to their area of gate coverage: 25 to 50 % gate coverage, 50 to 75 % gate coverage and 75 to 100 % gate coverage. This was done using a simple grid of four equal rectangles superimposed on top of microscopic pictures of low density cultures of SkMel28 cells (fig. 34).

Chips were characterized according to chapter 2.4.1 followed by impedance spectra measurements for cell-covered and cell-free transistor gates as described in chapter 2.4.2. All used channels showed g_m-values around 0.3 mS (fig. 35).
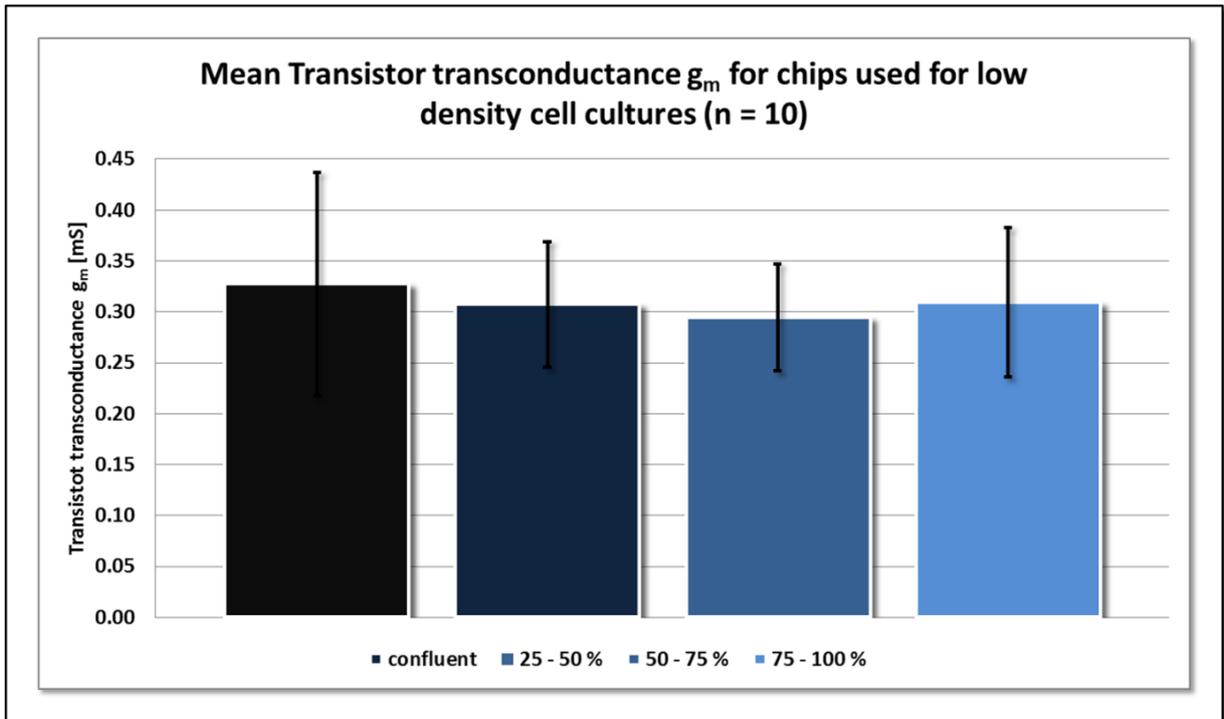
Fig. 35: Average g_m-values (obtained from chip characterization) for cell-covered transistor gates with different percentage of covered gate area (n = 10)

Statistical analysis of the mean g_m-values of transistor gates covered by SkMel28 cells covering different amounts of the transistor's surface did not show any significant difference. Statistical analysis was done using paired t-test with error bars representing the standard deviation.

3.3.1 Impedance spectra of low density cell cultures of SkMel28 cells

Cell-free transistor gates showed an ascent of the transfer function amplitude comparable to confluent cell cultures starting at around 100 kHz and becoming steeper till reaching the maximum height at around 800 kHz (fig. 36).
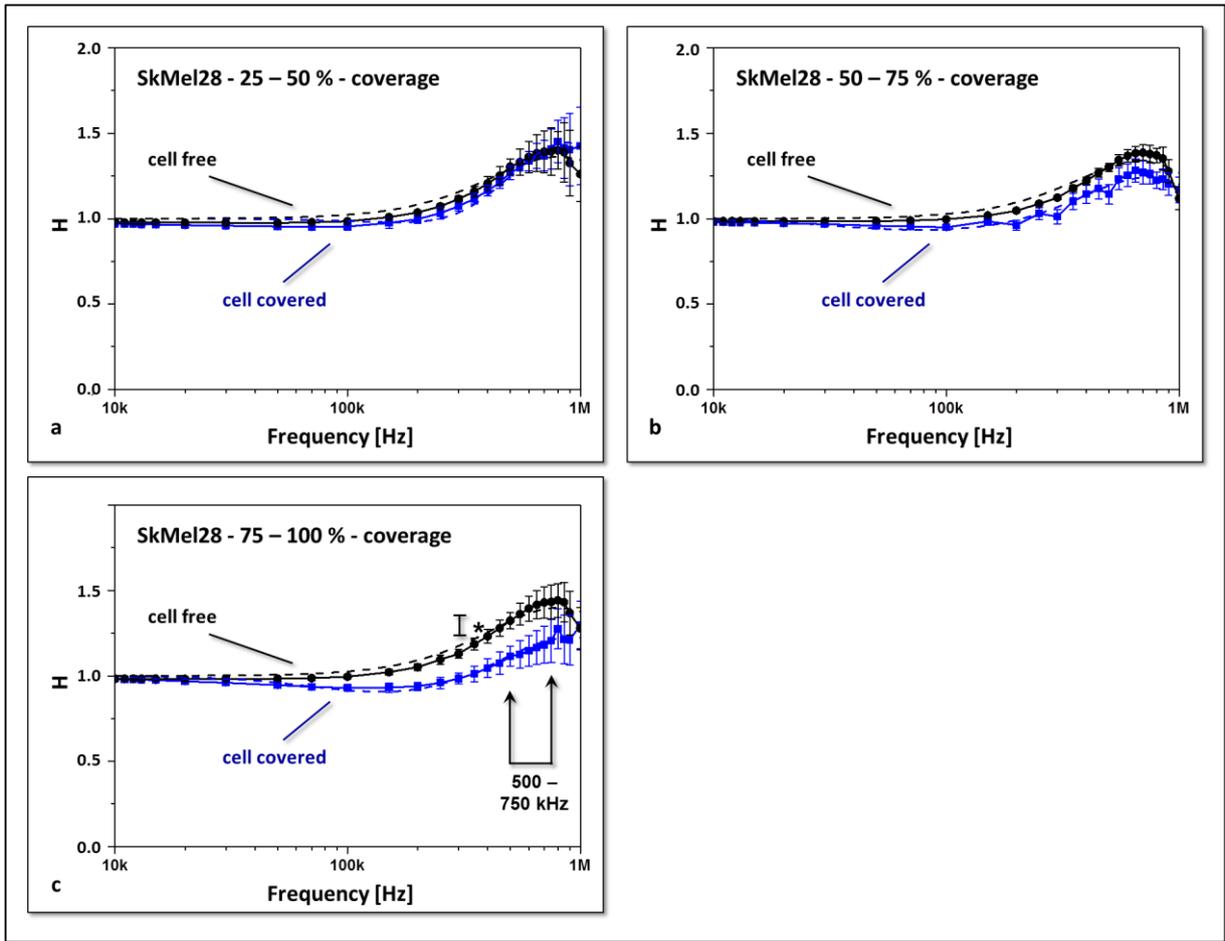
Fig. 36: Average impedance spectra for cell-covered transistor gates with different percentage of covered gate area (n = 10 individual channels)

a) 25 to 50 % gate coverage
b) 50 to 75 % gate coverage
c) 75 to 100 % gate coverage

Different percentage of covered gate area affects the TTF spectra of the respective gates. Tested transistor gates with covered gate area below 75 % did not show discernible differences between cell-covered and cell-free state a) and b). Fully covered transistor gates (75 – 100 %) show a significant difference in the frequency range of 500 to 750 kHz (p < 0.05). Dotted lines represent fitted data. Statistical analysis was done using two-way ANOVA with error bars representing the standard error.

Transistor gates with 25 to 50 % of their respective surface covered by an adhering cell showed no significant suppression of the transfer function. The same observation could be made for 50 to 75 % covered transistor gates with no significance difference between cell-covered and cell-free transistor gates (fig. 36 a & b).

Coverage of transistor gates exceeding 75 % led to a behavior comparable to the behavior of transistor gates covered by confluent cell layers with a significant suppression of the transfer function ($P < 0.05$) in the frequency range of 500 to 750 kHz (fig. 36 c).

Analysis of the differences between cell-covered transistor gates for the individual categories of transistor gate coverage showed significant differences between 25 – 50 % coverage and 50 – 75 % coverage only at four individual frequencies : 500 kHz ($P < 0.05$), 800 kHz ($P < 0.001$), 850 and 900 kHz ($P < 0.05$). Comparison of the categories of 25 – 50 % and 75 – 100 % showed significant differences ($P < 0.01$) for 500 and 550 kHz, in the frequency range of 600 to 900 kHz ($P < 0.001$) and at 1 MHz ($P < 0.05$). Comparison of the categories 50 – 75 % and 75 – 100 % showed no significant differences.
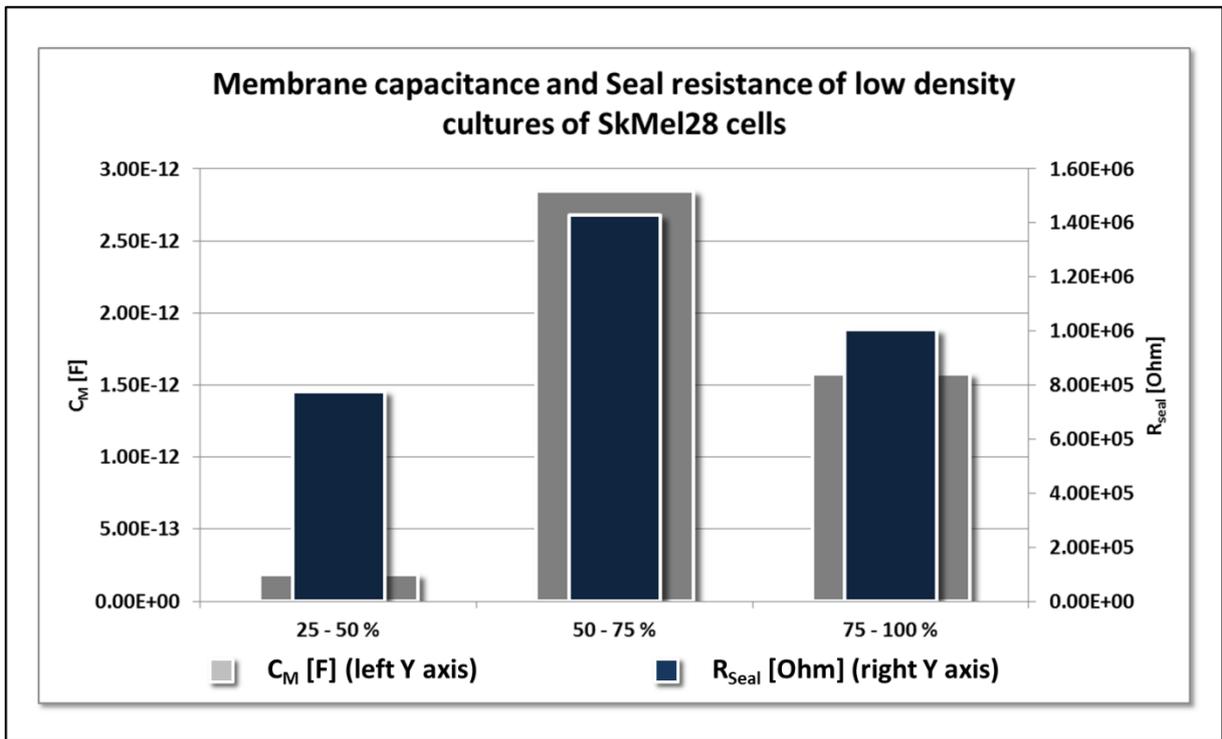
Fig. 37: C_M- and R_{seal}-values for cell-covered transistor gates covered by low density cultures of SkMel28 cells:

C_M- and R_{seal}-values of transistor gates covered by low density cultures of SkMel28 cells were extracted from averaged impedance spectra using the fitting procedure described under 2.9. The lowest membrane capacitance and seal resistance was observable for transistor gates with a gate coverage of 25 – 50 %.

Fig. 37 shows the membrane capacitance and seal resistance values for the three tested categories of gate coverage obtained from the data fitting of their respective impedance spectra. The membrane capacitance C_M was lowest for the category of 25 – 50 % as was the seal resistance R_{seal} with 0.186 pF and 0.78 MΩ, respectively. 50 – 75 % gate coverage lead to C_M and R_{seal} values of 2.85 pF and 1.43 MΩ while 75 – 100 % gate coverage showed C_M and R_{seal} values of 1.58 pF and 1.00 MΩ.

3.4   Impedimetric analysis of the nanotoxicity of the industrial nanoparticles NexSil20[5]

3.4.1   Analyzing the cytotoxicity of Nexsil20 nanoparticles using MTT-Assays

With the help of the FET system the cytotoxic effects of NexSil20 nanoparticles was analyzed using impedimetric analysis of cell adhesion as a marker of cell viability. Before impedimetric measurements were done the toxicity of the tested particle was assessed using MTT assays. For this purpose H441 cells, SkMel28 cells and EG 463 cells were seeded as described in the materials and methods section.

After incubation MTT assays were conducted using two different particle concentrations. A high concentration of 600 µg/ml (4.4 * 10^{13} particles/ml) and a low concentration 60 µg/ml (4.4 * 10^{12} particles/ml) were chosen according to a previous publication of Prof. Dr. Stauber's group (Kasper *et al.*, 2011). Both tested concentrations were already reported to cause a reduction of cell viability for the high concentration and to cause no significant loss of cell viability of for the lower concentration (Kasper *et al.*, 2011).

Treatment with the used nanoparticles caused drastic changes of the cell morphology. Treatment with the high particle concentration (600 µg/ml) led to cellular detachment and a generally round cell shape. Figure 37 shows the effect of the nanoparticle treatment on

---

[5] Results partially published in Results partially published in Biosensors & bioelectronics (2012) - *Monitoring nanoparticle induced cell death in H441 cells using field-effect transistors.* - Koppenhöfer, D; Susloparova, A; Docter, D; Stauber, R H; Ingebrandt, S

H441 cells. Before nanoparticle exposure, the cells grew in a dense and confluent culture and showed epithelial morphology. After 30 minutes of exposure, however the cells started to swell and turn round. These morphological changes indicated beginning cell damage.
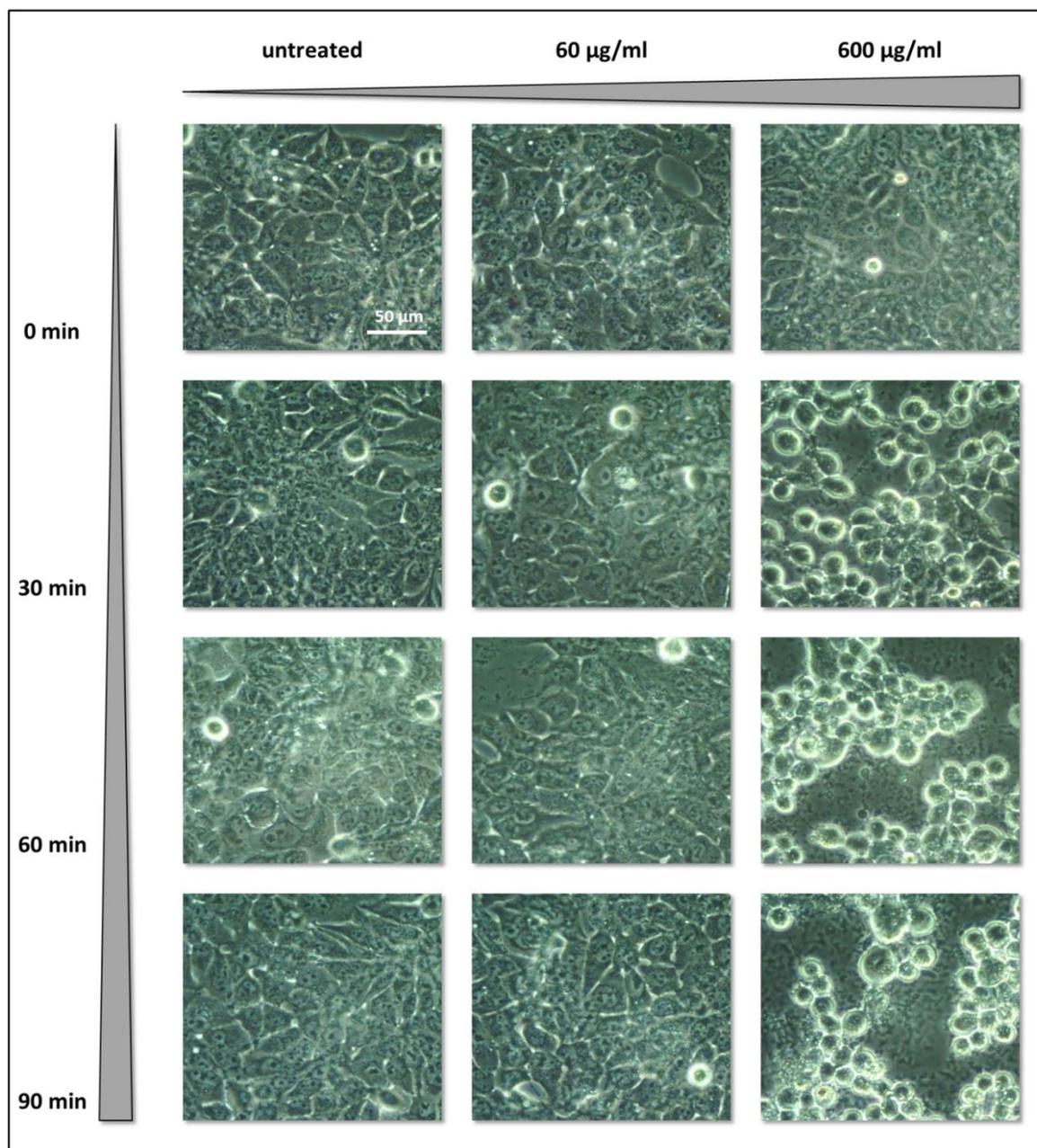
Fig. 38: Morphological changes in H441 cells induced by nanoparticle exposure

Treatment of H441 cells with NexSil20 particles causes concentration dependent cell damage. A dose of 600 µg/ml of nanoparticles caused swelling and partial detachment from the substrate. A lower dose of 60 µg/ml caused no effect.

Over the next hour of exposure all cells in the culture turned round and partially detached from the surface. After 90 minutes the cells were completely detached from the well surface and showed round and swollen cell morphology. Cellular debris is clearly visible (fig. 37).

To avoid particle aggregation and the formation of a protein corona, MTT assays were conducted for 6 hours in serum free medium with measurement points every hour. MTT-assays were conducted for 6 hours in serum free medium to avoid particle aggregation with measurement points every hour. For every experiment the number of independent cell cultures n = 4, while each n consists of 6 repeats and one blank measurement.
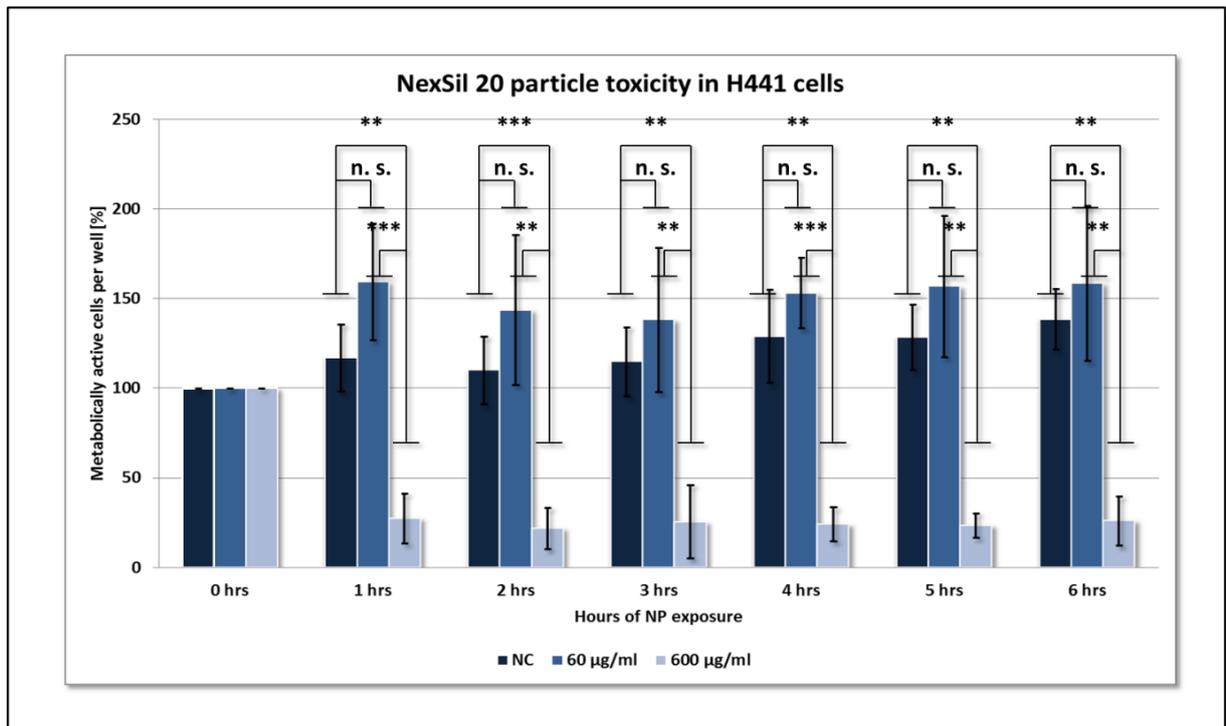
Fig. 39: Cytotoxicity of NexSil20 particles in H441 cells (n = 3 independent MTT assays)

A dose of 600 µg/ml of nanoparticles caused reduction of viable cells/well from 100 % before particle administration to 27.6 % after 1 hour, 25.6 % after 3 hours and 26.2 % after 6 hours. * = P < 0.05; ** = P < 0.01; *** = P < 0.001

Treatment with a particle concentration of 600 µg/ml showed a significant reduction of viable cells/well in H441 cells from 100% before particle administration (0 hours) to 27.6 % after 1 hour, 25.6 % after 3 hours and 26.2 % after 6 hours. Both the untreated control and cells treated with the lower particle concentration showed no significant reduction in cell

viability over time. Comparison of particle treatment with 60 µg/ml and 600 µg/ml showed significant differences (P < 0.01) for all measured time points (fig. 39). EG463 cells treated with the same particle concentration (600 µg/ml) showed a similar drop of cell viability from 100 % (0 hours) to 36.4 % after 1 hour, 19.2 % after 3 hours and 23.3 % after 6 hours. Treatment with the low particle concentration again did not lead to a significant reduction of cell viability. Additionally, there was no significant difference between treatment with 60 and 600 µg/ml in EG463 cells (fig. 40).
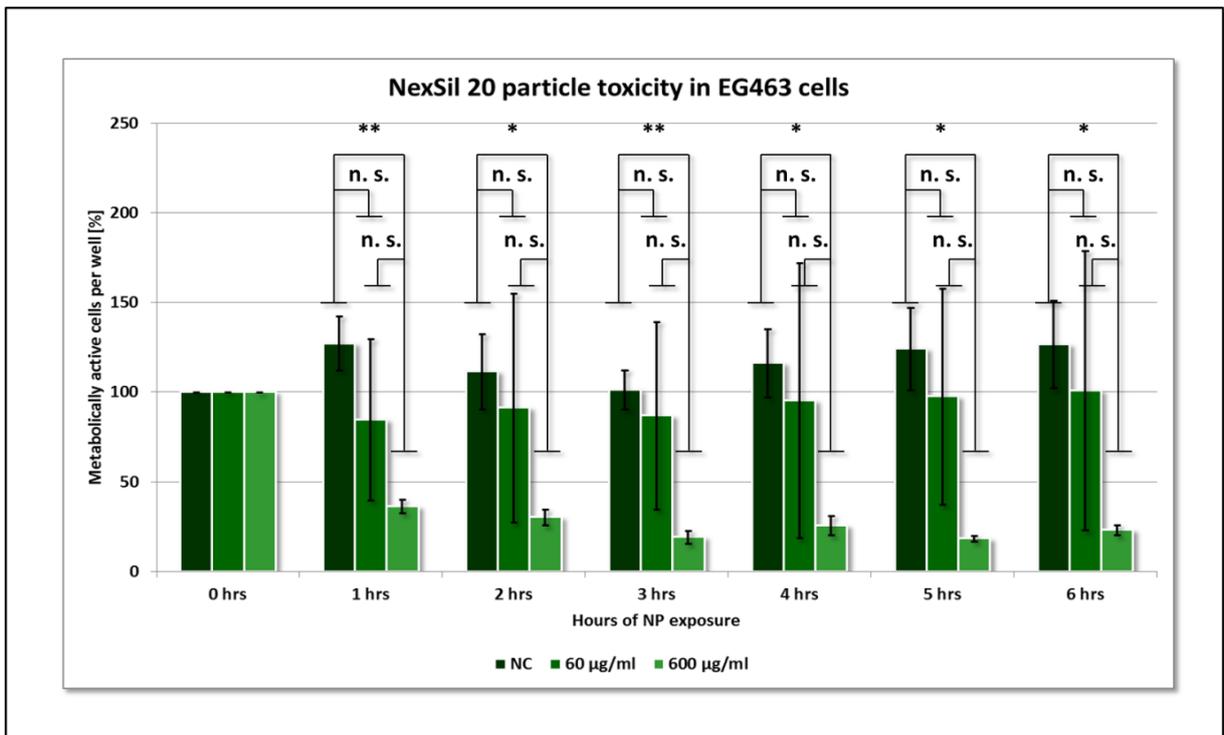
Fig. 40: Cytotoxicity of NexSil20 particles in EG463 cells (n = 3 independent MTT assays)

A dose of 600 µg/ml of nanoparticles caused reduction of viable cells/well from 100 % before particle administration to 36.4 % after 1 hour, 19.2 % after 3 hours and 23.3 % after 6 hours. * = P < 0.05; ** = P < 0.01; *** = P < 0.001

SkMel28 cells showed a much weaker effect of particle treatment for the high concentration of 600µg/ml with a reduction of cell viability from 100 % (0 hours) to 92.6 % after 1 hour, 84.8 % after 3 hours and 70 % after 6 hours. Treatment with the low particle concentration again did not lead to a significant reduction of cell viability. Additionally there was no significant difference between treatment with 60 and 600 µg/ml in SkMEl28 cells (fig. 41).
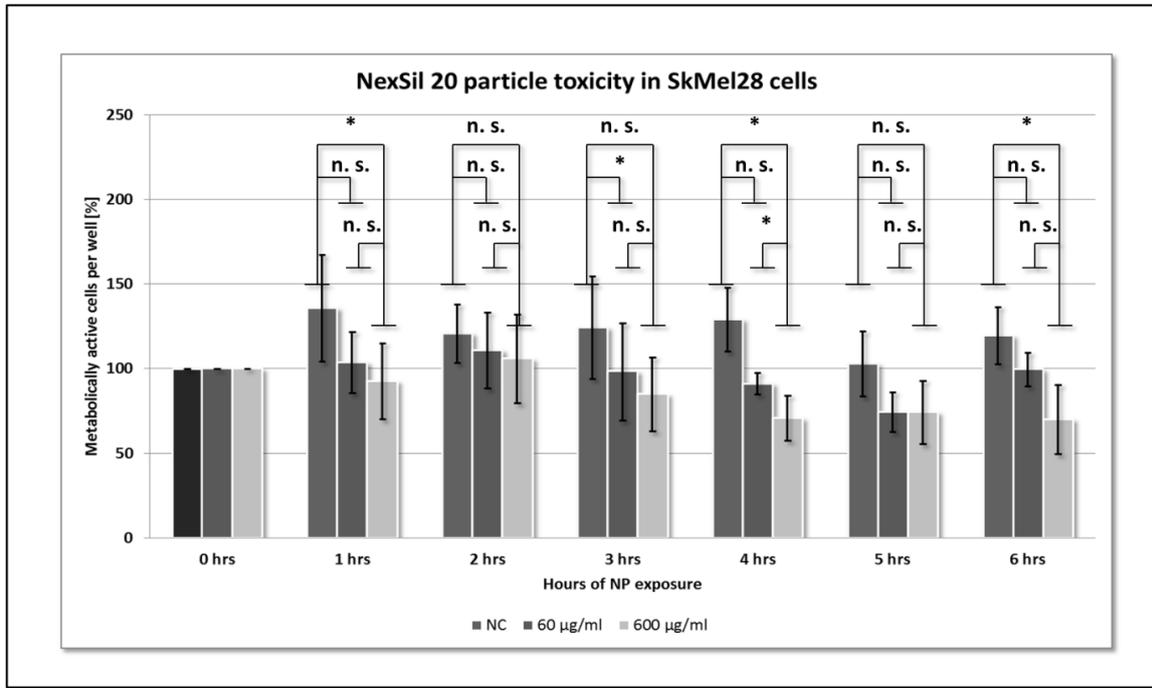
Fig. 41: Cytotoxicity of NexSil20 particles in SkMEl28 cells (n = 3)

A dose of 600 µg/ml of nanoparticles caused reduction of viable cells/well from 100 % before particle administration to 92.6 % after 1 hour, 84.8 % after 3 hours and 70 % after 6 hours. * = P < 0.05; ** = P < 0.01; *** = P < 0.001
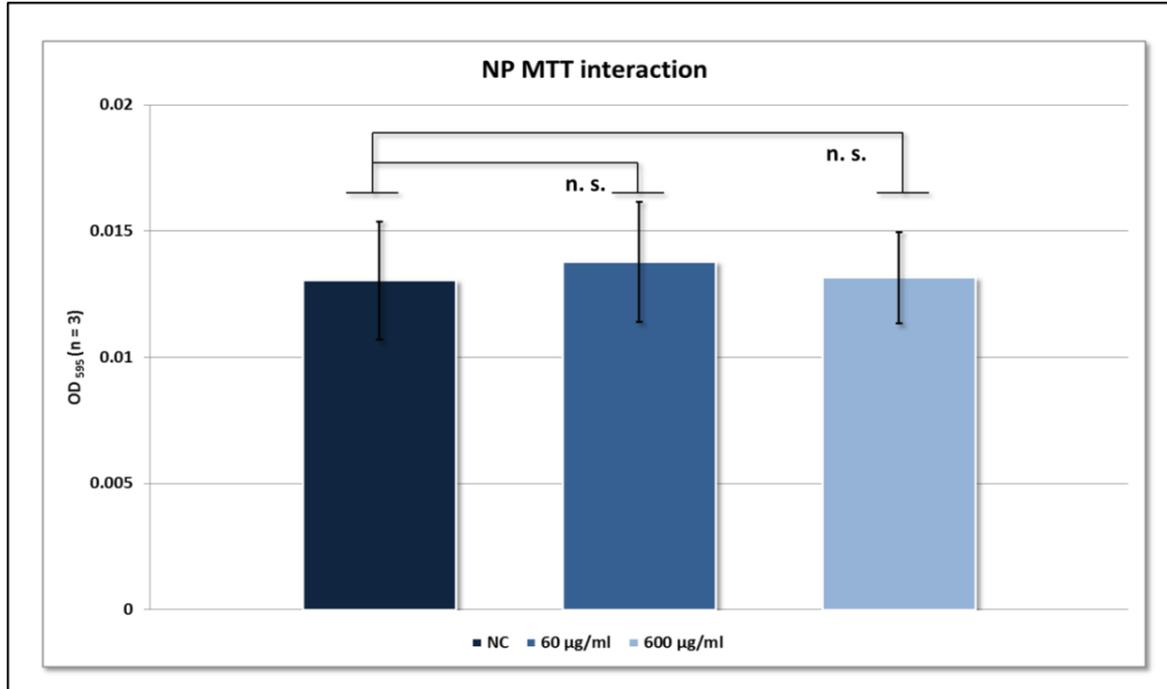
Fig. 42: Influence of NexSil20 particles on MTT assays (n = 3)

Presence of the NexSil20 particle did not lead to any significant impairment of the MTT assay.

To guarantee that the experiments have not been compromised by any possible interaction between the nanoparticles and the MTT reagent, control experiments using the same procedures and particle concentrations as mentioned for the cytotoxicity assays but without cells were conducted.

Presence of MTT reagent did not affect the applicability of the MTT assay as there were no discernable difference between the tested particle concentrations and the untreated control (n = 3, each n consisting of 12 repeats, Fig. 42).

Because of the severe effect of the tested particles after 1 hour of exposure, the effects of NexSil20 were analyzed impedimetrically with the ISFET sensors using real-time measurements under culture conditions (37°C, 5% CO_2). The main advantage is that a much higher time-resolution can be obtained in these experiments

3.4.2   Time series measurements of nanoparticle toxicity using ISFETs

H441 cells, SkMel28 cells and EG463 cells were used for the impedimetric assessment of nanoparticle toxicity. Therefore confluent cell cultures of these three cell lines were created on pre-coated transistor chips and cultivated for 24 hours (36° C, 5 % CO_2) until they reached full confluency (fig. 43).

After cultivating the cells for 24 hours, chips with attached cells were set to a working point of maximum transconductance. Following chip characterization, impedance spectra were measured to pick an optimal frequency for real-time measurements. Such real-time transfer function measurements were performed inside of the incubator under cell culture conditions (37°C, 5% CO_2) with each chip being measured for 2 hours. A constant frequency of 200 kHz was selected for measurements based on the impedance spectra analysis of H441 cells.

Measurements were performed using both high (600 µg/ml) and low (60 µg/ml) nanoparticle concentrations for cell-covered chips, cell-free chips with and without particle containing medium (600 µg/ml) and for cell-covered chips without nanoparticle exposure with n being 3 for all measurements presented in figure 44.
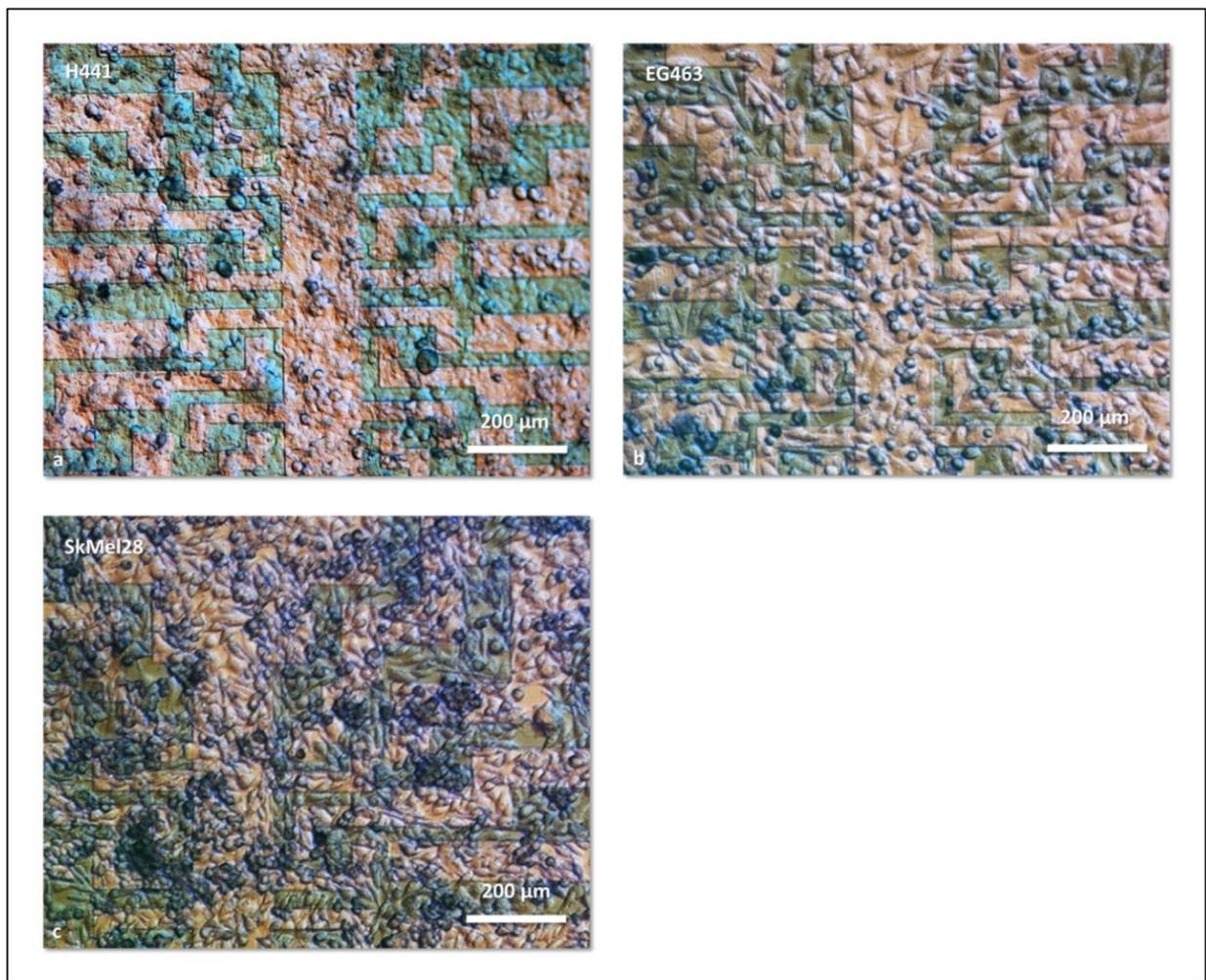
Fig. 43: FET surface covered by confluent cell cultures

    a)   **H441 cells**
    b)   **EG-463 cells**
    c)   **SkMEL28 cells**

Cells were seeded in a density of 5 000 to 10 000 cells per chip and cultivated for 24 hours (37°C, 5 % CO_2).

Cell-free chips treated with both particle concentrations (60 µg/ml and 600 µg/ml) showed almost no effect in their respective spectra (fig. 44 a).

The presence of the nanoparticle itself does not seem to affect the transfer function of the transistor gates as the real-time measurements showed a straight course for all tested channels with and without particles for the whole duration of 2 hours (fig. 44 a). Untreated cell cultures were used as negative control. Over the course of the measurement the negative control showed fluctuations of the transfer function signal (Fig. 44 b) with H441 cells showing the strongest fluctuations. It should be noted that the time courses contain fast spike artefacts due to a failure in the readout electronics. To analyze the data one should focus on the baseline variations only.

Figure 44 c shows the effects of low dose nanoparticle exposure in all three tested cell lines. A slight increase of the signal amplitude was observable for SkMel28 cells but not for H441 and EG463 cells. Treatment with the high dose of nanoparticles (600 µg/ml) resulted in an increase of the signal amplitude in the first 30 minutes of nanoparticle exposure for H441 cells and EG463 cells (fig. 44 d). As seen in figure 44 e the signal increase is not smooth but characterized by a fluctuating shape. After the increase of the transfer function amplitude all three cell lines showed a nearly straight course for the rest of the measurement (with observable fast spike artefacts in SkMel28 cells).
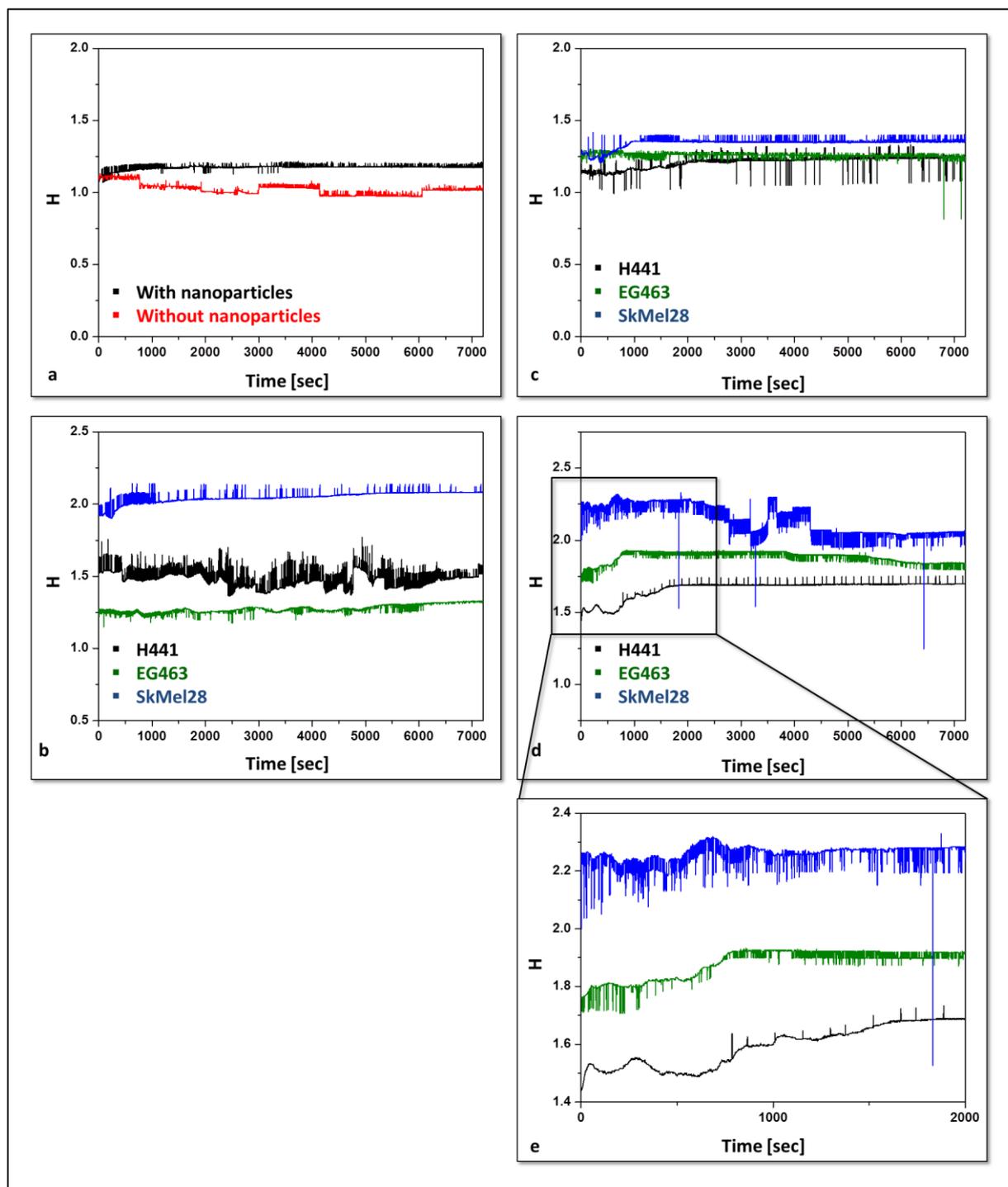
Fig. 44: Real-time transistor-transfer function measurements of cell-covered FET chips

a) Cell-free transistor gates with and without nanoparticles (600 µg/ml; negative control)
b) Cell-covered transistor gates without nanoparticle exposure in all 3 tested cell lines (positive control for viable cells)
c) Particle treatment (60 µg/ml) of H441, EG463 and SkMel28 cells (2 hours)
d) Particle treatment (600 µg/ml) of H441, EG463 and SkMel28 cells (2 hours)
e) Particle treatment (600 µg/ml) of H441, EG463 and SkMel28 cells (30 minutes, close up of d)

Each shown impedance profile represents an average of 3 individual cell covered channels. Standard errors were in the range of 0.16and 0.02 for measurements with and without particles (a); 0.2, 0.04 and 0.09 for untreated cells (b); 0.07, 0.12 and 0.03 for 60 µg/ml (c); 0.06, 0.09 and 0.13 for 600 µg/ml (d & e) in H441, EG463 and SkMel28 cells, respectively.

3.5   Impedimetric detection of cell adhesion of primary neuronal tissues on ISFET surfaces[6]
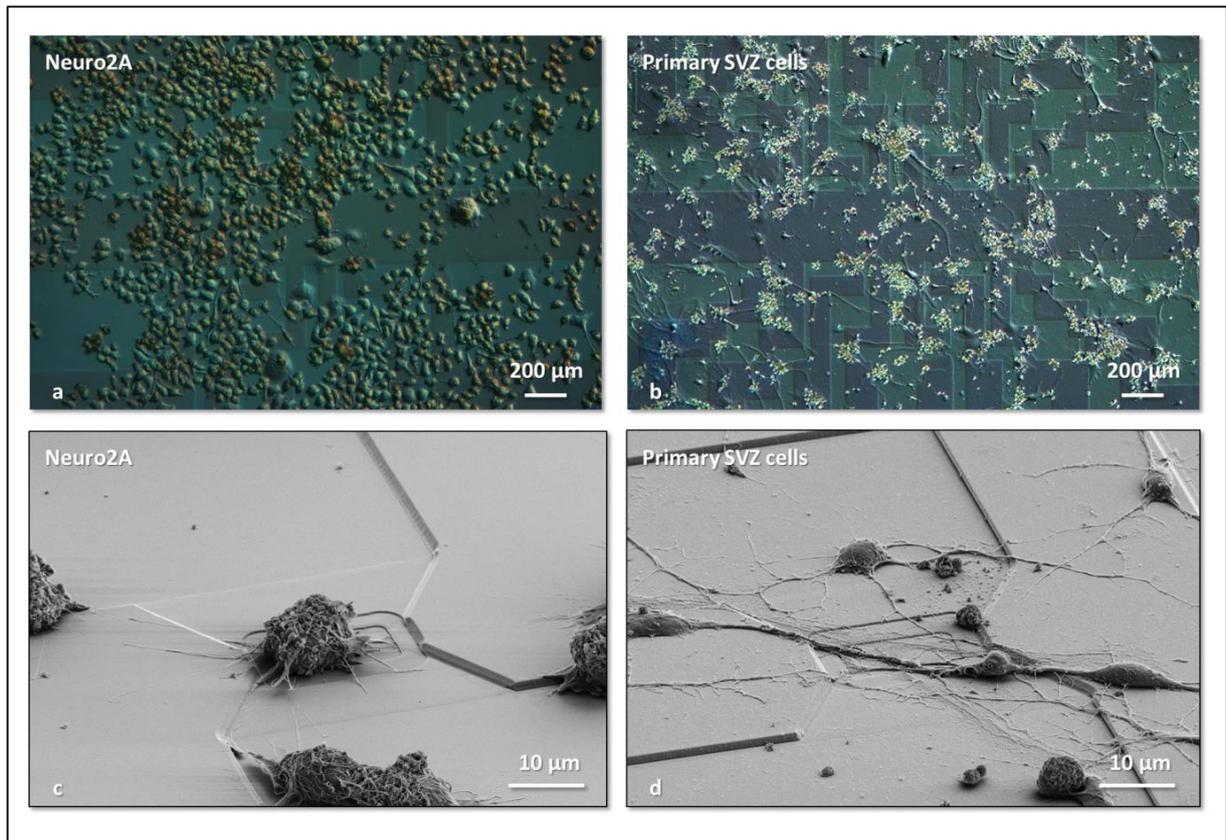
Fig. 45: Microscopic documentation of Neuro2A and primary SVZ cells on coated FET surfaces

a) **Neuro2A cells on fibronectin coated FET surface (reflected-light microscope)**
b) **Primary SVZ cells on PDL/laminin coated FET surface (reflected-light microscope)**
c) **Neuro2A cell on fibronectin coated transistor gate (SEM)**
d) **Primary SVZ cell on PDL/laminin coated transistor gate (SEM)**

The general applicability of the presented method and the associated system for studying pharmacological concepts for primary neuronal tissue was tested as a part of this thesis. To do so primary cells from the subventricular zone of 3 days old BALB/c mice and the established cell line Neuro2A were used for impedimetric analysis of cell adhesion. So far comparable metal electrode based systems are not able to provide a fast way of analyzing the adhesion (and thereby viability) of individual neuronal cells.

---

[6] Results published in Biosensors & bioelectronics (2014) - *Neurodegeneration through oxidative stress: Monitoring hydrogen peroxide induced apoptosis in primary cells from the subventricular zone of BALB/c mice using field-effect transistors.* - Koppenhöfer, D; Kettenbaum, F; Susloparova, A; Law, J K Y; Vu, X T; Schwab, T; Schäfer, K H; Ingebrandt, S

Neuro2A cells and primary SVZ cells were cultivated on fibronectin and PDL/laminin pre-coated FET chips, respectively (fig. 45 c & d). Primary SVZ cells were cultivated on chip for 7 days to allow for full cell differentiation before measurements were conducted, Neuro2A cells acted as a control.
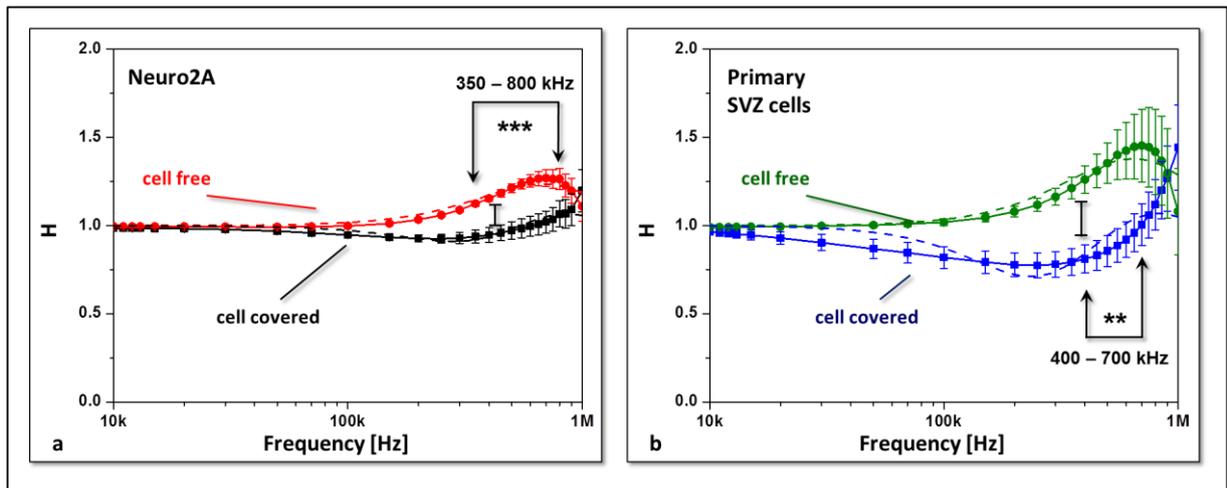
Fig. 46: Average impedance spectra of Neuro2A and primary SVZ cells (n = 20)

Impedance spectra measurements showed a significant difference between cell-covered and cell-free transistor gates for Neuro2A cells and primary SVZ cells within a frequency range 350 to 800 kHz (P < 0.001) and 400 to 700 kHz (P < 0.01), respectively. * = P < 0.05; ** = P < 0.01; *** = P < 0.001

Impedance spectroscopy of both cell types showed the already described ascent of the transistor-transfer function for cell-free transistor gates. Both cell types showed a characteristic suppression of the transfer function for cell-covered transistor gates (fig. 46 a & b). All used chips showed a g_m-value of around 0.3 mS (fig. 47), guaranteeing their correct operation.
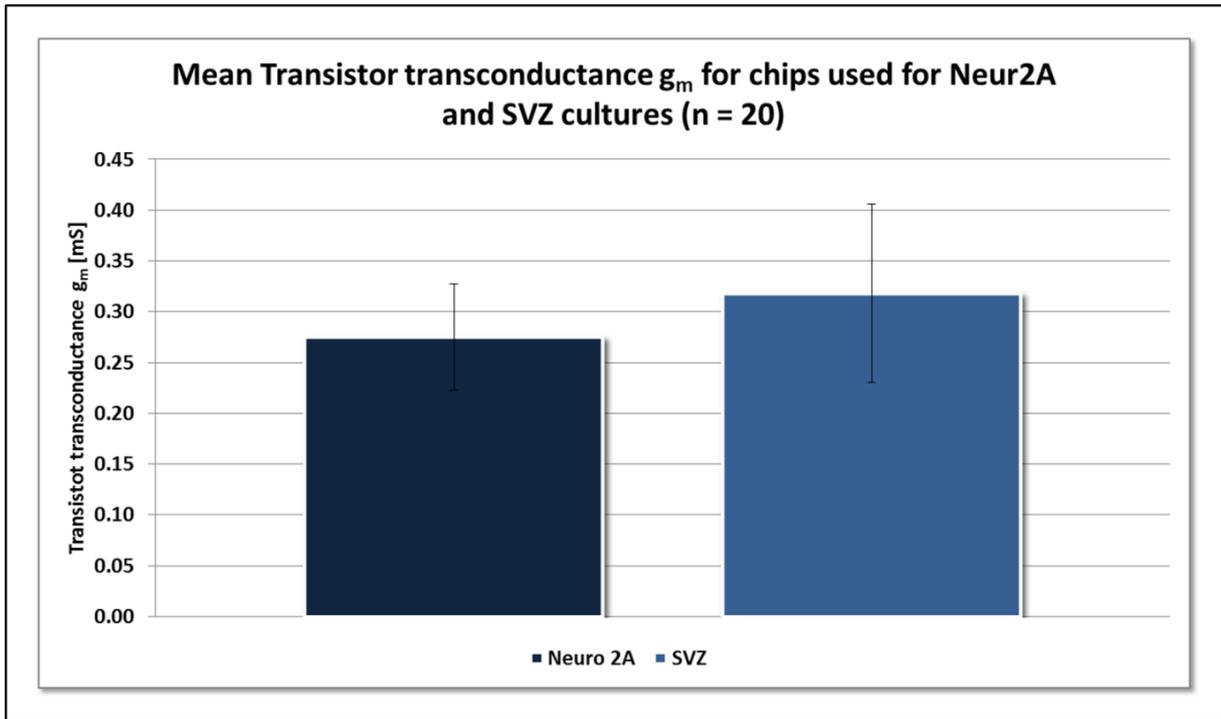
Fig. 47: Average g_m-values (obtained from chip characterization) for cell-covered transistor gates with (n = 20)

Statistical analysis of the mean g_m-values of transistor gates covered by Neuro2A and primary SVZ cells did not show any significant difference. Statistical analysis was done using paired t-test with error bars representing the standard deviation.

The transfer function of cell-covered transistor gates started to drop at around 50 kHz for Neuro2A cells and at 10 kHz for primary SVZ cells reaching the lowest level between 200 and 300 kHz for both tested cell types. Both impedance spectra showed a characteristic decrease in their amplitude for cell-covered transistor gates with a more prominent decrease visible for primary SVZ cells. In the frequency range of 350 to 800 kHz and 400 to 700 kHz a significant difference (P < 0.001) was observable for both Neuro2A and primary SVZ cells respectively (fig. 46).

Data fitting of the impedance spectra of Neuro2A and primary SVZ cells yielded information concerning the seal resistance R_{seal} and the membrane capacitance C_M. Primary SVZ cells and Neuro2A cells showed a membrane capacitance C_M of 0.22 pF and 0.54 pF and a seal resistance R_{seal} of 1.62 MΩ and 0.56 MΩ, respectively (fig. 48).
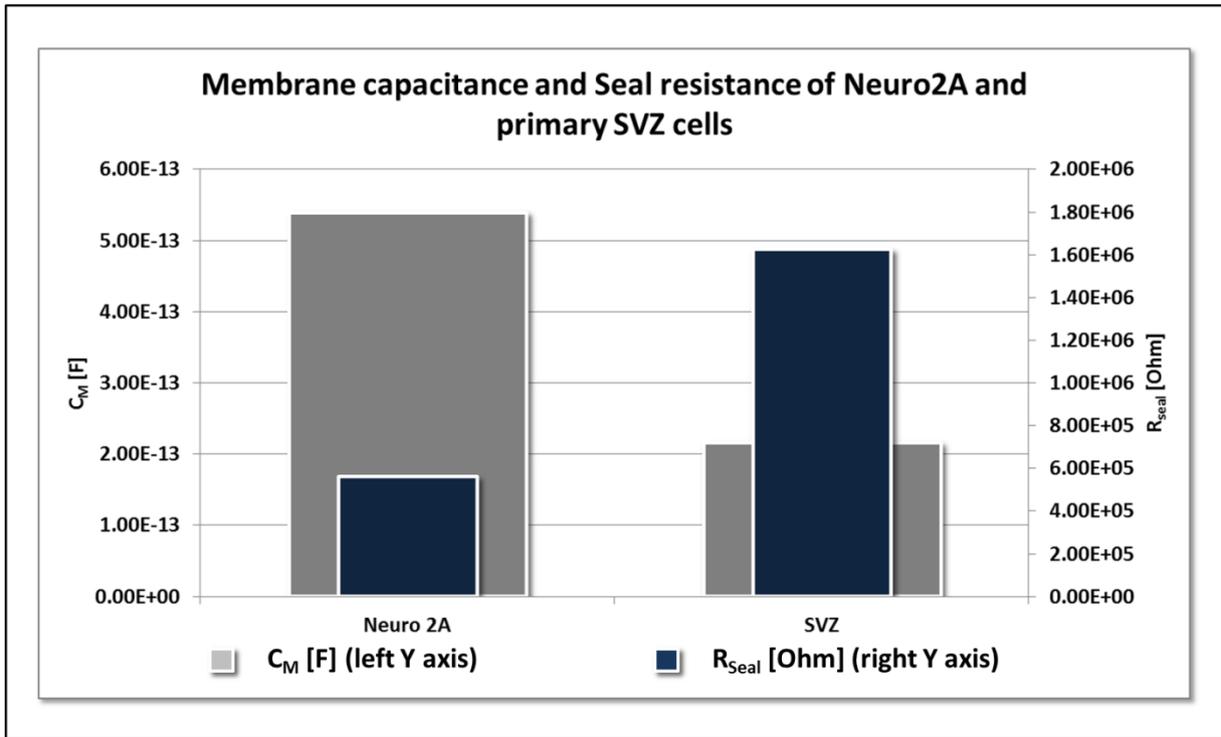
Fig. 48: C_M- and R_{seal}-values for transistor gates covered by Neuro2A and primary SVZ cells

C_M- and R_{seal}-values of transistor gates covered by Neuro2A and primary SVZ cells were extracted from averaged impedance spectra using the fitting procedure described under 2.9. Neuro2A cells showed a lower seal resistance (with 0.56 MΩ and 1.62 MΩ, respectively) and higher membrane capacitance compared to primary SVZ cells (with 0.54 pF and 0.22 pF, respectively).

3.6   Impedimetric analysis of neurodegeneration caused by oxidative stress in primary neuronal tissues

3.6.1   Hydrogen peroxide toxicity in cell culture medium and in HBSS

After first impedimetric measurements with primary neuronal tissue (SVZ) and Neuro2A cells were done analyzing the adhesion of these cell types, the toxicity of hydrogen peroxide (H_2O_2) was analyzed impedimetrically. As a control MTT assays were conducted using both cell types to assess the cytotoxicity of H_2O_2 and find the minimal cytotoxic concentration of H_2O_2 to be used for impedimetric measurements with the FET sensors.

MTT assays were conducted for both cell types in medium according to the protocol mentioned in chapter 2.2.2. Cells were then treated with culture medium containing various concentrations of hydrogen peroxide ranging from 50 mM to 10 µM, incubated under cell

culture conditions overnight and subsequently tested following the protocol for MTT assays described in chapter 2.2.2.

Neuro2A cells showed a significant drop of cell viability to around 65 % (P < 0.001) when treated with 1 mM H_2O_2 and to below 10 % compared to an untreated control only if treated with H_2O_2 concentrations above 10 mM (P < 0.001, fig. 49). Primary SVZ cells showed a similar behavior with a significant reduction of cell viability to 79.9 % for 10 mM H_2O_2 solution (P < 0.001) and to -2.7 % for 50 mM H_2O_2 solution (P < 0.001, fig. 49).
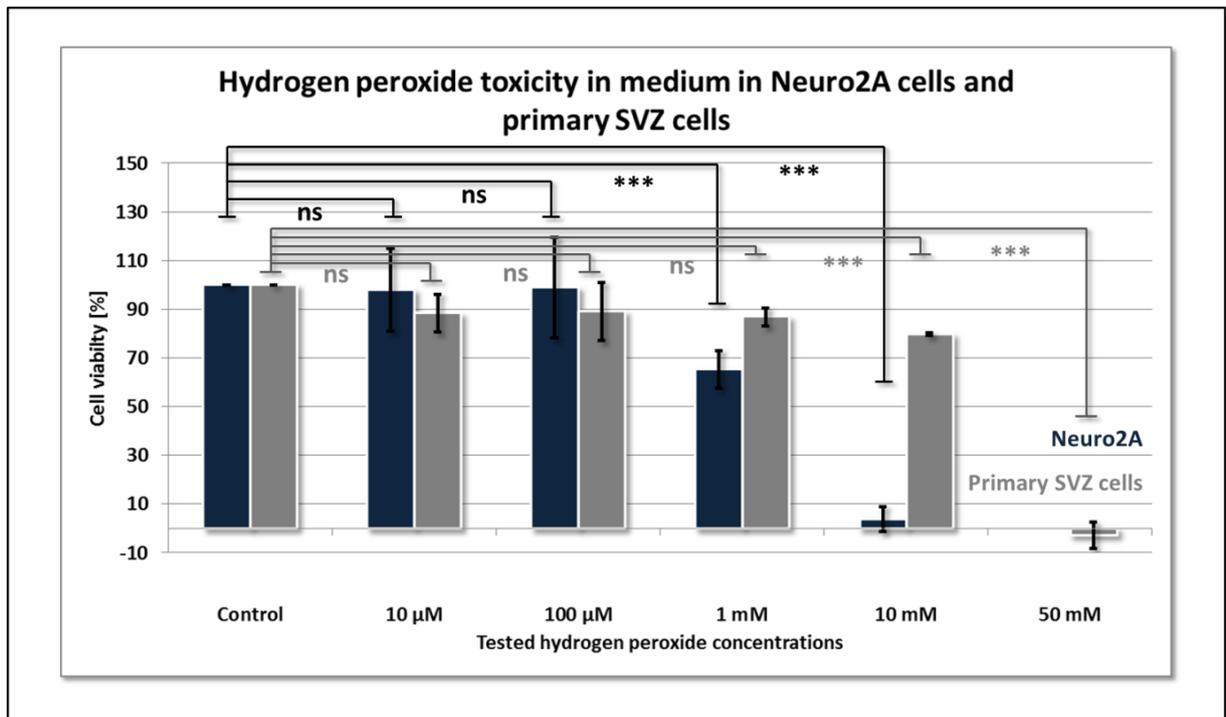
Fig. 49: Hydrogen peroxide toxicity (in cell culture medium) in Neuro2A and primary SVZ cells (n = 3)

H_2O_2 treatment led to a significant loss of cell viability in both Neuro2A and primary SVZ cells over 24 hours of exposition if treated with 10 mM and 50 mM H_2O_2, respectively, with both cell types dropping to below 10 %. Each n consists of 6 individual wells. * = P < 0.05; ** = P < 0.01; *** = P < 0.001

Since the cytotoxic effect of hydrogen peroxide was only observable for very high concentrations -much higher than what was expected- the cell culture media were replaced by HBSS to minimize possible interfering influences by serum or other components of the

used media. Therefor the viability of both cell types in HBSS was assessed using MTT assays under the same conditions as for the cytotoxicity assays.

Cell culture medium was replaced with HBSS (controls were kept in cell culture medium) and the cells were incubated for 3 hours, 6 hours and 9 hours and their viability assessed. Both cell types showed reduced viability in HBSS compared to their respective cell culture medium (fig. 50). After 3 hours viability of Neuro2A and primary SVZ cells was reduced to 49.3 % and 71.5 %, after 6 hours to 54.8 % and 58.6 % and after 9 hours to 31.2 % and 51.2 %, respectively. According to these results a 6 hour exposition to hydrogen peroxide containing HBSS was chosen for further cytotoxicity tests.
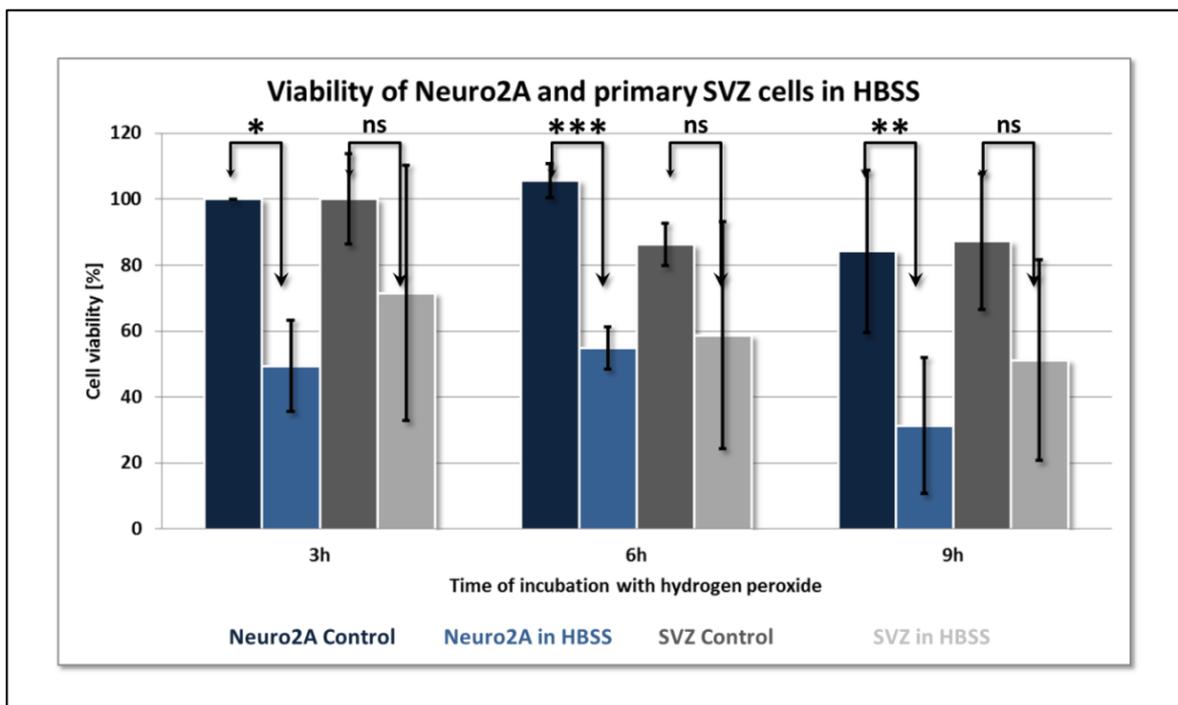
Fig. 50: Viability of Neuro2A cells and primary SVZ cells in HBSS (n = 3)

Both tested cell types showed reduced viability in HBSS compared to their respective cell culture medium with Neuro2A and SVZ cells dropping to 54.8 % and 58.6 % viability, respectively after 6 hours of incubation in HBSS under cell culture conditions (37°C, 5 % CO$_2$). Each n consists of 4 individual wells. * = P < 0.05; ** = P < 0.01; *** = P < 0.001

Reduction of cell viability comparable to what was observed in medium could be seen at a concentration of 1 mM H$_2$O$_2$ in HBSS (P < 0.01, Neuro2A; P < 0.001, SVZ cells) with cell

viability dropping to 18.3 % and 2.4 % compared to an untreated control for Neuro2A cells and primary SVZ cells, respectively (fig. 51).
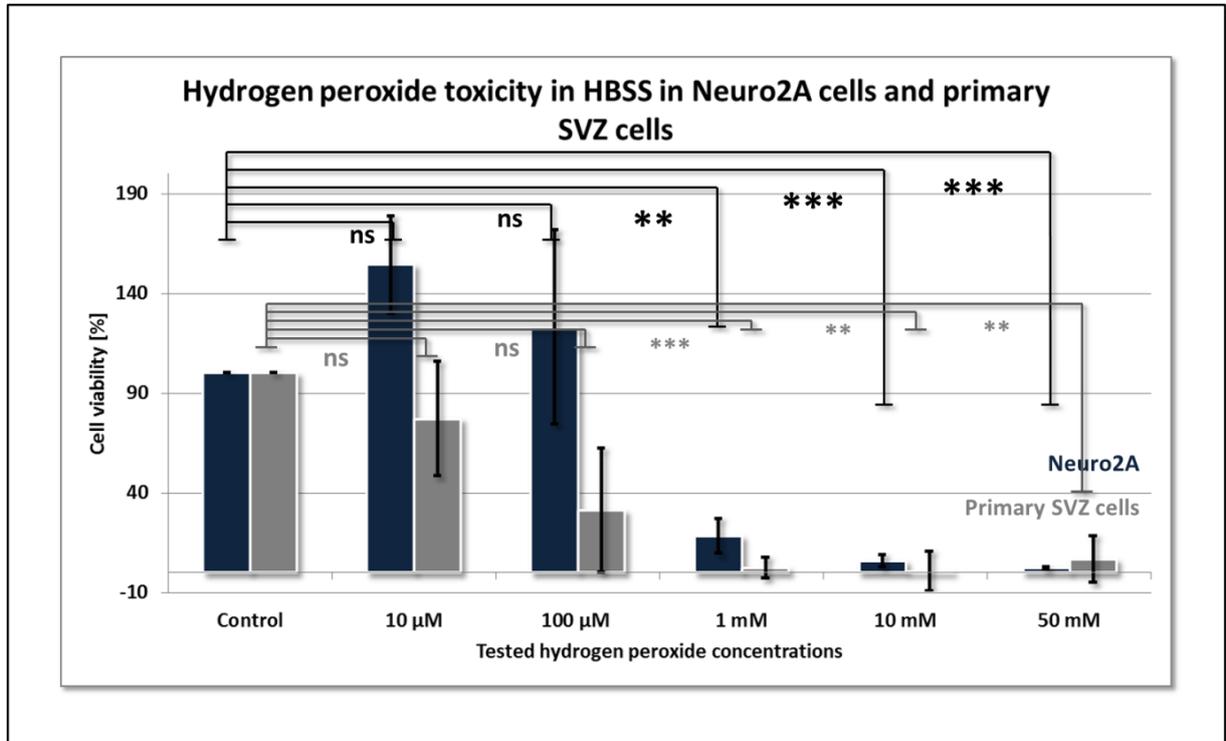
Fig. 51: Hydrogen peroxide toxicity (in HBSS) in Neuro2A and primary SVZ cells (n = 3)

H_2O_2 treatment led to a significant loss of cell viability in both Neuro2A and primary SVZ cells over 6 hours of exposition if treated with 1 mM H_2O_2, with Neuro2A cells dropping to below 20 %. Each n consists of 6 individual wells. * = P < 0.05; ** = P < 0.01; *** = P < 0.001

3.6.2 Impedimetric analysis of H2O2 toxicity in Neuo2A and primary SVZ cells

To analyze the cytotoxic effects of H_2O_2 in Neuro2A and primary neuronal cells obtained from the subventricular zone of postnatal BALB/c mice cells were seeded in a density of 7 500 cells on pre-coated parallel culture chips according to the protocol described in chapter 2.5. The cytotoxic effect of H_2O_2 on both cell types was analyzed in cell culture medium and HBSS.

Neuro2A cells and primary SVZ cells in cell culture medium were treated with concentrations of 10 mM and 50 mM H_2O_2, respectively and incubated under cell culture conditions (37°C, 5 % CO_2) for 24 hours. Microscopic examination of both cell types (fig. 52) showed shrinking of

the cell body and observable detachment from the transistor surface. In case of the SVZ cells a collapse of neuronal outgrowths was observable (fig. 52 d).

Impedance spectra were measured in cell culture medium without H_2O_2. Afterwards the cell culture medium was replaced with medium containing H_2O_2 (in case of the control cell culture medium without H_2O_2), incubated for 24 hours and another impedance spectrum in fresh cell culture medium was recorded. Chips were treated with 10 mM H_2O_2 and 50 mM H_2O_2 for Neuro2A and primary SVZ cells, respectively. Impedance spectra of both cell lines showed a suppression of their respective transfer functions (fig. 52) with stronger suppression for primary SVZ cells. After treatment with H_2O_2 the impedance spectra of both cell lines showed a transfer function comparable to cell-free transistor gates.

Comparison of the impedance spectra before and after hydrogen peroxide treatment revealed significant differences ($P < 0.001$) in Neuro2A cells and primary SVZ cells in the frequency ranges of 650 kHz to 1 MHz and 150 to 900 kHz, respectively (fig. 53 b & d). The impedimetric assessment of H_2O_2 toxicity in Neuro2A and primary SVZ cells was repeated in HBSS instead of in cell culture medium. Cells were cultivated under the same conditions as for the measurements in cell culture medium with the medium being replaced by HBSS free of H_2O_2 for untreated measurements. Afterwards the buffer was replaced by HBSS containing 1 mM H_2O_2 (normal HBSS in case of the untreated control) and the chips were again incubated for 6 hours. Incubation was followed by the careful exchange of the HBSS containing H_2O_2 against H_2O_2-free HBSS for final impedance spectroscopy.
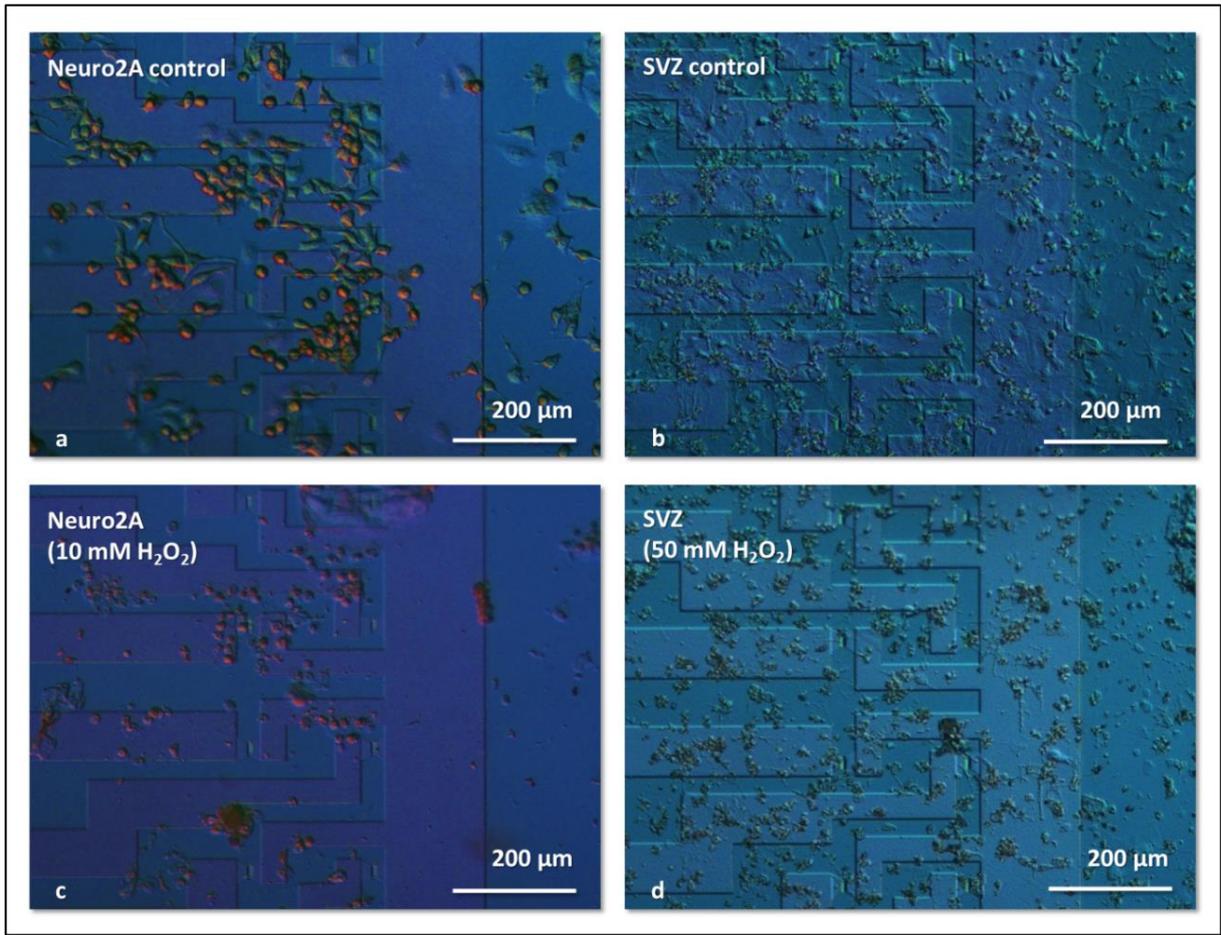
Fig. 52: Microscopic documentation of hydrogen peroxide toxicity in Neuro2A and primary SVZ cells (in medium)

  a)   **Neuro2A cells (control) in medium on fibronectin coated FET surface**
  b)   **Primary SVZ cells (control) in medium on PDL/laminin coated FET surface**
  c)   **Neuro2A cells after 24 hours of H_2O_2 (10 mM) exposition**
  d)   **Primary SVZ cells after 24 hours of H_2O_2 (50 mM) exposition**

H_2O_2 exposition led to severe morphological changes in both cell types ranging from shape changes to a round cell shape, collapse of outgrowths in SVZ cells and detachment from the transistor surface.

Microscopic examination of H_2O_2 treated on-chip cultures revealed similar changes to their respective cell morphology like in medium. Changes included breakdown of outgrowths in primary SVZ cells, shrinking cell bodies in both cell types and detachment from the transistor surface (fig. 54 c & d). Impedance spectroscopy in HBSS yielded unexpected results.

 In both cell types no significant differences between before and after H_2O_2 treatment were observable. Suppression of the transistor-transfer function was very low in general, being stronger in primary SVZ cells (fig. 55).

.
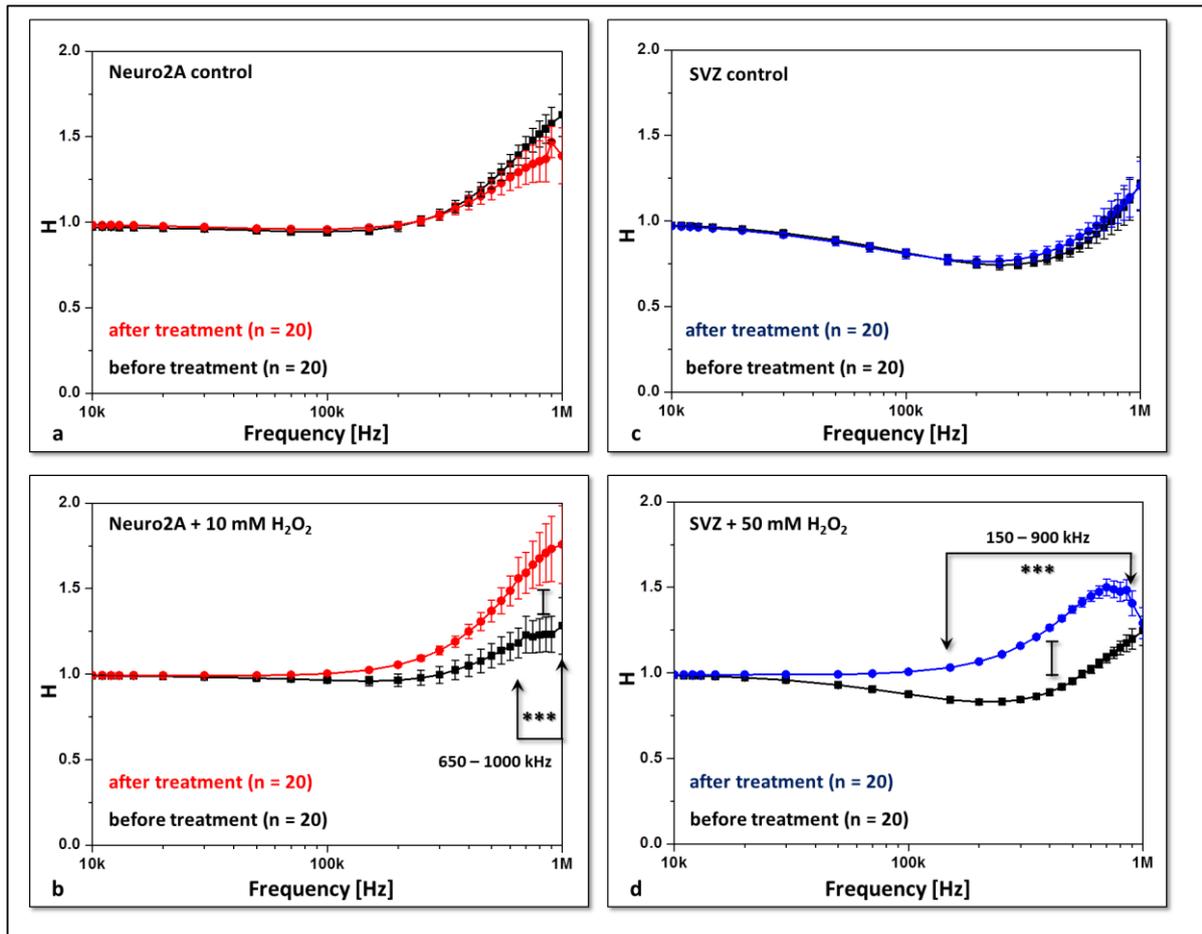
Fig. 53: Impedimetric analysis of H₂O₂ toxicity (in medium) in Neuro2A and primary SVZ cells (n = 20)

Impedimetric measurements of H₂O₂ toxicity showed a significant difference for treated cell cultures (650 – 1000 kHz, Neuro2A; 150 – 900 kHz; b & d) and showed no significant difference for untreated controls (a & c). * = P < 0.05; ** = P < 0.01; *** = P < 0.001
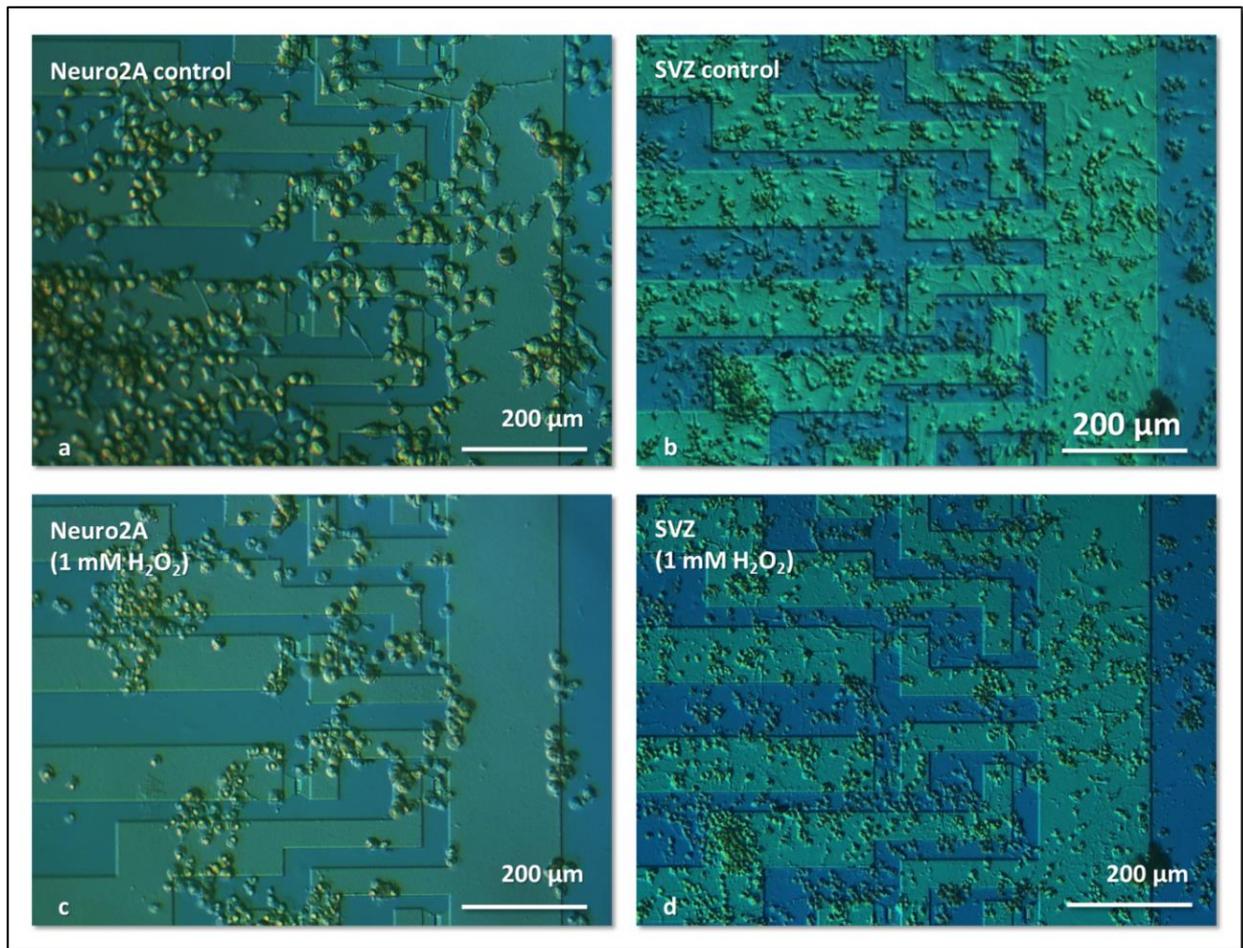
Fig. 54: Microscopic documentation of hydrogen peroxide toxicity in Neuro2A and primary SVZ cells (in HBSS)

a)   **Neuro2A cells (control) in medium on fibronectin coated FET surface**
b)   **Primary SVZ cells (control) in medium on PDL/laminin coated FET surface**
c)   **Neuro2A cells after 6 hours of H_2O_2 (1 mM) exposition**
d)   **Primary SVZ cells after 6 hours of H_2O_2 (1 mM) exposition**

H_2O_2 exposition led to severe morphological changes in both cell types ranging from shape changes to a round cell shape, collapse of appendages in SVZ cells and detachment from the transistor surface.
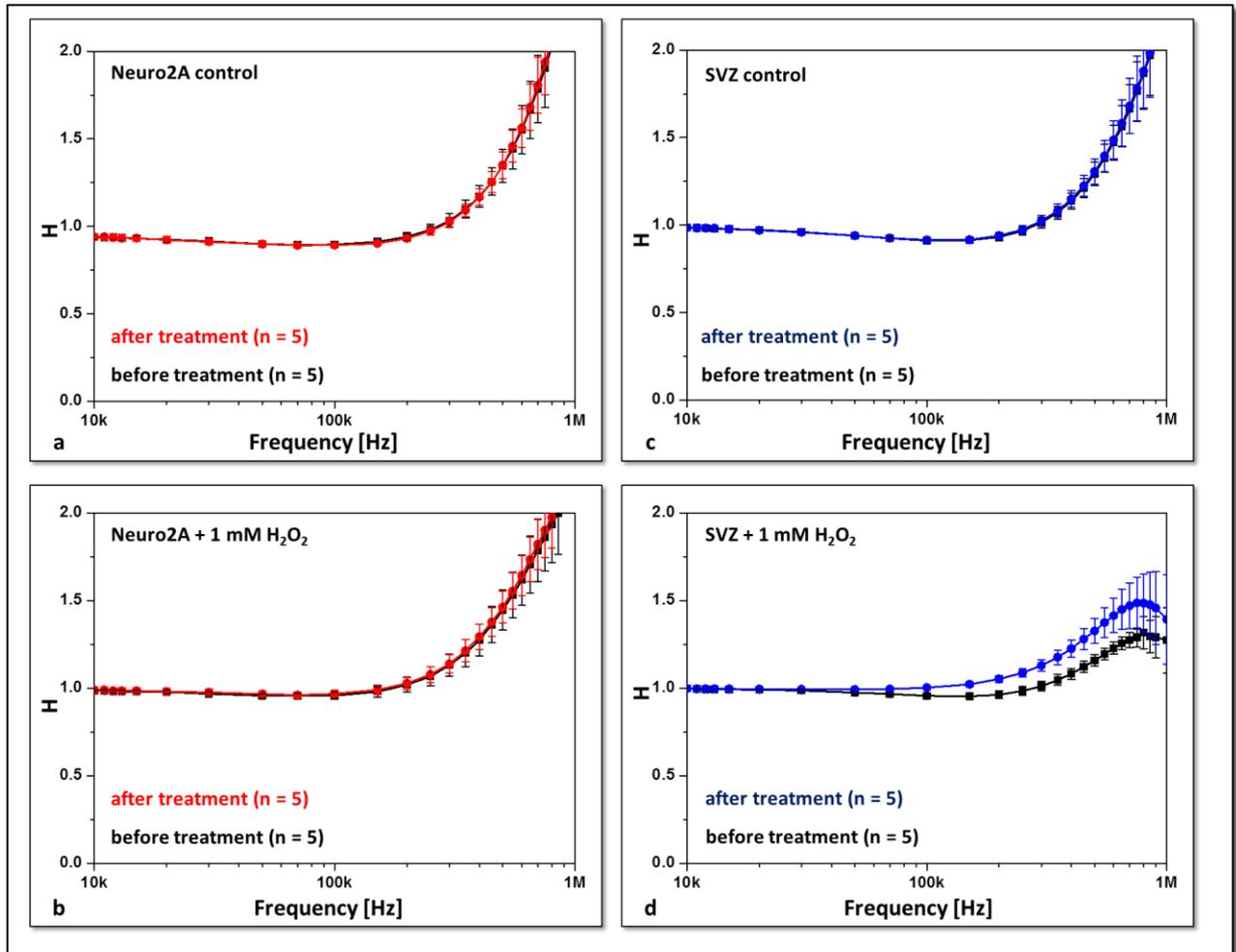
Fig. 55: Impedimetric analysis of H_2O_2 toxicity (in HBSS) in Neuro2A and primary SVZ cells (n = 5)

Impedimetric measurements of H_2O_2 toxicity showed no significant differences for treated cell cultures (b & d) and showed no significant difference for untreated controls (a & c). * = P < 0.05; ** = P < 0.01; *** = P < 0.001

4.   DISCUSSION

4.1   Performance deterioration of individual transistor gates used in cell culture

For impedimetric measurements done in this thesis work (except measurements concerning hydrogen peroxide toxicity) field-effect transistors with an almost completely flat topography were used. For these optimized chips the transistor transconductance g_m was analyzed to verify the chip performance compared to older chips used in our group and their life span.

The g_m-values of the quasi-planar chips used for the impedimetric measurements were obtained during the chip characterization process conducted during the preparation of the individual measurements. A total amount of 144 individual g_m-values were analyzed over a course of 13 measurements, as described in chapter 2.4.4. Channels were considered working channels if they showed a g_m-value over 0.1 mS. 88 channels showed a g_m-value of above 0.1 mS for all 13 measurements and were used to analyze the decline of the g_m-values over time, while 38 channels broke down over time and 18 channels were not working at all. Working channels showed a decline of the g_m-value of 55 % starting at 0.47 mS and ending at 0.21 mS.

Older devices previously used showed an average g_m-value of 0.2 mS (Koppenhöfer *et al.*, 2013; Susloparova *et al.*, 2013). The generally higher g_m-values of the newly developed quasi-planar transistors (in the range of 0.3 mS) match the predicted values for these new chips (Susloparova *et al.*, 2015), with the gate dimensions and the thinner gate oxide compared to older devices (Susloparova *et al.*, 2015) being responsible for these higher g_m-values. Since higher g_m-values are beneficial for the sensitivity of the transistor to adhering

cells, thereby leading to stronger suppression of the transistor-transfer function, these higher values represent a major improvement.

The reusability of the used FETs, however, is limited by their relatively sharp performance decline. This decline might be caused by mechanical stress during the cleaning procedure can damage the gate oxide layer and thereby lower the sensitivity or break the chip entirely.

4.2   Impedimetric detection of cell adhesion of confluent cell cultures on ISFET surfaces

The experiments conducted during this thesis work using morphologically different cell lines for the impedimetric analysis of cellular adhesion on FET surfaces showed a distinct difference between cell-covered and cell-free states for SkMel28 cells, RBL-2H3 cells and H441 cells. All three tested cell lines showed a significant suppression of their respective transistor-transfer function for cell layers fully covering the transistor surface compared to the transistor-transfer function of cell-free transistor gates. The TTF suppression was strongest in the range of 150 − 850 kHz for H441 cells, 200 − 800 kHz for SkMel28 cells and 150 − 700 kHz for RBL-2H3 cells respectively. This effect has already been described as typical behavior of adherent cell lines covering transistor surfaces in confluent cell layers (Schäfer *et al.*, 2009; Susloparova *et al.*, 2013; Koppenhöfer *et al.*, 2013).

The morphological differences of the three tested cell lines as described in section 2.2.1 led to individual combinations of the cells seal resistance R_{seal} and membrane capacitance C_M. The C_M values shown in this thesis are not identical to the membrane capacitance commonly used in patch clamping, instead representing the combined capacitance of free membrane parts and parts in contact with the transistor. The observed C_M values for the tested cell lines indicate a correlation to the height of the measured cell (Susloparova *et al.*, 2015) with the highest values having been extracted from measurements using H441 cells while the

membrane capacitance for RBL-2H3 cells and SkMel28 cells were smaller. This observation can be correlated to the documented height of the tested cell line, with H441 cells being documented with a height of 29 µm, while the height of RBL-2H3 cells was documented at 11 µm (Donnellan *et al.*, 1997; Woolhead *et al.*, 2006). Since C_M and R_{seal} values of SkMel28 cells and RBL-2H3 cells were comparable, one might assume a comparable height of SkMel28 cells and RBL-2H3 cells.

In addition to higher membrane capacitance the H441 cells also showed a higher seal resistance compared to SkMel28 and RBL-2H3 cells. This indicates an effectively smaller gap between the cell layer and the transistor surface. One possible explanation for this behavior might be a possibly tighter connection between individual H441 cells. Microscopic analysis of confluent cell layers of H441 cells adhered to the transistor surface revealed a very tight connection between individual cells. Assuming the effective gap between the transistor surface and adhering cells is influenced by the contacts between individual cells and effects taking place at the edges of said area of contact this possibly tighter connection might affect the sealing properties of the adhering cell layer. In addition H441 cells were unable to form low density cultures with individual isolated cells, instead always forming small confluent patches of cells. Both RBL-2H3 and SkMel28 cells showed a loser connection between individual cells, being able to form cell cultures with individual cells being isolated from each other.

The FETCIS system presented in this thesis is capable to analyze cell adhesion of both confluent and low density cell cultures of morphologically different cell types. Measuring cell adhesion as a measure of cell viability is a well-established approach in impedance based biosensing (Asphahani and Zhang, 2007). As has been mentioned before, cells adhering to a transistor surface affect the impedance spectrum of said gate and thereby their detachment

from said surface leads to a measurable shift in the TTF spectrum. This shift seems to be characteristic for cell lines stemming from different histological sources as indicated by the results obtained from analyzing the TTF spectra of different cell lines. The observed difference between morphologically distinguishable cell types leads to the possibility of using the presented measuring technique to identify specific cell types using their impedimetric fingerprint. This would lead to an impedimetric alternative to classic histological methods creating an impedimetric histology technique (Ingebrandt *et al.*, 2014 - *Device and method for measuring biological and/or electronic properties of a sample, and uses thereof,* Application number PCT/DE2015/100040). Utilizing this particular capability of the shown system opens new possibilities in the field of individualized cancer therapy providing a fast method to analyze the histological composition of solid tumors using tissues obtained from biopsy cultivated on the surface of field-effect transistors.

4.3   Impedimetric detection of cell adhesion of low density cell cultures on ISFET surfaces

In addition to impedimetric measurements utilizing confluent cell layers, experiments were conducted during this thesis work using low density cultures of SkMel28 cells to analyze the effects of incomplete coverage of the transistor surface. The cell line SkMel28 was chosen for these experiments due to their relatively large cell body (and resulting capacity to seal the transistor gate completely with a single cell) and their ability to grow isolated from one another in low density cultures.

As can be found in the results section transistor gates with coverage of below 75 % of their respective surface did not show any discernible suppression of the transfer function for cell-covered transistor gates. The presented data fitting technique made it possible to extract values for both seal resistance and membrane capacitance. Meeting the expectations the

4.   DISCUSSION

R_{seal} value was lowest for a rate of transistor coverage of 25 to 50 %, while a rate of gate coverage of 50 to 75 % lead to a comparable seal resistance like the one observed for a rate of transistor coverage above 75 %. Since lower amounts of gate coverage equal limited sealing of the transistor by the adhering cell these results were no surprise.

Since the C_M value is defined by the characteristics of the individual cell type, it should be comparable for confluent and low density cultures of the same cell type. Therefor the main parameter responsible for the different behavior of adhering cells with varying rates of transistor coverage should be the seal resistance R_{seal}. However the presented fitting approach is not yet able to provide absolute data concerning C_M and R_{seal} based on the data acquired during this thesis work (as indicated by the differing C_M values observed for confluent and low density cultures of SkMel28 cells). Since the data fitting was done using averaged impedance spectra this could be one reason for this behavior.

According to these results it can be concluded that the sealing of the transistor gates by adhering cells needs to be above 50 % of the transistor surface. Therefore in future designs the size of the ISFET should be miniaturized. In this work, with the sensor designs available, the SkMel28 cells were chosen for low density cell culture experiments due to their comparably large cell bodies, making it easier to achieve high rates of gate coverage. In case of different cell types with different morphologies, for example the RBL-2H3 cells, this is possible to achieve utilizing smaller transistor gates.

These findings strongly indicate the applicability of the proposed system to monitor the activity of cells, which are normally not acting as a part of a confluent cell layer. So far the ECIS system was the most frequently used system for impedimetric measurements regarding cell viability, membrane integrity or cellular migration. However such systems use metal

electrode arrays interacting with larger cell populations, meaning that the obtained results can only be interpreted as the response of an averaged cell to the applied stimulus. Studies aiming to analyze the effects of physiological or chemical stimuli on primary tissues might not be conducted as efficiently, since the effect of the applied stimulus might not be the same for every cell type present in the cell sample. The composition of most primary tissues is not necessarily homogeneous, consisting of different cell types that might react differently to external stimuli. Other examples where an averaged observation might be a disadvantage are cell types stemming from the immune system (e.g. T-cells, Law *et al.*, 2014) or primary neuronal tissues, which do not form necessarily form tight connections to other cells and are thereby hard to analyze using a system utilizing large metal electrodes. This holds especially true for solid tumors, which can show a high rate of heterogeneity stemming from their high rate of chromosome instability. Therefor it is of utmost importance to analyze the response of individual cells to treatment with potentially selective compounds (Lips *et al.*, 2008; Asphahani *et al.*, 2011).

Coupled with the already described capability of the presented system to differentiate between individual cell types, its ability to impedimetrically monitor cytological responses on single cell level provides us with the possibility to monitor the response of malign and benign tissue to antineoplastic drugs, simultaneously. In addition it would provide a possibility to analyze the composition of a biopsy sample of a solid tumor to analyze the effectiveness of the planned treatment before it is administered, thereby advancing the possibilities of individualized therapy.

The difficulty in assessing the response of individual cells is mainly caused by the electrode size. In general it can be assumed that the lower size limit for metal electrodes in bio-impedance assays is 25 µm in diameter, with the main problem being the double layer

capacitance formed at the metal-liquid interface dominating the overall impedance (Xiao *et al.*, 2002). The ion-sensitive FET devices utilized in this work are considerably smaller than the area of even circular electrodes with sizes below 20 µm diameter (Koppenhöfer *et al.*, 2015).

4.4   Impedimetric analysis of the nanotoxicity of the industrial nanoparticle NexSil20

During this thesis experiments were conducted analyzing the cytotoxic effect of the nanoparticle NexSil20 on the human papillary adenocarcinoma cell line H441. This cell line has been used by Prof. Dr. Roland Stauber as part of a model simulating particle absorption via the lung (Kasper *et al.*, 2011). Cells were cultivated on top of pre-coated transistor surfaces and exposed to particle concentrations whose toxicity was already described as being apoptosis inducing (Kasper *et al.*, 2011).

Particle treatment led to significant reduction of cell viability in MTT assays as described in the results section. Microscopic examination showed typical signs of cellular detachment (round shape, bright edges; Okano *et al.*, 1995). This observed reduction of cell viability matched the already published results of Prof. Dr. Stauber's research group and provided an ideal system to test the real-time monitoring capabilities of the FETCIS impedance measurement setup. Therefore H441 cells were cultivated in confluent cell layers on pre-coated FET surfaces and the cytotoxic effects of the NexSil20 particles were analyzed via real-time monitoring of the transistor-transfer function using a fixed frequency of 200 kHz.

Monitoring the transfer function of FETs covered by H441 cells revealed a rise of the transfer function in the first 30 min after nanoparticle exposure (600 µg/ml) began. The observed shift can be correlated to the MTT assay results were the cytotoxic effect was shown to take place in the first hour after particle administration. The observed change in the amplitude of

the measured transfer function indicates progressive cellular damage occurring after particle administration. In addition, control measurements using untreated H441 cells showed fluctuations of the transistor-transfer function. These fluctuations have already been described as the reaction of the impedance sensor to activity (e.g. membrane fluctuations) of living cells (Koppenhöfer *et al.*, 2013).

Nanostructures are more and more something of a hot topic in the scientific community. Keeping the scope of this work in mind their possible application in cancer diagnosis and therapy is of special interest. As has been mentioned in the introduction chapter such structures can be used for tumor targeting, drug delivery or as a therapeutical compound themselves. In this context the analysis of their toxic effects is of major interest for the development of new selective antineoplastic compounds based on nanoscale structures.

The real-time monitoring of the cytotoxic effects of NexSil20 particles using impedance spectroscopy via field-effect transistors demonstrates the applicability of the presented system as an alternative to standard toxicity or cell viability assays like MTT or LDH, especially in the context of nanoparticle toxicity. These assays must be used with precaution given that the used chemicals tend to interact with the tested nanoparticles and thereby influence the results (Monteiro-Riviere *et al.*, 2009; Wörle-Knirsch *et al.*, 2006). As a consequence it is of importance to use more than one assay to reach solid conclusions (Lewinski *et al.*, 2008). The proposed FET system provides another possible solution to analyze the toxicity of such particles providing a platform for real-time analysis of cytotoxicity. Standard procedures (e.g. MTT, LDH) do not provide the possibility to monitor affected cells in real-time if they are not expressing GFP or any other live-cell marker.

The presented FET system can be used to not only impedimetrically analyze changes in cell adhesion in a time-resolved manner but could simultaneously be used to monitor pH changes in the cell medium at a low frequency. One further advantage is the possibility to obtain impedimetric results of individual cells in a confluent culture, while measuring several channels under cell culture conditions (Schäfer *et al.*, 2009), thereby generating a high amount of data for statistical analysis.

Taking the results obtained from the impedimetric analysis of cell adhesion (in both confluent and low density cell cultures) into account it becomes clear that the presented system can provide researchers with an impedimetric multiparametric live-cell measurement setup, vastly widening the possible applications of impedance-based biosensors.

4.5   Impedimetric detection of cell adhesion of primary neuronal tissues on ISFET surfaces

To further substantiate the usefulness and versatility of the presented FETCIS approach additional experiments were conducted using Neuro2A cells and primary neuronal cells obtained from the subventricular zone of postnatal BALB/c mice.

The impedimetric analysis of Neuro2A and primary SVZ cells showed an expected suppression of the transistor-transfer function for cell-covered transistor gates comparable to the suppression caused by the previously tested cell lines. As mentioned before such suppression has already been described as characteristic for the used field-effect transistors with an attached cell on top of it (Schäfer *et al.*, 2009; Koppenhöfer *et al.*, 2013; Susloparova *et al.*, 2013; Koppenhöfer *et al.*, 2015; Susloparova *et al.*, 2015). The minor differences observed between the impedance spectra of the tested cell types seem to be caused by their

different morphologies and adhesion strength and might be interpreted as a kind of fingerprint of these specific cell types as has been detailed in section 4.2.

4.6   Impedimetric analysis of neurodegeneration caused by oxidative stress in primary neuronal tissues

As a continuation of the aforementioned experiments and further expansion of the possible applications of the presented system, a new encapsulation procedure was formulated leading to a new parallel culture platform utilizing two individual FET-chips with separated cell culture receptacles. These chips were then used for experiments analyzing the cytotoxic effect of hydrogen peroxide to simulate oxidative stress in primary neuronal tissues obtained from the subventricular zone of postnatal BALB/c mice. During these experiments primary SVZ cells were cultivated in both cell culture receptacles and were treated with hydrogen peroxide to induce oxidative stress. Neuro2A cells were used as a control. MTT assays in cell culture medium and HBSS were done before impedimetric measurements to find appropriate concentrations of hydrogen peroxide for impedimetric measurements.

Cell culture medium with 10 mM of H_2O_2 induced a reduction of cell viability in Neuro2A cells to below 10 % of the untreated control, while in primary SVZ cells a H_2O_2 concentration of 50 mM was necessary to achieve a similar reduction of cell viability. If cell culture medium was replaced with HBSS the concentration of H_2O_2 could be lowered to 1 mM to achieve a reduction of viability to below 15 % in both cell types.

The concentrations of hydrogen peroxide needed to induce a nearly total reduction of cell viability in cell culture medium are much higher than what should be expected based on the literature (25 to 50 µM; Da´vila and Torres-Aleman, 2008). This effect is most probably caused by a combination of several factors inherent to the used cell culture technique, like

the presence of glia cells in the primary cell culture and the presence of beta-mercaptoethanol (acting as an antioxidant) in the cell culture medium. The primary cell culture created from the cells obtained from the subventricular zone of mice is a mixture of different cell types and contains both neurons and glia cells. The presence of glia cells in the used culture leads to a reduction of the effective H_2O_2 concentration due to detoxification by the glia cells (Desagher *et al.*, 1996). To lower the needed hydrogen peroxide concentration and reduce possible interference from components of the cell culture medium the cell culture medium was replaced with HBSS. Using HBSS instead of cell culture medium allowed for a reduction of the H_2O_2 concentration to 1 mM. However it must be kept in mind that HBSS is not suited to sustain long term cell culture, in our case longer than 6 hours. To properly study the effects of hydrogen peroxide induced oxidative stress longer time periods would be beneficial.

Impedimetric analysis of H_2O_2 toxicity using adhered Neuro2A cells and primary SVZ cells was done to examine the cytotoxic effects of hydrogen peroxide treatment and to monitor the damaging effects of oxidative stress on neuronal tissue. Both cell types were impedimetrically analyzed using H_2O_2 containing cell culture medium (10 mM and 50 mM) and HBSS (1 mM), respectively. Both cell types showed the already described suppression of the transistor-transfer function for healthy cells adhering to a transistor gate. Hydrogen peroxide treatment (in medium) led to the abolition of said suppression due to massive cellular damage caused by the oxidative stress, indicating cellular detachment and cell death. However such suppression could not be observed in HBSS. The difference between HBSS and cell culture medium mainly seem to stem from the buffer itself. Keeping in mind that a loss of viability of 40 % was observable in HBSS in untreated cells, one can assume that the exposition to HBSS might have been enough to damage the cells to the point of not

adhering strong enough to cause the expected suppression of the transistor-transfer function. However, the results of experiments using hydrogen peroxide containing cell culture medium still yielded useful results with measurement taking roughly five minutes of time and not needing additional chemicals or incubation periods. It has to be kept in mind though, that the experiments done in this particular study were not meant to emulate *in vivo*-conditions and the used cells and stimulus do not necessarily represent a clinically relevant experimental setup.

5.   CONCLUSION AND OUTLOOK

During this thesis work a measurement system using field-effect transistors for the impedimetric measurement of cellular adhesion was used to establish first methods and testing protocols for toxicity testing, cell viability monitoring and pharmacological testing. To this purpose three sub-projects were conducted using different cell types to analyze the systems applicability in different experimental setups.

In the first step of the first sub-project general cell adhesion was analyzed using three different cell types grown in confluent cell layers, revealing distinct patterns in their respective impedance spectra implicating possible impedance-based histological analysis of tissue samples using the presented system. The second part of the first sub-project used low density cultures of SkMel28 cells to test the system's ability to monitor individual cells for several applications. Finding that transistor gate coverage of around 75 % is necessary to see an individual cellular binding event impact the TTF spectrum proves the possible application of the presented systems to study individual cellular reactions to specific stimuli.

During the second sub-project the focus was shifted from assessing cell adhesion using impedance spectroscopy to analyzing cytotoxicity of nanoparticles using real time monitoring of the transistor-transfer function. H441 cells were grown in confluent cultures and exposed to the nanoparticle NexSil20 and their reaction was analyzed using MTT assays and impedimetric real time measurements. Both MTT assays and impedimetric monitoring revealed an apoptosis-inducing effect taking place during the first 30 minutes of particle exposure.

The third and final sub-project focused on the impedimetric analysis of the viability of primary neuronal cells obtained from the subventricular zone of postnatal BALB/c mice

(Neuro2A cells were used as a control). The sub-project was divided into two parts. Cells were isolated from postnatal mice and cultivated on top of pre-coated FET-surfaces. During the first part of this sub-project the obtained neuronal tissue was cultivated on standard 16-channel FET-chips and analyzed impedimetrically using impedance spectroscopy. Both primary cells and Neuro2A cells showed significant suppression of the transistor-transfer function comparable to the suppression observed in other cell types. This is the first time that such cell types were successfully used in impedance asays. For the second part the obtained primary cells were cultivated on top of pre-coated 2 x 8-channel FET-parallel culture-chips and treated with hydrogen peroxide. Attached cells were expected to cause the already observed suppression of the transistor-transfer function, while cells damaged by their exposure to hydrogen peroxide were expected to detach from the transistor surface. The expected observations could only be made when cell culture medium (with and without hydrogen peroxide) was used but not for HBSS.

The measurement and analysis system developed in our group and tested in this work is primarily meant for pharmacological testing. In this context it could provide researchers with a fast working system capable of analyzing the effects of new pharmacological compounds, side effects of existing compounds or the possible effects of micro-environmental conditions (e.g. temperature, pH value, etc.) both in real time and under cell culture conditions.

Considering the amount of time needed for one individual measurement of an impedance spectrum, which is roughly 5 minutes, the system could in the future be used in a high throughput manner. In addition to its ability for fast measurements it also provides the possibility of multiparametric readouts, since not just the impedance spectra can be measured but also possible changes of the pH (not done in this thesis).

In addition to its possible application in pharmacological testing the presented system should also be usable in individualized cancer diagnostics and therapy. Based on the implied possibility to measure the adhesion of individual cells and to differentiate between different cell types using their impedimetric fingerprints could allow for the development of an impedimetric histology system. Starting with tissue obtained from a biopsy, which can then be dissociated and cultured on top of a transistor array, individual transistor gates could provide the impedance spectra of the individual cell types present in the tumor. By utilizing devices with small transistor gates and a high density of individual measurement points the presented system could be used to analyze the dissociated primary tissue and identify the present cell types.

It has been shown that the FETCIS system is very well capable to monitor the adhesion and the detachment of individualized cells accurately. Since the ability of cells to adhere to a surface can be used as a way to monitor their viability (Susloparova *et al*., 2013; Koppenhöfer *et al*., 2013) the system could potentially be used to monitor the effects of planned cancer treatment before it is actually administered to the patient. Again starting with cells obtained from dissociated biopsy tissue primary cultures of the tumor could be created on top of the transistor surface. Such cell cultures would represent a cross section of the actual tumor and therefor provide a possibility to analyze the effectiveness of the planned chemotherapy. By applying the planned chemotherapy procedure and impedimetrically monitoring the cell adhesion over a defined period of time the responsible medical doctors could adjust their treatment regiment according to the results of the FETCIS analysis. This would allow for both changes to the planned treatment or the general scrapping of it, if the treatment proves to be ineffective before the patient would have to deal with side effects and a loss of quality of life. Since the process of impedimetrically

measuring the cell adhesion and cell viability is fairly fast this technique could provide medical doctors a possibility to optimize the treatment of solid tumors and thereby tailor it to an individual patient.

By combining the two possible applications described above the presented system could in the future provide researchers and medical doctors with an integrated system able to monitor the cell adhesion (as a measure of cell viability) and changes of the pH in the electrolyte impedimetrically to analyze the effects of pharmacological or physical stimuli. Thereby this system could be used to test pharmacological compounds, optimize therapeutical procedures like chemotherapy and to analyze the composition of primary cell samples.

However the presented system is not without disadvantages. In general the system is only able to monitor changes of cell adhesion and therefor is unable to document the intracellular mechanism of action of pharmacological compounds if it is not directly tied to cell adhesion.

In addition the system itself is not yet fully developed, with the density of individual transistors being too low for efficient medical or scientific application. By raising the number of individual measurement points on top of the chip surface the amount of generated data per measurement will grow considerably thereby generating a better basis for reproducible experiments.

Performance stability of the proposed system is another point of concern for future applications. During this thesis the presented system proofed difficult to use for long term measurements because of excess heat produced by the electrical components. The

mentioned excess heat is enough to heat up the cell culture medium to 40 °C thereby influencing the cell viability assay.

Chip feasibility and deterioration are further major problems of the system. So far it seems that the chips can be reused roughly 15 times before becoming defective, indicated by a reduction of the transconductance g_m to a value of below 0.1 mS. This decline of chip performance combined with the complex fabrication process leads to a reduced long term usability, making it necessary to establish cheaper and more robust chip platforms.

Nevertheless the described FETCIS measurement setup is a promising tool for future research, providing researchers with a fast, reliable and label-free method to study the interaction of individual cells and their reaction to external stimuli under cell culture conditions. Its applicability in a wide range of research fields, ranging from pharmacological testing to individualized cancer diagnostics and treatment or impedance-based histological analysis, coupled with the high resolution down to individual cells make it an ideal tool for the rapidly growing field of individualized medicine.

6.   APPENDIX

App. 1: Abbreviations

AC	Alternating current
ATP	Adenosine triphosphate
BHF	Buffered hydrofluoric acid
BSA	Bovine serum albumin
C_L	Contact line capacitance
C_M	Combined membrane capacitance
CNT-FET	Carbon nanotube field effect transistor
C_{Ox}	Gate oxide capacitance
C_T	Cytotoxic T lymphocyte
DMEM	Dulbecco's modified Eagle's Medium
DMSO	Dimethyl sulfoxide
DNA	Deoxyribonucleic acid
e.g.	exempli gratia
ECIS	Electrical cell-substrate impedance sensing
ECM	Extracellular matrix
EEC	Electrical equivalent circuit
EGF	Epidermal growth factor
EPR	Enhanced permeability and retention
FCS	Fetal calf serum
FET	Field effect transistor
FETCIS	FET system for ECIS measurements
f_g	Cutoff frequency of the operational amplifier
FGF	Fibroblast growth factor
Fig.	Figure
g_m	Transistor transconductance
HBSS	Hank's balanced salt solution
HEK293	Human embryonic kidney cells 293
HF	Hydrofluoric acid
HNE	4-hydroxyl-2,3-nonenal
IDAM	Interdigitated array microelectrode
I_{DS}	Drain-source current
I_{GS}	Gate-source current
ISFET	Ion sensitive field effect transistor
LCC	Leaded chip carrier
MEM	Minimum essential medium
MOSFET	Metal oxide semiconductor field effect transistor
MTT	3-(4,5-dimethylthiazol-2-yl)-2,5-diphenyltetrazolium bromide
NEAA	Non-essential amino acids
OECT	Organic electrochemical transistors
OTFT	Organic thin-film transistor
PBS	Phosphate buffered saline
PCB	Printed circuitry board

PDL	Poly-D-lysine
PDMS	Polydimethylsiloxane
PEDOT:PSS	Poly(3,4-ethylenedioxythiophene) polystyrene sulfonate
poly-Si NWFET	Polycrystalline silicon nanowire field effect transistor
PSA	Prostate specific antigen
R_{el}	Serial resistance of electrolyte and reference electrode
$R_{feedback}$	Feedback resistance
rhEGF	Recombinant human epidermal growth factor
RNA	Ribonucleic acid
ROS	Reactive oxygen species
rpm	Rotations per minute
RPMI	Roswell Park Memorial Institute medium
R_{seal}	Seal resistance
SEM	Scanning electron microscopy
SVZ	Subventricular zone
TTF	Transistor-transfer function
V_{DS}	Drain-source voltage
V_{GS}	Gate-source voltage

App. 2: Chemicals, cell culture supplies and devices used during this work in alphabetical order

Item	Abbreviations	Provider
3-(4,5-dimethylthiazol-2-yl)-2,5-diphenyltetrazolium bromide	MTT	Carl Roth, Germany
AccuMax		PAA Laboratories, Germany
Accutase		PAA Laboratories, Germany
Adhesive 377 1LB		Epoxy Technology, USA
Alpha medium		Biochrom, Germany
B27		Gibco Life technologies, Germany
Bovine serum albumin	BSA	AppliChem, Germany
Dimethylsulfoxide	DMSO	AppliChem, Germany
Dulbecco's modified Eagle's medium	DMEM	PAN Biotech, Germany
Dulbecco's modified Eagle's medium nutrient mixture F-12	DMEM F12	Gibco Life technologies, Germany
Fetal calve serum	FCS	PAN Biotech, Germany
Fibronectin		AppliChem, Germany
Genios microplate reader		Tecan, Switzerland
Glutaraldehyde		Sigma Aldrich, Germany

Hank's balanced salt solution	HBSS	Sigma Aldrich, Germany
Hellmanex III		Sigma Aldrich, Germany
Hydrogen peroxide		AppliChem, Germany
Laminin		Sigma Aldrich, Germany
Lead Chip Carrier	LCC carrier	Global chip Materials, USA
L-Glutamine	Q	PAN Biotech, Germany
Minimum Essential Medium	MEM	PAN Biotech, Germany
Non-essential amino acids	NEAA	PAN Biotech, Germany
Penicillin/Streptomycin	PS	PAN Biotech, Germany
Phosphate buffered saline	PBS	PAA Laboratories, Germany
Polydimethylsiloxane (Silicon adhesive Kit 96-083)	PDMS	Dow Corning, Germany
Poly-D-Lysine (70 kDa)	PDL	Sigma Aldrich, Germany
Printed circuit board dip chip carrier		LeitOn, Germany
Roswell Park Memorial Institute medium	RPMI	PAN Biotech, Germany
Scanning electron microscope Supra 40	SEM	Carl Zeiss AG, Germany
Sulfuric acid		AppliChem, Germany
Sylgard silicone elastomer 184		Dow Corning, Germany
Trypsin/EDTA (0.5%)		PAN Biotech, Germany
Upright microscope Axiotech vario 100 HD		Carl Zeiss AG, Germany

App. 3: Graphs and figures

7.   LITERATURE

7.1   Books

B. Alberts, A. Johnson, J. Lewis, M. Raff, K. Roberts, P. Walter, *Molecular Biology of the Cell, 4th edition (2004)*

H. Leischner, *Oncology, 3rd edition (2014)*

P. Kaatsch, C. Spix, A. Katalinic, S. Hentschel, *Cancer in Germany 2007/2008, 8th edition (2012)*

7.2   Patents

S. Ingebrandt, A. Susloparova, X. T. Vu, D. Koppenhöfer, "Device and method for measuring biological and/or electronic properties of a sample, and uses thereof", Application number PCT/DE2015/100040

M. Zeppezauer, H- P- Leinenbach, "Cytostatic and cytotoxic agent combination for therapeutical use", Application number 90125093.6

7.3   Papers

M. Abdolahad, H. Taghinejad, A. Saeidi et al., "Cell Membrane Electrical Charge Investigations by Silicon Nanowires Incorporated Field Effect Transistor (SiNWFET) Suitable in Cancer Research", *RSC Advances 4 (2014)*, 7425–7431

F. Alexander, D. T. Price, S. Bhansali, "Optimization of Interdigitated Electrode (IDE) Arrays for Impedance Based Evaluation of Hs 578T Cancer Cells", *Journal of Physics: Conference Series 224 (2010)*, 1–4

J. K. Andersen, "Oxidative Stress in Neurodegeneration: Cause or Consequence?", *Nature Medicine 10 (2004)*, S18–25

M. M. G. Antonisse, B. H. M. Snellink-Rue, R. J. W. Lugtenberget al., "Membrane Characterization of Anion-Selective CHEMFETs by Impedance Spectroscopy", *Analytical Chemistry 72 (2000)*, 343–48

F. Asphahani, K. Wang, M. Theinet al., "Single-Cell Bioelectrical Impedance Platform for Monitoring Cellular Response to Drug Treatment.", *Physical Biology 8 (2011)*, 1–23

F. Asphahani, M. Zhang, "Cellular Impedance Biosensors for Drug Screening and Toxin Detection.", *The Analyst 132 (2007)*, 835–841

K. J. Barnham, C. L. Masters, A. I. Bush, "Neurodegenerative Diseases and Oxidative Stress", *Nature Reviews Drug Discovery 3 (2004)*, 205–214

C. Behl, "Alzheimer's Disease and Oxidative Stress: Implications for Novel Therapeutic Approaches", *Progress in Neurobiology 57 (1999)*, 301–323

J. S. Bertram, "The Molecular Biology of Cancer", *Molecular Aspects of Medicine 21 (2000)*, 167–223

7. LITERATUR

J. N. Blattman, P. D. Greenberg, "Cancer immunotherapy: a treatment for the masses.", *Science 305 (2004)*, 200-205

J. F. Boivin, "Second Cancers and Other Late Side Effects of Cancer Treatment. A Review.," *Cancer 65 (1990)*, 770–775

R. J. Bold, P. M. Termuhlen, D. J. McConkey, "Apoptosis, Cancer and Cancer Therapy", *Surgical Oncology 6 (1997)*, 133–142

L. Brannon-Peppas, J. O. Blanchette, "Nanoparticle and Targeted Systems for Cancer Therapy", *Advanced Drug Delivery Reviews 64 (2012)*, 206–212

I. Brigger, C. Dubernet, P. Couvreur, "Nanoparticles in Cancer Therapy and Diagnosis", *Advanced Drug Delivery Reviews 54 (2002)*, 631–651

J. Broeders, S. Duchateau, B. Van Grinsven et al., "Miniaturised Eight-Channel Impedance Spectroscopy Unit as Sensor Platform for Biosensor Applications", *Physica Status Solidi (A) Applications and Materials Science 208 (2011)*, 1357–1363

D. A. Carson, J. M. Ribeiro, "Apoptosis and Disease", *The Lancet 341 (1993)*, 1251-1254

T. M. Curtis, J. Tabb, L. Romeo et al., "Improved Cell Sensitivity and Longevity in a Rapid Impedance-Based Toxicity Sensor", *Journal of Applied Toxicology 29 (2009)*, 374–380

D. Da´vila, I. Torres-Aleman, "Neuronal Death by Oxidative Stress Involves Activation of FOXO3 through a Two-Arm Pathway That Activates Stress Kinases and Attenuates Insulin-like Growth Factor I Signaling", *Molecular Biology of the Cell 19 (2008)*, 2014–2025

S. Desagher, J. Glowinski, J. Premont, "Astrocytes Protect Neurons from Hydrogen Peroxide Toxicity.", *The Journal of Neuroscience : The Official Journal of the Society for Neuroscience 16 (1996)*, 2553–2562

J. Devy, R. Wargnier, M. Pluot et al., "Topotecan-Induced Alterations in the Amount and Stability of Human DNA Topoisomerase I in Solid Tumor Cell Lines", *Anticancer Research 24 (2004)*, 1745–1751

M. Donnellan, D. R. McKenzie, P. W. French, "Effects of Exposure to Electromagnetic Radiation at 835 MHz on Growth, Morphology and Secretory Characteristics of a Mast Cell Analogue, RBL-2H3.", *Cell Biology International 21 (1997)*, 427–439

E. Eccleston, B. J. Leonard, J. S. Lowe et al., "Basophilic Leukaemia in the Albino Rat and a Demonstration of the Basopoietin", *Nature New Biol 244 (1973)*, 73–76

Y. Fang, "Label-Free Biosensors for Cell Biology", *International Journal of Electrochemistry 2011 (2011)*, 1–16

T. Finkel, M. Serrano, M. A. Blasco, "The Common Biology of Cancer and Ageing.", *Nature 448 (2007)*, 767–774

J. Fogh, J. M. Fogh, T. Orfeo, "One Hundred and Twenty-Seven Cultured Human Tumor Cell Lines Producing Tumors in Nude Mice", *JNCI Cancer Spectrum 59 (1977)*, 221–226

7. LITERATUR

I. H. Frazer, "Prevention of Cervical Cancer through Papillomavirus Vaccination.", *Nature Reviews. Immunology 4 (2004)*, 46–54

I. Giaever, C. R. Keese, "Micromotion of Mammalian Cells Measured Electrically.", *Proceedings of the National Academy of Sciences of the United States of America 88 (1991)*, 7896–7900

I. Giaever, C. R. Keese, "A Morphological Biosensor for Mammalian Cells.", *Nature 366 (1993)*, 591–592

J. F. Harrison, S. B. Hollensworth, D. R. Spitz et al., "Oxidative Stress-Induced Apoptosis in Neurons Correlates with Mitochondrial DNA Base Excision Repair Pathway Imbalance", *Nucleic Acids Research 33 (2005)*, 4660–4671

L. E. Hebert, P. A. Scherr, J. L. Bienias et al., "Alzheimer Disease in the US Population", *Arch Neurol 60 (2003)*, 1119–1122

Y. Huang, C. Wu, C. Chuang et al., "Real-Time and Label-Free Detection of the Prostate-Specific Antigen in Human Serum by a Polycrystalline Silicon Nanowire Field-Effect Transistor Biosensor.", *Analytical Chemistry 85 (2013)*, 7912–7918

S. Ingebrandt, Y. Hana, F. Nakamura et al., "Neuron-Transistor Coupling: Interpretation of Individual Extracellular Recorded Signals", *European Biophysics Journal 34 (2005)*, 144–154

S. Ingebrandt, C. Yeung, M. Krause et al., "Label-Free Detection of Single Nucleotide Polymorphisms Utilizing the Differential Transfer Function of Field-Effect Transistors", *Biosensors and Bioelectronics 22 (2007)*, 2834–2840

A. Jemal, R. Siegel, E. Ward et al., "Cancer Statistics, 2008", *CA: A Cancer Journal for Clinicians 58 (2008)*, 71–96

J. Kasper, M. Hermanns, C. Bantz et al., "Inflammatory and Cytotoxic Responses of an Alveolar-Capillary Coculture Model to Silica Nanoparticles: Comparison with Conventional Monocultures.", *Particle and Fibre Toxicology 8 (2011)*

J. F. Kerr, C. M. Winterford, B. V. Harmon, "Apoptosis. Its Significance in Cancer and Cancer Therapy.", *Cancer 73 (1994)*, 2013–2026

A. B. Kharitonov, J. Wasserman, E. Katz et al., "The Use of Impedance Spectroscopy for the Characterization of Protein-Modified ISFET Devices : Application of the Method for the Analysis of Biorecognition Processes ", *Journal of Physical Chemistry B 105 (2001)*, 4205-4213

J. P. Kim, B. Y. Leeb, J. Lee et al., "Enhancement of Sensitivity and Specificity by Surface Modification of Carbon Nanotubes in Diagnosis of Prostate Cancer Based on Carbon Nanotube Field Effect Transistors", *Biosensors and Bioelectronics 24 (2009)*, 3372–3378

D. Kloß, R. Kurz, H. G. Jahnke et al., "Microcavity Array (MCA)-Based Biosensor Chip for Functional Drug Screening of 3D Tissue Models", *Biosensors and Bioelectronics 23 (2008)*, 1473–1480

T. Kottke, F. Errington, J. Pulidoet al., "Broad Antigenic Coverage Induced by Vaccination with Virus-Based cDNA Libraries Cures Established Tumors.", *Nature Medicine 17 (2011)*, 854–859

F. W. Kreth, A. Berlis, V. Spiropoulou et al., "The Role of Tumor Resection in the Treatment of Glioblastoma Multiforme in Adults", *Cancer 86 (1999)*, 2117–2123

A. Kulczycki, C.Isersky, H. Metzger, "The Interaction of IgE with Rat Basophilic Leukemia Cells", *The Journal of Experimental Medicine 139 (1974)*, 600–616

J. K. Y. Law, A. Susloparova, X. T. Vu et al., "Human T Cells Monitored by Impedance Spectrometry Using Field-Effect Transistor Arrays: A Novel Tool for Single-Cell Adhesion and Migration Studies", *Biosensors and Bioelectronics 67 (2015)*, 170–176

N. Lewinski, V. Colvin, R. Drezek, "Cytotoxicity of Nanopartides", *Small 4 (2008)*, 26–49

P. Lin, F. Yan , J. Yu et al., "The Application of Organic Electrochemical Transistors in Cell-Based Biosensors", *Advanced Materials 22 (2010)*, 3655–3660

E. H. Lips, R. van Eijk, E. J.R. de Graaf et al., "Progression and Tumor Heterogeneity Analysis in Early Rectal Cancer", *Clinical Cancer Research 14 (2008)*, 772–781

R. R. Love, H. Leventhal, D. V. Easterling et al., "Side Effects and Emotional Distress during Cancer Chemotherapy.", *Cancer 63 (1989)*, 604–612

D. Mazia, G. Schatten, W. Sale, "Adhesion of Cells to Surfaces Coated with Polylysine. Applications to Electron Microscopy", *Journal of Cell Biology 66 (1975)*, 198–200

M. R. Mcdevitt, D. Chattopadhyay, B. J. Kappel et al., "Tumor Targeting with Antibody-Functionalized, Radiolabeled Carbon Nanotubes", *The Journal of Nuclear Medicine 48 (2007)*, 1180–1189

W. L. McKeehan, R. G. Ham, "Stimulation of Clonal Growth of Normal Fibroblasts with Substrata Coated with Basic Polymers", *Journal of Cell Biology 71 (1976)*, 727–734

R. Medert, A. Schuster, L. K. Schwarz et al., "Spiking Rate of Myenteric Neurons Recorded from Multi-Electrode Arrays Depending on Local Microenvironment", *Physica Status Solidi (C) Current Topics in Solid State Physics 10 (2013)*, 877–881

P. Mohanty, Y. Chen, X. Wang et al., "Field Effect Transistor Nanosensor for Breast Cancer Diagnostics", *arXiv preprint arXiv:1401.1168 (2014)*, 1–25

N. A. Monteiro-Riviere, A. O. Inman, L. W. Zhang, "Limitations and Relative Utility of Screening Assays to Assess Engineered Nanoparticle Toxicity in a Human Cell Line", *Toxicology and Applied Pharmacology 234 (2009)*, 222–235

T. Mosmann, "Rapid Colorimetric Assay for Cellular Growth and Survival: Application to Proliferation and Cytotoxicity Assays", *Journal of Immunological Methods 65 (1983)*, 55–63

C. Nutting, D. P. Dearnaley, S. Webb, "Intensity Modulated Radiation Therapy: A Clinical Review", *British Journal of Radiology 73 (2000)*, 459–69

A. Offenhausser, C. Sprössler, M. Matsuzawa et al., "Field-Effect Transistor Array for Monitoring Electrical Activity from Mammalian Neurons in Culture", *Biosensors and Bioelectronics 12 (1997)*, 819-826

7. LITERATUR

T. Okano, N. Yamada, M. Okuhara et al., "Mechanism of Cell Detachment from Temperature-Modulated, Hydrophilic-Hydrophobic Polymer surfaces", *The Biomaterials: Silver Jubilee Compendium 16 (2006)*, 109–115

C. W. Olanow, W. G. Tatton, "Etiology and Pathogenesis of Parkinson's Disease", *Annual Review of Neuroscience 22 (1999)*, 123–144

Z. Ou, B. Wu, D. Xing et al., "Functional Single-Walled Carbon Nanotubes Based on an Integrin αvβ3 Monoclonal Antibody for Highly Efficient Cancer Cell Targeting", *Nanotechnology 20 (2009)*, 105–102

D. Peer, J. M. Karp, S. Hong et al., "Nanocarriers as an Emerging Platform for Cancer Therapy", *Nature Nanotechnology 2 (2007)*, 751–760

M. Peeters, P. Csipai, B. Geerets et al., "Heat-Transfer-Based Detection of L-Nicotine, Histamine, and Serotonin Using Molecularly Imprinted Polymers as Biomimetic Receptors", *Analytical and Bioanalytical Chemistry 405 (2013)*, 6453–6460

A. Poghossian, S. Ingebrandt, A. Offenhäusser et al., "Field-Effect Devices for Detecting Cellular Signals", *Seminars in Cell and Developmental Biology 20 (2009)*, 41–48,

A. Ramanavicius, F. W. Herberg, S. Hutschenreiter et al., "Biomedical Application of Surface Plasmon Resonance Biosensors (Review)", *Acta Medica Lituanica 12 (2005)*, 1–9

M. T. Santini, G. Rainaldi, P. L. Indovina, "Apoptosis, Cell Adhesion and the Extracellular Matrix in the Three-Dimensional Growth of Multicellular Tumor Spheroids", *Critical Reviews in Oncology/Hematology 36 (2000)*, 75–87

S. Schäfer, S. Eick, B. Hofmann et al., "Time-Dependent Observation of Individual Cellular Binding Events to Field-Effect Transistors", *Biosensors and Bioelectronics 24 (2009)*, 1201–1208

R. B. M. Schasfoort, G. J. Streekstra, P. Bergveld et al., "Influence of an Immunological Precipitate on D.C. and A.C. Behaviour of an Isfet", *Sensors and Actuators 18 (1989)*, 119–129

M. J. Schöning, A. Poghossian, "Recent Advances in Biologically Sensitive Field-Effect Transistors (BioFETs)", *The Analyst 127 (2002)*, 1137–1151

C. W. Scott, M. F. Peters, "Label-Free Whole-Cell Assays: Expanding the Scope of GPCR Screening", *Drug Discovery Today 15 (2010)*, 704–716

C. L. Shapiro, A. Recht, "Side Effects of Adjuvant Treatment of Breast Cancer", *New England Journal of Medicine 344 (2001)*, 1997–2008

E. Urcan, U. Haertela, M. Stylloua et al., "Real-Time xCELLigence Impedance Analysis of the Cytotoxicity of Dental Composite Components on Human Gingival Fibroblasts", *Dental Materials 26 (2010)*, 51–58

F. Uslu, S. Ingebrandt, D. Mayer et al., "Labelfree Fully Electronic Nucleic Acid Detection System Based on a Field-Effect Transistor Device", *Biosensors and Bioelectronics 19 (2004)*, 1723–1731

M. Varshney, Y. Li, "Interdigitated Array Microelectrodes Based Impedance Biosensors for Detection of Bacterial Cells", *Biosensors and Bioelectronics 24 (2009)*, 2951–2960

7.   LITERATUR

O. Windl, H. Lorenz, C. Behrens et al., "Construction and Characterization of Murine Neuroblastoma Cell Clones Allowing Inducible and High Expression of the Prion Protein.", *J Gen Virol 80 (1999)*, 15–21

A. M. Woollhead, D. L. Baines, "Forskolin-Induced Cell Shrinkage and Apical Translocation of Functional Enhanced Green Fluorescent Protein-Human αENaC in H441 Lung Epithelial Cell Monolayers", *Journal of Biological Chemistry 281 (2006)*, 5158–5168

J. M. Wörle-Knirsch, K. Pulskamp, H. F. Krug, "Oops They Did It Again! Carbon Nanotubes Hoax Scientists in Viability Assays", *Nano Letters 6 (2006)*, 1261–1268

G. Wrobel, R. Seifert, S. Ingebrandt, et al., "Cell-Transistor Coupling: Investigation of Potassium Currents Recorded with P- and N-Channel FETs", *Biophys J 89 (2005)*, 3628–3638

C. Xiao, B. Lachance, G. Sunahara et al., "Assessment of Cytotoxicity Using Electric Cell-Substrate Impedance Sensing: Concentration and Time Response Function Approach", *Analytical Chemistry 74 (2002)*, 5748–5753

E. Yavin, Z. Yavin, "Attachment and Culture of Dissociated Cells From Rat Embryo Cerebral Hemispheres on Poly Lysine-Coated Surface", *The Journal of Cell Biology 62 (1974)*, 540–546

8.   AUTHOR'S LIST OF PUBLICATIONS

D. Koppenhöfer, A. Susloparova, D. Docter et al., "Monitoring Nanoparticle Induced Cell Death in H441 Cells Using Field-Effect Transistors", *Biosensors and Bioelectronics 40 (2013)*, 89–95

D. Koppenhöfer, A. Susloparova, J. K. Y. Law et al., "Electronic Monitoring of Single Cell-Substrate Adhesion Events with Quasi-Planar Field-Effect Transistors", *Sensors and Actuators, B: Chemical 210 (2015)*, 776–83

D. Koppenhöfer, F. Kettenbaum, A. Susloparova et al., "Neurodegeneration through Oxidative Stress: Monitoring Hydrogen Peroxide Induced Apoptosis in Primary Cells from the Subventricular Zone of BALB/c Mice Using Field-Effect Transistors", *Biosensors & Bioelectronics 67 (2015)*, 490–496

R. Lanche, V. Pachauri, D. Koppenhöfer et. al., "Reduced graphene oxide-based sensing platform for electric cell–substrate impedance sensing ", *Physica Status Solidi (A) Applications and Material Science 211 (2014)*, 1404–1409

A. Susloparova, D. Koppenhöfer, X. T. Vu et al., "Impedance Spectroscopy with Field-Effect Transistor Arrays for the Analysis of Anti-Cancer Drug Action on Individual Cells", *Biosensors and Bioelectronics 40 (2013)*, 50–56

A. Susloparova, X. T. Vu, D. Koppenhöfer et al., "Investigation of ISFET Device Parameters to Optimize for Impedimetric Sensing of Cellular Adhesion", *Physica Status Solidi (A) Applications and Materials Science 211 (2014)*, 1395-1403

A. Susloparova, D. Koppenhöfer, J. K. Y. Law et al., "Electrical Cell-Substrate Impedance Sensing with Field-Effect Transistors Is Able to Unravel Cellular Adhesion and Detachment Processes on a Single Cell Level", *Lab Chip 15 (2015)*, 668-679

9.   SUMMARY / ZUSAMMENFASSUNG

9.1   Summary

Cancer is one of the most common cause of death and one of the most severe diagnoses patients can receive in modern medicine. Its treatment normally involves a combination of chemotherapy, tumor resection and radiation therapy, often accompanied by severe side effects causing high psychological strain. In recent years treatment shifts from general approaches to individual therapy regiments for individual patients. A similar situation can be assumed for neurodegenerative diseases like Alzheimer's or Parkinson's disease, for which oxidative stress is a common contributing factor.

For both cancer and neurodegenerative diseases the development of new pharmacological compounds and treatment strategies is a high priority goal facilitating the need for fast and efficient screening and testing platforms. The objective of this thesis was the establishment of an impedance spectroscopy-based high throughput testing system using silicon-based field-effect transistors. During this thesis work three subprojects were conducted.

The first subproject of this thesis covered the topic of the analysis of cellular adhesion. Morphologically and histologically different cell lines were compared with regard to their respective impedance spectra (for both confluent and low density cultures) and unique characteristics of the tested cell lines were identified, demonstrating the ability of the presented system to differentiate between cells of different cell types down to the single cell level.

In the second subproject the toxicity of an industrial silica nanoparticle was monitored in real time under cell culture conditions using the presented FETCIS system. Observed transfer-function suppression between 30 and 60 min after particle administration could be

correlated with the observed cytotoxic effect of the used particle NexSil20. By analyzing the toxicity of an already described particle via real-time impedance monitoring, the applicability of the proposed system was further substantiated.

During the third subproject of this thesis work the applicability of the presented system to simultaneously monitor the reaction of primary neuronal tissue to external stimuli using a parallel-culture setup. Primary SVZ cells were exposed to hydrogen peroxide to induce apoptosis and monitored for their response to this treatment. By analyzing the effects of hydrogen peroxide toxicity in neuronal tissues the capability to open up new research applications in Alzheimer's and Parkinson's disease of the presented system could be shown.

The measurement and analysis system presented in this thesis work is primarily meant for pharmacological testing both in real time and under cell culture conditions, providing a fast working method of analyzing the effects of external stimuli like pharmacological compounds or effects of micro-environmental conditions (e.g. temperature, pH value, etc.). As a second possible application the presented system should also be usable in the field of individualized cancer diagnostics and therapy. By differentiating between the impedimetric fingerprints of different cell types an impedimetric histology system would be possible.

9.2   Zusammenfassung

Krebs ist eine der häufigsten Todesursachen und gleichzeitig eine der erschütterndsten Diagnosen der modernen Medizin, die Patienten erhalten können. Die Behandlung besteht normallerweise aus Chemotherapie, Tumorresektion und Strahlentherapie zusammen, wobei die Behandlung häufig mit starken Nebenwirkungen und einem hohen Leidensdruck verbunden ist. In den letzten Jahren verlagert sich die Behandlung von Krebs weg von generischen Behandlungsansätzen hin zur individuell auf einzelne Patienten zugeschnittenen

Therapie. Eine ähnliche Entwicklung lässt sich bei der Behandlung neurodegenerativer Erkrankungen wie Alzheimer oder Parkinson erkennen, bei denen oxidativer Stress als gemeinsamer begünstigender Faktor eine Rolle spielt.

Sowohl für Krebs als auch neurodegenerative Erkrankungen ist die Entwicklung neuer Wirkstoffe und Behandlungsansätze ein Ziel mit hoher Priorität, was die Etablierung von schnellen und effizienten Screening-Plattformen nötig macht. Ziel der vorliegenden Arbeit war die Etablierung einer auf Impedanzspektroskopie basierenden Hochdurchsatz-Plattform, die siliziumbasierte Feldeffekt-Transistoren verwendet. Im Verlauf dieser Arbeit wurden drei Unterprojekte bearbeitet.

Im Verlauf des ersten Unterprojekts wurde die Zelladhäsion dreier morphologisch und histologisch unterschiedlicher Zelltypen untersucht und bezüglich ihrer jeweiligen Impedanzspektren verglichen (sowohl für konfluente als auch nicht-konfluente Zellkulturen). Dabei wurden für die verschieden Zelltypen charakteristische Merkmale beobachtet, die die Fähigkeit des vorgestellten Systems zur Unterscheidung spezifischer Zelltypen voneinander mit einer Auflösung bis zur Einzelzellebene belegt.

Im Zuge des zweiten Unterprojekts wurde die Toxizität eines industriellen Silica-Nanopartikels in Echtzeit unter Zellkulturbedingungen mittels des präsentierten FETCIS-Systems untersucht. Dabei konnte eine Unterdrückung der Transistor-Transferfunktion zwischen 30 und 60 min nach Partikelapplikation beobachtet werden, die mit bereits veröffentlichten Toxizitätsergebnissen des verwendeten Partikels NexSil20 korrelieren. Durch die Analyse der Zytotoxizität eines bereits beschriebenen Partikels via Echtzeit-Impedanzmessung konnte die Anwendbarkeit der beschriebenen Methode in pharmakologischen Studien weiter belegt werden.

Das dritte Unterprojekt der vorliegenden Arbeit diente dem Beleg der Nutzbarkeit des vorgestellten Systems zur simultanen Untersuchung der Reaktion primären neuronalen Gewebes auf externe Stimuli mittels eines Parallel-Kultur-Setups. Primäre SVZ-Zellen wurden mit Wasserstoffperoxid behandelt um Apoptose zu induzieren, anschließend wurde die Reaktion der Zellen auf diese Behandlung beobachtet. Durch die Analyse der Wasserstoffperoxid-Toxizität in neuronalem Gewebe konnte die Fähigkeit des vorgestellten Systems gezeigt werden neue Forschungsanwendungen in den Bereichen Alzheimer und Parkinson zu eröffnen.

Das in dieser Arbeit vorgestellte Mess- und Analysesystem soll primär für pharmakologische Untersuchungen in Echtzeit und unter Zellkulturbedingungen verwendet werden und stellt dabei eine schnelle Methode dar die Effekte externer Stimuli, wie pharmakologische Wirkstoffe oder Veränderungen der Umgebungsbedingungen (z.B. Temperatur, pH-Wert, etc.) zu untersuchen. Eine zweite mögliche Anwendung des vorgestellten Systems liegt im Feld der individualisierten Krebsdiagnostik und –therapie. Durch die Unterscheidung der impedimetrischen Fingerabdrücke unterschiedlicher Zelltypen ist eine impedimetrische Histologie möglich.

10. ACKNOWLEDGEMENT